国立大学法人
東京農工大学
Tokyo University of Agriculture and Technology

**Tokyo University of Agriculture and Technology**

**A thesis submitted to the Tokyo University of Agriculture and Technology**

**For the degree of Doctor of Engineering**

# Coordination-Assembled Nanomedicine Based on Reactive Oxygen Species (ROS) for Anti-Inflammatory and Anti-Tumor Therapy

**2022**

**Bio-Applications and Systems Engineering**

**Department of Bio-Functions and Systems Science**

**Xiaoyan Ma**

## List of contents

**Abstract**

Reactive oxygen species (ROS) play a double-edged-sword role on various physiological functions. The low or normal level of ROS can participate in the regulation of redox homeostasis, immune function and associated cell signaling. Nevertheless, the high level of ROS can induce cellular dysfunction and increase risk of chronic diseases and carcinogenesis. Therefore, excessive generation of ROS in lesion site has been a new target for treating diseases. Recently, nanomaterials-regulated *in vivo* ROS have received increasing attention, which dynamically guide process of ROS in biological milieu. This a new-generation therapeutic methodology ascribes to advances of ROS science, including ROS chemistry, ROS biology ROS nanotechnology. Especially, the advance of ROS nanotechnology promotes to fabricate various nanomaterials with ROS-regulating properties.

## Chapter 1. 1. Introduction

Reactive oxygen species (ROS) are crucial for physiological functions of every aerobic organism. It not only is deemed as critical second messengers for regulating cell signaling pathways, but also plays a significant role on cell survival and death.[1] Chemically speaking, ROS are also defined as collective term that is comprised of incomplete reduction of oxygen. It includes hydroxyl radical (•OH), singlet oxygen ($_1O^2$), superoxide anion($O_2•^-$) and hydrogen peroxide ($H_2O_2$). Importantly, ROS are double-edged sword. At lower or moderate levels, the intracellular ROS are necessary for redox homeostasis, immune function and cell signaling.[2] A wide factors, such as pathogen invasion, ages, radiation, etc., and imbalance of ROS generation and scavenging activity from endogenous antioxidant, cause excessive ROS generation. The high level of ROS leads to severe damage to cell structure, normal function, cellular components (such as lipids, DNA and proteins), elevation of cytosolic $Ca^{2+}$ and other impairment to cells, even resulting in cell death (Figure 1.1a).[3]

Excessive ROS can lead to the necrosis and/or apoptosis malignant cells, exhibiting a potential therapeutic strategy for tumor therapy. Therefore, materials that can assist to produce more ROS, has received increasing attention from scientists. With introduction of different exogenous stimulus, for example, light, ultrasound and radiation, various dynamic therapy strategies, such as photodynamic, sonodynamic radiation therapies have been developed.

Additionally, massive accumulation of ROS can exacerbate oxidative stress, which affects the transcription and expression of genes towards abnormal level, change crucial signaling pathways of cell and modulate inflammatory responses. Therefore, the oxidative stress leads to many serious diseases, for example, inflamed diseases (inflammatory bowel disease, periodontitis, sepsis), neurodegenerative disease (Alzheimer's Disease, Parkinson's Disease), atherosclerosis, cardiac repair and some other diseases **(**Figures 1.1b, c, d). These diseases have a serious impact on human health and quality of life.[4] Based on unpredictability of related biological processes about ROS, it is of great significance in regulating and controlling ROS concentrations within an expected threshold for initiating optimally therapeutic effects.

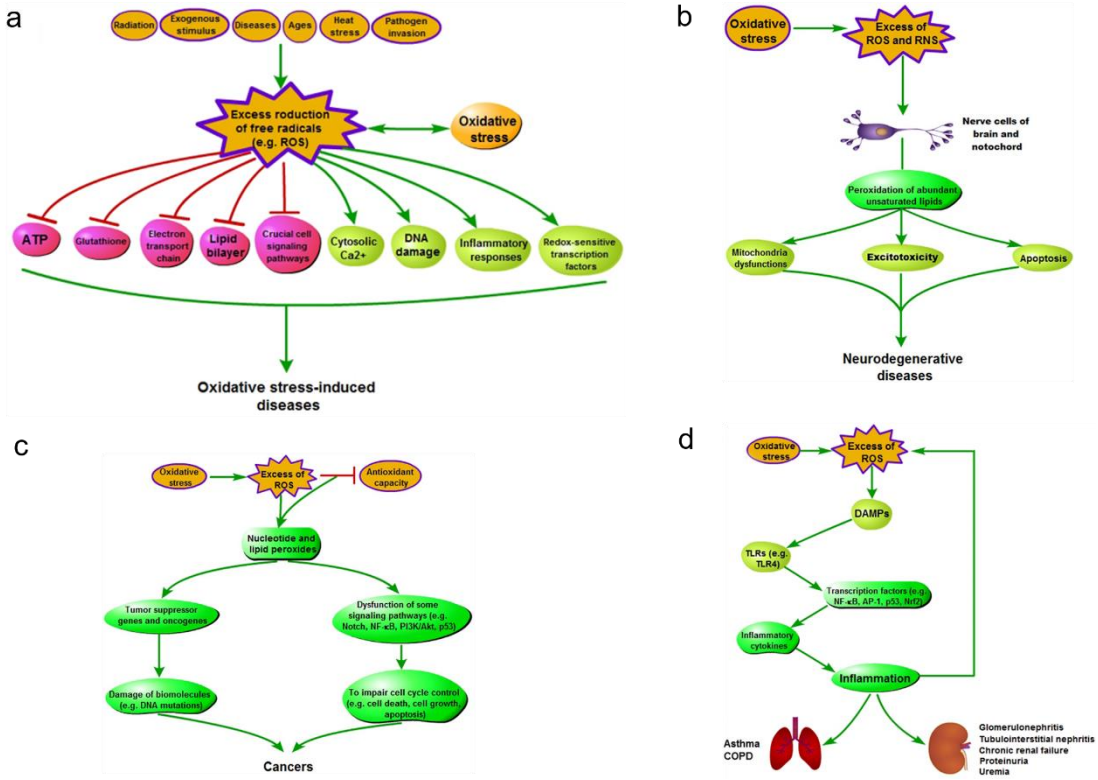


**Figure 1.1** (a) The schematic diagram of oxidative stress-induced diseases.[3] (b) The mechanism diagram of oxidative stress-induced neurodegenerative diseases. (c) The pathogenesis diagram of oxidative stress-induced cancers. (d) The pathogenesis diagram of oxidative stress-induced related diseases of inflammation.

## 1.2 ROS science

In the past century, the ROS generation processes and physiological roles of ROS in organisms were gradually unveiled by biologists. The reaction mechanisms involved ROS, such as pathways and kinetics, were gradually investigated by chemists. On this basis, nanomaterials for guiding dynamic behaviors of ROS were designed by materials scientists. Thanks to more and more ROS-related researches, artificially ROS-related materials and nanotechnology, the concept of "ROS science" is proposed. ROS-based chemical mechanisms, nanomaterials and biological effects are integrated into one, which is believed to be an emerging discipline. Attributing to three subdisciplines of ROS biology, ROS chemistry, and ROS nanotechnology, ROS science provides new and rational therapeutic strategies for various therapeutic modalities, for example, tumor therapy, anti-inflammatory therapy, wound disinfection and cellular detection (Figure 1.2).[5] According to different biological scenarios, ROS-based nanomedicine are designed to regulate ROS generation, depletion processes, realizing remarkable ROS-based therapeutic effect.

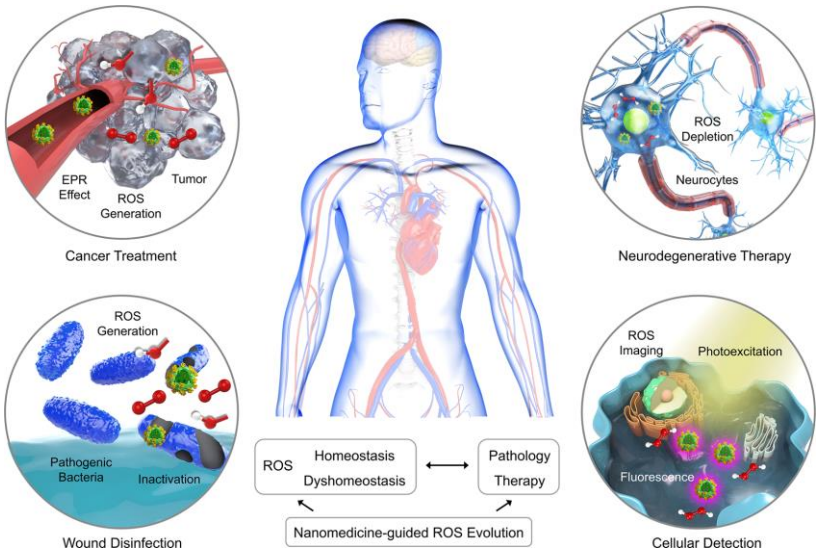


**Figure 1.2** ROS-based nanomedicine for various applications.[5]

Self/co-assembly has drawn huge interesting on change from disorder into order.[6] The phenomenon of self/co-assembly can be seen everywhere. From inorganic substance to organic substance, from lipid, amino acid and nucleic acid molecules to phospholipid bilayer, protein structure and double helix structure of genetic material, and from individual cells to tissues, even living organisms. Therefore, self/co-assembly plays a crucial role in the structure, functions, and properties of natural substance.[7] Inspired by nature, the development of multifunctional and advanced nanomaterials has exhibited huge potential through self-assembling strategy. From the molecular building blocks to complex nanomaterials are bridged by self-assembly method via complicated intermolecular interactions. The self/co-assembling method possesses a few advantages, including high encapsulation efficiency, reduced system toxicity and easy maneuverability. With the development of self-assembly technology and regulation of self-assembling process, multifunctional and different-structured nanomaterials have exhibited huge potential to fabricate for various applications.

### 1.2.1 Physiological roles of ROS

ROS generation is involved in UV light exposure, environmental stress and byproduct from many physiological processes. As canonical ROS sources, mitochondria easily generate ROS for ATP synthesis due to the imperfect electron transport chain.[8] Moreover, the process of disulfide bond formation from oxidative protein in the endoplasmic reticulum lumen, is primary source of ROS.[9] NADPH oxidases are another source of ROS production in cell membranes.[10] Additionally, pathogens-killed phagosomes and peroxisomes are as classic examples of organelles for locally generating ROS.[11,12]

ROS can serve as intracellular signaling molecules, play a vital role in multiple layers of control to mediate physiological functions.[13] For example, ROS can regulate cell migration, promote stem cell proliferation and influence subsequent neurogenesis.[14,15] All coins have two sides, thence ROS is no exception. In normal cells, ROS at the redox

homeostasis can carry out physiological regulation as messengers, which can not only sustain the normal physiological functions and reduce the risk of diseases. However, excessive ROS can cause damage to tissues and cells, including DNA, proteins, and lipid. It was first demonstrated that ROS could induce carcinogenesis in 1981 due to characteristic of increased aerobic glycolysis existing at different forms of cancer cells. Therefore, excessive ROS can induce cellular dysfunction and increase risk of several chronic diseases and carcinogenesis. Ulteriorly, excessive ROS are produced in cancer cells, which further induce upregulation of endogenous cellular antioxidants for self-survival through shift of redox dynamics.[16] This process maintains new redox homeostasis and low toxic threshold ROS level, leading to cancer cells metastasis. In summary, ROS associated redox homeostasis play a significant role in normal tissue and cancer cells.

### 1.2.2 Chemistry exploration of ROS

ROS chemistry has made great progress and gradually uncovered intercorrelations between ROS and materials, biological milieu since reported Fenton reaction in 1894. ROS generation is ubiquitous in chemistry. Materials can assist exogenous energy to converse to ROS through different catalytic reactions. For example, $H_2O_2$ is capable of generating explosive ROS in the presence of transition metal ions such as $Cu^{2+}$ and $Fe^{2+}$; $TiO_2$ was used as photocatalysis to catalyze $H_2O$ for ·OH generation.[17] With the in-depth study of ROS-generating catalysts, increasing materials provided ROS generation are developed for applications of disease treatment. It has emerged enormous potential for application of ROS biology.

Another source of ROS generation is biological systems. Especially, mitochondria are as main location. ROS generation derived from $O_2$ molecules electrons can react with electrons get off the mitochondrial respiratory. Moreover, isoforms of NADPH oxidase complexes in cytomembranes, flavoenzyme ERO1 loaded in the endoplasmic reticulum promote to generate ROS in some cancer cells. In addition, catalytic ROS generation is developed via lipoxygenases, cyclooxygenases, xanthine oxidase, and metal ions (such as $Fe^{2+}$ and $Cu^{2+}$).

Importantly, the reaction characteristics of ROS is high reactivity, specificity and diffusibility. High reactivity of ROS exhibits nonequilibrium state and involves different various ROS reactions. Then specific ROS can further mediate various redox arrays. The diffusibility of ROS demonstrates that compartmentalization of ROS is existent. Therefore, it is of great important significance to explore ROS biology with advances in ROS chemistry.

### 1.2.3 Nanotechnology innovation of ROS

The development of nanotechnology is an important bridge between physiological function of ROS and chemical materials with ROS depletion, generation, or transition functions. Therefore, multifunctional nanomaterials constructed by nanotechnology are participated in regulating ROS level for maintaining cellular redox status. ROS-based nanotherapeutic modalities are gradually developed.

Materials are extracted from nature or created to novel materials by synthetic chemists.

Materials are further optimized through decreasing to nanoscale for promoting the tissue penetration and cellular uptake, providing binding sites for ambient reactive molecules. Notedly, designed nanomaterials are endowed with ROS-regulating functionals via the integration of intrinsic characteristics, especially chemical features, and extrinsic properties, such as particle size. The ROS-based nanomaterials are employed in therapeutic application, which has obtained fulfilling therapeutic effects and further promote nanomedicine innovation.

The great progress has been made in ROS-based nanomedicines. Nevertheless, the thorny issues, such as biocompatibility, bioavailability, biodegradability, loading efficiency and extra immune response, still exist, which limit bioapplication of nanomedicine. It needs researchers to explore more efficient technology with fewer side effects for design nanomedicines. It is of great significance for advances in nanomedicine applications.

### 1.3 Assembly nanotechnology

Nanotechnology as an emerging technique, is capable of constructing multitudinous nanomaterials for diagnosis and therapy. Assembly as one of nanotechnologies has made great progress for fabricating nanomedicine.

Based on that the phenomenon of assembly can be seen everywhere, from inorganic substance to organic substance, from lipid, amino acid and nucleic acid molecules to phospholipid bilayer, protein structure and double helix structure of genetic material, and from individual cells to tissues, even living organisms. It follows that assembly plays a crucial role. Inspired by this, self-assembly or co-assembly strategies are gradually employed for fabricating diverse nanomaterials. The assembly process is accompanied by noncovalent interactions, including hydrogen bond, hydrophobic interaction, electrostatic interaction, π–π stacking, Van der Waals interaction, coordination interaction, and covalent interaction.[18]

The hydrogen bond drives from mutual attraction between hydrogen atoms and electronegative atoms via dipole-dipole interaction. The common electronegative atoms include nitrogen, oxygen and fluorine atoms. The strength and direction of single hydrogen bond is not favorable to construct stable supermolecular structure. Therefore, the development of multiple hydrogen bonds is an important approach for stable supramolecular structure with ordered structure.[19] Moreover, pH value, temperature and solvent polarity effectively impact the strength and direction of hydrogen bond.[20,21] Thence, the polymer materials with unique response property, structure and morphology are designed according to actual demand. It is benefit for further targeted application at the disease site for the purpose of personalized medicine.

The hydrophobic interaction is a force caused by the close proximity of hydrophobic groups to avoid water. It plays an important role in the self-assembly of molecules containing hydrophobic groups, which is a spontaneous process to fabricate more stable material structure. For example, hydrophobic ammonia acid side chains, nucleic acid bases and hydrocarbon chains of fatty acids in biomolecule structures. Yan's group has reported that hydrophobic structure in bovine serum albumin is chose as carries to load photosensitizer pheophorbide a. The constructed nanodrugs are applied for anti-tumor

through photothermal effect.[22]

The electrostatic interaction is a force formed between ions with charges. It includes attraction of inversely charged groups and repulsion of same charged groups. Importantly, electrostatic interaction is closest to covalent interaction in strength compared with the other noncovalent interactions, which can be employed for fabricating preliminarily designed nanoparticles. Additionally, electrostatic interaction also used to adsorb motivated molecules for further researches. For example, Ma's group has reported that calcium ions were chelated with acidic residues on the outer membrane of bacterial outer membrane vesicles to facilitate the CaP nucleation.[23]

The π–π stacking interaction is a kind of weak interaction between aromatic rings based on the special spatial arrangement of aromatic compounds.[24] In biological systems, the π–π stacking interactions play an important role on nuclear bases in DNA and RNA molecules, protein folding, template-guided synthesis and molecular recognition. The introduction of π–π stacking interaction into supramolecular polymer materials has also greatly promoted the development of materials science with the deep understanding of π–π stacking.

Fluctuations of electron distribution on the groups cause changes in the dipole moment, and the interaction between the corresponding dipoles is called the van der Waals interaction. Van der Waals interaction is a universal weak force between atoms and molecules, showing much weaker than hydrogen bond. Therefore, Van der Waals interaction is rarely main driving force in self-assembly systems.

Coordination interaction is a special kind of covalent bond. The coordination bond is formed through one atom alone supplying a pair of electrons to another atom without any electrons. There are many inorganic complexes in living organisms, which are formed by the coordination between biological ligands and metals, such as metalloenzymes, chlorophyll, vitamin B12. Coordination interaction plays an important role in mediating assembly.[25]

Polyvalence and synergy of interactions are beneficial for constructing stable nanoparticles. Because the single intermolecular interaction is very weak and unstable. Additionally, organisms formed organizational structures and performed biological functions adopt "polyvalent" and "synergistic" strategies. Inspired by these, designed nanomedicines are fabricated by multiple interactions. Yan's group has reported assembled peptide−porphyrin photothermal nanodots (PPP-NDs) (Figure 1.3a).[26] During assembly process, π-stacking and hydrophilic interaction as main driving forces promote to self-assemble nanodots (Figure 1.3b). Especially, strong π-stacking plays a significant role, which both completely quenches fluorescence and inhibits ROS generation for achieving highly efficient light-to-heat energy conversion. Moreover, multifunctional photodynamic drugs are fabricated via assembly of amphiphilic peptides, $Mn^{2+}$ and photosensitizer chlorin e6 (Figure 1.3c).[27] This assembled process depended on coordination, hydrophobic, and π−π stacking interactions. These examples mentioned above demonstrate that a stable structure depends on multiple forces.

As-prepared nanoparticles constructed by multiple noncovalent interactions perform many favorable advantages: Firstly, the preparation approach is simple manufacturing process. Secondly, nanoparticles possess multiple noncovalent coordination and

noncovalent interactions for fabricating nanomedicines, achieving robust construct for long blood circulation and susceptible response to environmental variations for targeted burst release. Thirdly, nanoparticles possess high encapsulation efficiency. These advantages indicate that the assembly approach has potential to fabricate specialized nanoparticles for bioapplications.

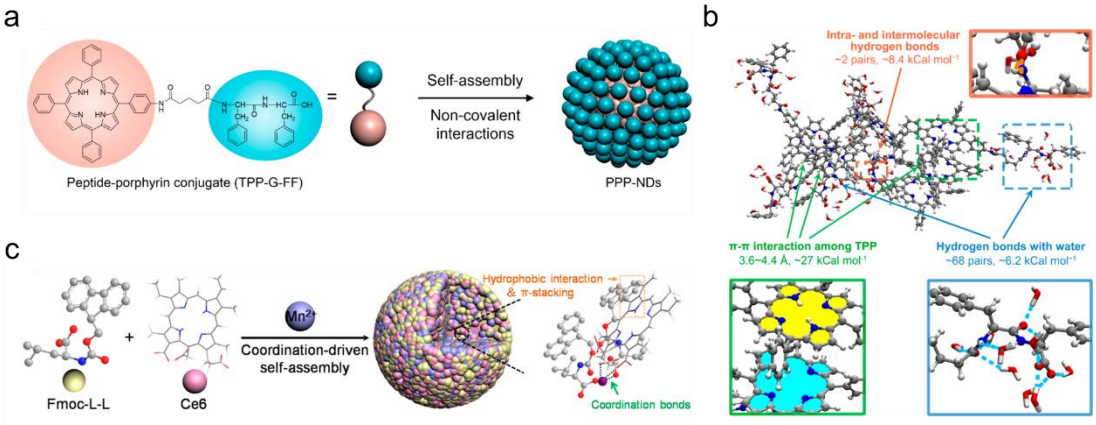


**Figure 1.3** (a) The schematic illustration of the self-assembled PPP-NDs.[26] (b) A molecular dynamics simulation of self-assembled PPP-NDs. (c) The schematic illustration of the self-assembled photodynamic drugs through the synergy of coordination bonds, π–π stacking and hydrophobic interactions.[27]

## 1.4. Bioapplication

### 1.4.1 Anti-inflammatory therapy

Inflammation is an essential and natural defense response to tissue damage or pathogenic infection in the body. Uncontrolled inflammation can induce the development and progression of various diseases associated with inflammation, seriously affecting human health. ROS as an important signal in inflamed sites, are overprocessed and perform negative effects on tissues. Therefore, targeted strategy to ROS is a potential approach.

Aiming at the overproduction of ROS, a large amount of antioxidants are developed for scavenging excessive ROS. The ROS scavenging mechanisms of various antioxidants have reported.[28] For polyphenol scavengers, including teas, coffee, fruits, fruit juices, vegetables, etc., the mechanisms of antioxidant activity are ascribed to chelate with metal ions, activate antioxidant enzymes, inhibit oxidases and transfer electrons of free radicals (Figure 1.4a). For polysaccharides scavengers, their protective effects attribute to chelate metal catalysts, promote activation of enzymatic defense system, and act on oxygen removal, singlet oxygen quenching and free radical breaking (Figure 1.4b). For poly(amino) and peptides scavengers, the mechanisms are ascribed to chelate metal and inactivate free radicals (Figure 1.4c). For mimetic enzyme-based scavengers, mimetic enzymes can be complete to scavenge excessive ROS. Additionally, other synthetic polymeric ROS scavengers are developed for achieving ROS clearance, but are few employed for clinical appliacation.[29,30] Many antioxidant enzymes, such as glutathione

peroxidase (GPx) and superoxide dismutase (SOD), and naturally antioxidant small molecules, such as vitamin C and vitamin E, can prevent cells and tissues from oxidative damage, even associated inflammatory diseases. Nevertheless, these antioxidant enzymes and antioxidant small molecules are restricted in their low bioavailability owing to instability in hostile conditions. In addition, chemically synthesized antioxidants are very common in life, for example, butylated hydroxyanisole, butylated hydroxytoluene, ethoxyquin and propyl gallate. They play multiple roles on radioprotection, anti-tumor activity, antimutagenic activity, and acute toxicity of chemicals prevention. But the synthesized antioxidants can cause adverse effects, such as increased toxicity of other chemicals, increased mutagen activity, even increased risk of other cancers. Recently, naturally occurring, small-molecule bioactive compounds, such as curcumin, resveratrol, bilirubin, rosmarinic acid and epigallocatechin gallate, have drawn increasing attention for their anti-inflammatory, antimicrobial, and anticancer activities. However, the poor water solubility and further induced low bioavailability severely hinder bioapplication and further translation to clinical development.[30]

To overcome these disadvantages, carry strategies are developed, including liposome, polymer, biomimetic bacteria and inorganic nanomaterials. Nevertheless, low loading efficiency, systemic toxicity, easy leak, tedious manufacture, extra inflammatory and immune response derived from the synthetic components, still need to be addressed, which seriously hinder bioapplication and clinical application. Therefore, it is of great importance to develop creative, valuable and ideal drugs for disease treatment. Notedly, fabricated multifunctional nanodrugs by the assembly strategy perform favorable advantages, such as high loaded-drug rate and reduced system toxicity. Some researchers have made great progress for various diseases treatment.

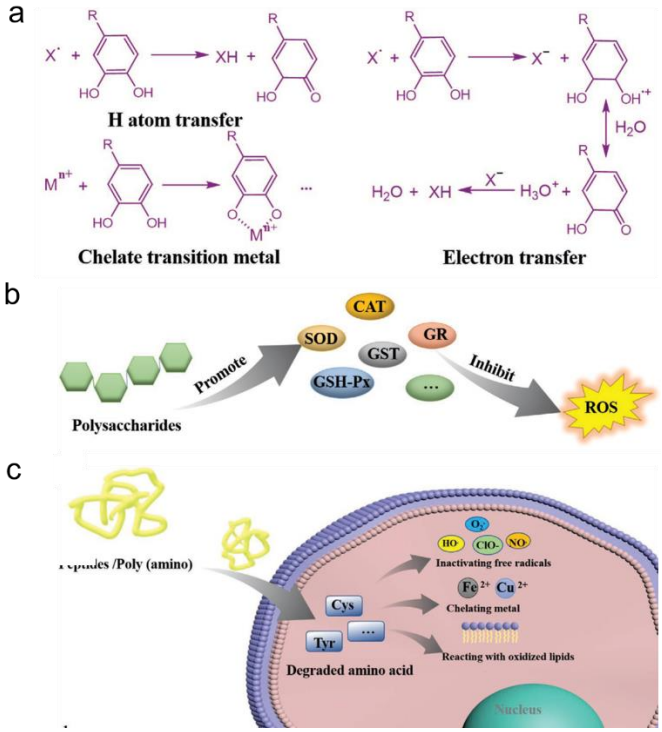


**Figure 1.4** (a) The mechanisms of polyphenol scavengers.[28] (b) The mechanisms of

polysaccharides scavengers. (c) The mechanisms of poly(amino) and peptides scavengers.

#### 1.4.1.1 Anti-inflammatory bowel disease therapy

Inflammatory bowel disease (IBD) as one of main threats to public health, significantly decreases life quality of patients and increases risk of colon cancer.[31] Current therapeutic drugs include antibodies, antibiotics and small molecular drugs, which lead to antibiotic resistance, multiple complications and immunological response.[32] In recent years, enzyme proteins have received increasing attention due to high specificity compared with other therapeutic drugs. Nevertheless, enzyme proteins easily suffer from hydrolysis and enzymatic degradation in hostile conditions, such as stomach acid, proteases. To overcome these problems, encapsulation strategies of various nanocarriers and chemical modification from hydrophilic and neutral polymers have been developed. Chen's group propose targeted nanoparticle for the local IBD treatment.[33] Firstly, SOD is selected as desirable antioxidant that could alleviate mucosal injury. Secondly SOD-containing lipid−polymer hybrid nanoparticles are prepared by self-assembly approach and modified with folate ligands to obtain SNP-FA (Figure 1.5a). As-made SNP-FA exhibit many advantages, including good stability, long residence time and high permeability at mucosa, and targeted ability in the inflamed colon (Figure 1.5b). *In vivo* results demonstrate that SNP-FA nanoparticles can effectively mitigate inflammation in colitis mice.

Moreover, the mechanism of delivered drugs need to be further clarified. The therapeutic drugs are generally loaded by covalent conjugation or physical loading methods. Because the non-covalent conjugation way via non-covalent forces greatly affects loaded-drug capacity and efficiency, drug stability and drug release kinetics. It is more potential to explore non-covalent interactions between drug molecules and carrier material in drug delivery systems. Jianxiang Zhang and his colleagues investigate the self-assembly of cyclodextrins (CDs) with hydrophilic copolymers could be mediated by guest molecule.[34] In this work, CD-containing polymers are used to fabricate nanosystems, then are interacted with Tempol (Tpl) that acts as superoxide dismutase mimetic for antioxidant and anti-inflammatory through host–guest interaction as (Figure 1.5c). In comparison with free Tpl at the same dose, the inhibited expression levels of pro-inflammatory cytokines by the assembled Tpl/PEG-P(bCD) nanoparticles are not altered, indicating that assembled nanoparticles still release Tpl. It demonstrates that CDs with block copolymers are expected to be developed drug delivery systems for various disease treatment by non-covalent interactions.

With the in-depth study of IBD, the gut microbial ecosystem is closely related to IBD, exhibiting reduced diversity of gut microbiota due to the unbalance between pathogenic and commensal microorganisms.[35] Tea polyphenols have performed preventive antioxidant effects on anti-inflammatory, antimicrobial. However, their water-insoluble characteristic and low bioavailability limit their bioapplication and clinical development. In addition, the interrelations with the gut microbiota in IBD have been unclear. Inspired by the above, Raffaele Mezzenga uses amyloid fibrils as templates to combine with polyphenol compound epigallocatechin-3-gallate (EGCG) for IBD

therapy (Figure 1.5d). Due to highly self-associate tendency in water, EGCG molecules accumulatively self-assembled on structural support amyloid fibrils. As-obtained hybrids perform high loading efficiency, good chemical stability, utilization of high concentration compared with single polyphenols. During treating IBD, EGCG can inhibit the enrichment of gut microbiotas associated with inflammation, such as Aestuariispira (OTU17), Escherichia (OTU3) and Bacteroides thetaiotaomicron (OTU8). Formed hybrid nanofilament based on EGCG deposited on the surface of the amyloid fibrils perform both prolonged retention time and regulation of gut microbial, achieving remarkable anti-inflammatory effect.

In summary, assembled nanomedicines effectively overcome disadvantages of instability of antioxidant enzymes in hostile conditions, release drugs, and improve bioavailability of hydrophobic drugs for IBD treatment.

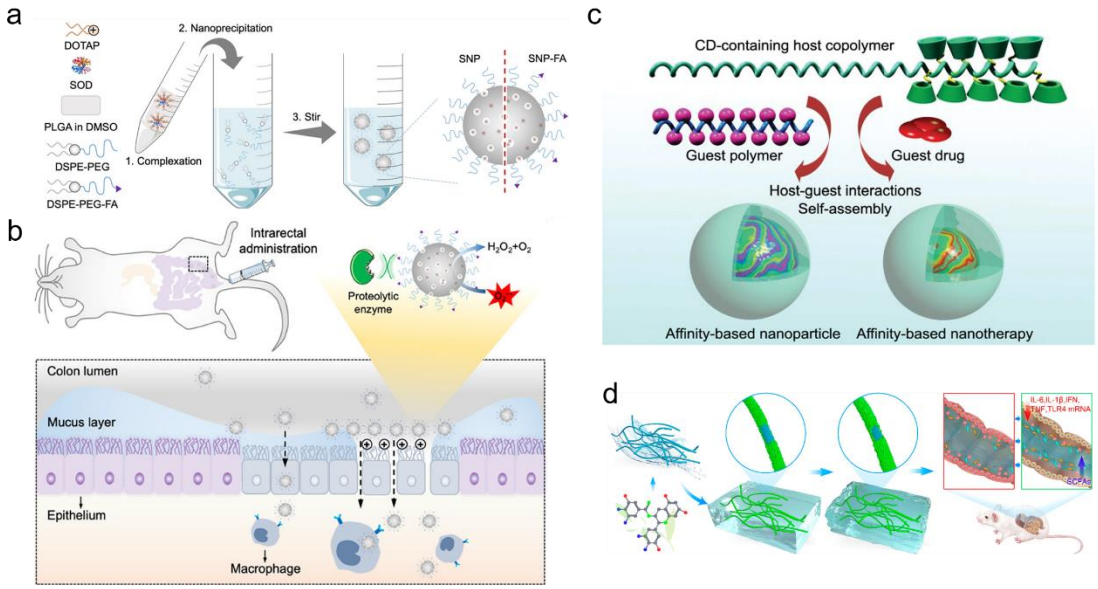


**Figure 1.5** (a) The preparation process of SOD-containing lipid−polymer hybrid nanoparticles.[33] (b) As-prepared SNP and SNP-FA nanoparticles for IBD therapy through oral administration. (c) Schematic of affinity nanoparticles by self-assembling CD-containing host copolymers and guest polymer and drug by host–guest interactions.[34] (d) The schematic diagram of as-obtained hybrid nanofilament by combining amyloid fibrils with polyphenol for treating IBD through anti-inflammatory and the regulation of gut microbial dysbiosis.[35]

### 1.4.1.2 Periodontal disease (PD) therapy

PD is chronic inflammatory disease induced by oral polymicrobial pathogens and microbiological plaque, and companied with lots of ROS generation for aggravating inflammation.[36] If PD is not treated in time, it will be caused tooth loss and destruction of adjacent connective tissue. The current strategy for PD is antimicrobial agents, such as antibiotics that inhibit recolonization of pathogenic bacteria.[37] However, long-term use of antimicrobial agents easily induces many side effects, including drug resistance, gastrointestinal intolerance, hypersensitivity.[38] In addition, antimicrobial agents are difficult to reach enough antibacterial concentrations at the disease site. Therefore, local

drug application can effectively bypass these disadvantages. Bernd Kreikemeyer and his team design self-assembling peptides (SAP) hydrogel.[39] Hydrogel agents intrinsically possess favorable properties, such as adhesion benefit for retention in periodontal pocket, controlled and prolonged drug release, syringability. Moreover, as-obtained two SAP hydrogels (P11-4 and P11-28/29) exhibit many advantages of intrinsic antimicrobial characteristic, drug delivery capacity and regenerative potential. This P11-SAP hydrogel provides new thought for PD therapy.

To meet the severe change of antimicrobial resistance, many researchers have made a lot of efforts. Polypeptide-based nanostructures are developed to effectively destroy bacteria due to membrane disruption mechanisms of antimicrobial peptides. If bacterial protein or cytoplasm cannot be completely attacked, antimicrobial resistance is difficult to overcome. To address this issue, Jianzhong Du and his group fabricate dual corona vesicles with intrinsic antibacterial activity for biofilm-caused periodontitis.[40] In this work, two block copolymers of PCL-b-P(Lys-stat-Phe) and PEO-b-PCL are co-assembled into a dual corona vesicle. PEO has capability of penetrating polymeric substances on the cell surface, and P(Lys-stat-Phe) has intrinsic antibacterial activity ascribed to positive charges. Obtained result demonstrates that the antibiofilm activity is remarkably improved through the combination of PEO and P(Lys-stat-Phe). In this work, ciprofloxacin hydrochloride as broad-spectrum antibiotic is loaded into the dual corona vesicle, effectively eradicating biofilm and mitigating periodontal symptoms.

In a word, antibacterial peptides and copolymers with intrinsically broad-spectrum antibacterial activity are selected to self-assembled unique dosage form for loading antibiotic drugs. As-obtained antibiotic-loaded dual corona vesicles achieve desirable treatment effect with reduced dosage of 50%, benefiting for reducing side effects of antibiotic resistance.

#### 1.4.1.3 Sepsis therapy

Sepsis is a disease derived from dysregulation of the host immune response to infection, threatening people's health seriously due to high morbidity and mortality.[41] Except for bacteria, ROS generation can also trigger multi-organ failure during sepsis, scavenging ROS as a significant target is able to prevent sepsis.[42] Many antibiotics and anti-inflammatory agents are employed to attenuate inflammation response. However, the concern problems, including rapid metabolism, high toxicity and poor bioavailability, still exist. In addition, poor targeting to infectious tissues severely handers therapeutic effect. It has been reported that microenvironments (IMEs) exhibit activated blood vessels, more bacterial enzymes, low pH. Enlightened by the features of IMEs, Wang's team designed bioresponsive nanoparticles to target IMEs for sepsis treatment.[43] Firstly, amphiphilic block copolymer (Biotin-PEG-b-PAE(-g-PEG-b-DSPE)-b-PEG-Biotin) with pH/enzyme responses was synthesized and self-assembled into nanoparticles. Secondly, the anti-inflammatory agent (2-[(amino-carbonyl) amino]-5-(4-fluorophenyl)-3-thiophenecarboxamide, TPCA-1) and antibiotic (ciprofloxacin, CIP) were encapsulated with aforementioned nanoparticles. Finally, intercellular adhesion molecule-1 (ICAM-1) antibody was used to coat on the surface of as-prepared nanoparticles for targeting infectious tissues. As-prepared multifunctional nanodrugs

can effectively treat the mouse sepsis.

Furthermore, Zhou's group designed antioxidant melatonin (Mel)-deliveried ROS-responsive nanoparticles for attenuating sepsis-caused liver injury.[44] Due to that Mel is well known as promising broad-spectrum antioxidant and free radical scavenger. Nevertheless, its narrow therapeutic window and low bioavailability severely restrict therapeutic effect. Therefore, diblock copolymers of poly (-propylene sulfide) (PPS) and poly (ethylene glycol) (PEG) were self-assembled delivery system (mPEG-b-PPS-NPs) to encapsulate Mel, which overcame poor pharmacokinetic properties. Importantly, the platform performed sustained and on-demand release merits. *In vivo* results demonstrated that Mel-loaded mPEG-b-PPS-NPs showed high efficiency in alleviating oxidative stress, and subsequent liver injury.

In summary, self-assembled nanoparticles not only perform biological responsiveness, but also are expected as cargoes to deliver antioxidants, antibiotics and anti-inflammatory agents, achieving targeted function and overcoming poor pharmacokinetic properties. Major mechanism of targeting property ascribes to the imbalance of assembly-disassembly between noncovalent interactions.

### 1.4.2 Atherosclerosis therapy

Atherosclerosis is regarded as a chronic inflammatory disease, threatening human's health, even causing death worldwide.[45] Oxidative stress induced by the elevated level of ROS is directly related to atherosclerosis pathogenesis. Because low density lipoproteins are oxidized, further trigger development of atherosclerotic lesions. Thence, an increasing number of antioxidants have been developed for reducing ROS generation, alleviating oxidative stress, further achieving the treatment of atherosclerosis. However, so many problems, including no targeting property, distribution, rapid metabolism, short retention time of antioxidants still exert, leading to afford unsatisfactory effects. Therefore, Hu's group has designed a broad-spectrum ROS-scavenging nanoparticles for atherosclerosis therapy. In this work, superoxide dismutase mimetic agent Tempol is covalently conjugated with a hydrogen-peroxide-eliminating compound of TPCD (phenylboronic acid pinacol ester onto a cyclic polysaccharide β-cyclodextrin). As-prepared TPCD is self-assembled to TPCD nanoparticles.[46] As-obtained nanoparticles are capable of scavenging multiple species of ROS, of effectively alleviating oxidative stress-induced relevant product, and of further preventing the atherosclerosis progression. Importantly, TPCD nanoparticles have the targeted characteristics of atherosclerotic plaque through i.v. administration, effectively improving efficiency of atherosclerosis therapy.

The activated platelets and water-fast fibrins as two blood factors can trigger thrombus, further atherosclerosis. Tirofiban as antiplatelet agents can effectively attenuate arterial thrombosis. Tissue plasminogen activators are famous for lysing thrombus and degrading fibrin. Nevertheless, their side effects and narrow therapeutic window of antiplatelet agents restrict clinical applications. With in-depth learning about ROS biology, ROS chemistry, and ROS nanotechnology, creative nanodrugs are developed. Dongwon Lee and colleagues design fibrin-targeted and $H_2O_2$-responsive FTIAN nanoparticles for atherosclerosis therapy.[47] Due to a burst of $H_2O_2$ generation during

activating platelet, boronate antioxidant polymer (BAP) with $H_2O_2$-responsive is used to scavenge $H_2O_2$ and convert HBA. Next, obtained HBA is used for antiplatelet and anti-inflammatory owing to Gastrodia elata. The fluorescent dye IR820 is conjugated with BAP to obtain fBAP. achieving noninvasive photoacoustic imaging about atherosclerotic plaque structure and composition. Then fBAP is assembled to FTIAN nanoparticles. This work provides a promising nanotheranostic agent with integration of diagnosis and treatment for the atherosclerosis therapy.
In summary, based on the knowledge of ROS biology, and chemistry, self-assembled nanoparticles possess $H_2O_2$-responsive property for targeting atherosclerosis therapy.

### 1.4.3 Neuroprotective disease therapy

Neurodegenerative diseases with increased morbidity and mortality, for example, Parkinson's disease (PD) and Alzheimer's disease (AD), have always been a medical challenge. Lots of researches have substantiated that excessive generation of ROS can exacerbate neurodegeneration. For example, higher than normal levels of ROS can cause dysregulation of intracellular $Ca^{2+}$ signaling, leading to more production of ROS for inducing an apoptotic cascade.[48] The pathogenesis is diversified that ROS are involved with neurodegenerative disorders. In AD, amyloid-β peptide (Aβ) acts as an important key to induce intracephalic oxidative stress. To address this difficulty, an increasing number of nanomedicines have been developed to inhibit Aβ aggregation. Qu's group select Aβ15-20 (Ac-QKLVFF-$NH_2$) as targeted amyloid specific sequence and poly oxometalates (POMs) Wells-Dawson-type phosphotungstate ($K_8[P_2CoW_{17}O_{61}]$) as Aβ aggregation inhibitors to prepare POM/peptide composites (POM@P) by straightforward self-assembly method.[49] As-made POM@P nanoparticles exhibit favorable advantages, including specific targeted-Aβ ability, enhanced inhibition efficiency and increased side effects of POM. This work has been spotlighted as a potential targeting agent for treating AD.
Moreover, it has been reported that a zinc-finger-like supramolecular complex is capable of targeting and binding 16-23 region of the Aβ peptide with α-helix form for preventing Aβ from aggregating. Therefore, Qu's group fabricate nanoparticles through self-assembling bioactive hexapeptide (Ac-QKLVFF-$NH_2$) extracted from Aβ and M-enantiomer (NiM) to prepare NiM@P nanoparticles. As-prepared NiM@P nanoparticles with well-defined spherical structures not only enhance the local density of peptide mass, but also improve targeting efficiency for inhibiting Aβ aggregation.[50]
In conclusion, the integration of ROS biology, ROS chemistry and ROS nanotechnology promote development of multifunctional nanomedicines for treating various diseases Especially, lots of biomolecules, such as peptide and DNA, are introduced to prepare well-defined supramolecular architectures with multifunctionality for treating different diseases under clear disease mechanism.

### 1.4.4 Cardiac repair

Myocardial infarction (MI) as one of cardiac diseases has high morbidity. Retained stem cells are threatened by oxidative stress damage induced by ROS, and are restricted to adhere to extracellular matrices of the heart tissue because of disrupted focal contacts,

causing low survival rate of implanted stem cells.[51]Moreover, implanted stem cells are unevenly distributed in MI area, resulting that the disrupted cell−cell communication is deteriorated. To solve this shortcoming, injectable hydrogel has been developed to deliver stem cells into MI area, and effectively enhance the retention time of stem cells.[52] To further overcome the triggered oxidant stress damage from ROS in MI area, an injectable hydrogel with favorable antioxidant activity has been reported by Yang team. The injectable hydrogel is employed as cargoes of stem cells for cardiac repair.[53] In this work, fullerenol/alginate hydrogel are prepared by ionic cross-linking method and can remove excessive ROS to fullerenol cage through transferring electrons. Importantly, it further mitigates JNK phosphorylation induced by $H_2O_2$ and activates the p38 MAPK signaling for achieve a protection mechanism. The experimental results substantiate that as-prepared fullerenol/alginate hydrogel not only prevents cell damage from ROS, but also enhance the survival and proliferative capacity of brown adipose derived stem cells, exhibiting potential therapeutic value for MI.

Owing to that peptides possess many favorable advantages of easy preparation and functionalization, clear metabolic pathway, low immunogenicity and excellent biocompatibility, self-assembled peptide hydrogels have drawn wide attention for huge potential.[54] Self-assembled peptide hydrogels exhibit many advantages, including shear thinning and recovery characteristics, stable β-sheet form, targeted modification.[55] Inspired by the above, A. Saiani and colleagues prepare FEFEFKFK hydrogels by assembly method (F: phenylalanine; E: glutamic acid; K: lysine). The FEFEFKFK peptides possess pH response, which benefits for forming mechanical properties of hydrogel similar to a range of human tissues. Additionally, cell-adhesion motif RGD (R: arginine; G: glycine; D: aspartic acid) is employed to functionalize the hydrogel for enhancing cell adhesion to the hydrogel scaffold. As-obtained RGDSP-functionalized FEFEFKFK hydrogel achieves retention and delivery of cardiac progenitor cells into the injured heart tissue.[56]

In short, in consideration of oxidative stress damage to stem cells and low retention of stem cells in the MI area, various self-assembled hydrogel agents that are similar to a range of human tissues and possess antioxidant activity, are gradually developed. Based on the needs of the cardiac repair, hydrogel agents achieve special treatment.

### 1.4.5 Contrast-induced nephropathy (CIN) therapy

The high dosage of iodinated contrast agents required in computed tomography (CT) angiography can induce excessive generation of ROS in kidneys, and further lead to iatrogenic renal failure. Therefore, it is of great significance to design novel CT contrast agents for avoiding iodine-induced nephrotoxicity. Du's team design renoprotective angiographic polymersomes (RAPs).[57] In present work, PEO45-b-P[(Lys-IBC)$_{45}$-stat-(Lys-PAPE)$_{15}$] are utilized to self-assemble polymersomes RAPs. Lys-PAPE segments play a major role in scavenging ROS, Lys-BIC repeat units are utilized for CT imaging. As-prepared RAPs not only increase renoprotection but also prolong angiographic live time, which provided a new strategy for overcoming the risk of CIN.

In a word, Excessive ROS can lead to different diseases, thence redox regulation by ROS-based nanomedicine has become a promising therapeutic strategy. More and more

researches have opened a new pathway for optimized therapeutic efficacies based on scavenging ROS-related nanotherapies.

### 1.4.6 Dynamic therapy

High ROS generation in cancer cells promotes cells to upregulate antioxidant for new redox homeostasis, which maintains cancer cells alive under the hypotoxicity ROS level. Thus, the destruction of the adaptively endogenous redox homeostasis can be as an attractive strategy to destroy cancer cells. ROS-mediated therapeutic methods, such as exogenous interventions of ROS-generating nanomaterials and antioxidant inhibitors, have made great progress in favorably therapeutic effect for treating cancer. In this section, ROS-generating nanomaterials are described, such as photosensitizers (PS), sonosensitizers, microwave sensitizers and nanozyme, which are employed for therapeutic intervention.

#### 1.4.6.1 Photodynamic therapy (PDT)

PDT as a noninvasive and lower side effect manner, has exhibited satisfactory therapeutic efficacy toward neoplastic diseases, such as skin, lung cancer, etc.[58] PDT efficiency is involved with the three necessary components, including light, PS and tissue oxygen. PS can absorb photon during light irradiation and convert into its excited singlet state ($S_1$). Then the PS need to return to its ground state ($S_0$) by transferring its energy into fluorescence or heat due to unstable and short-lived state. In addition, intersystem crossing can induce excited triplet state $T_1$, in which PS are capable of converting its energy into chemically reactive species and phosphorescence through two types of reactions. In a type I reaction, superoxide anion radicals are generated via oxygen reacts with reformed PS by reacting with an electron donating substrate. In a type II reaction, singlet oxygen ($^1O_2$) as highly ROS are processed by directly reacting with ground state oxygen $^3O_2$ (Figure 1.6). [59] The superoxide anion radicals and $^1O_2$ can lead to cytotoxicity for damaging cells by reacting directly with lipid, protein, nucleic acid and other biomolecules. $^1O_2$ reacts with cell membrane lipids, causing lipid peroxidation and further the destruction of cell membrane. Moreover, it can also react with amino acids to mediate apoptosis by impairing the function of important proteins. In contrast to surgery, chemotherapy and radiotherapy, PDT has several major advantages: firstly, PDT as a noninvasive treatment strategy can collectively exert targeted cytotoxicity toward nonmalignant and neoplastic diseases; secondly, Due to ROS damage to cells, PDT has a wide application prospect; thirdly, PDT has almost no resistance. Finally, PDT can be used alone or in combination with other treatments, including surgery, chemotherapy, radiotherapy, photothermal therapy and immunotherapy, achieving a highly efficient treatment effect.

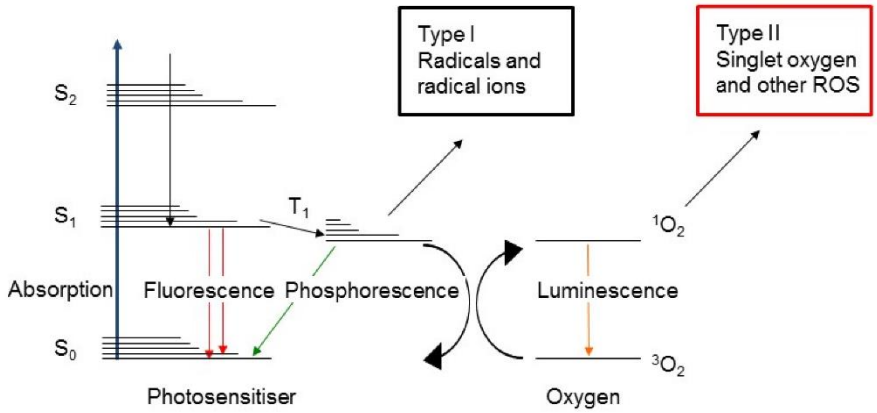


**Figure 1.6** Schematic representation of photosensitizer activation under laser irradiation.[59]

PS play a significant role in therapeutic effect. PS have been optimized for three generations. From poor tissue selectivity and low light absorption of first generation PS to third generation PS modified with biologic conjugates, enhances their physical, chemical and therapeutic properties. However, frequently-used PS have many disadvantages, such as poor water solubility and low bioavailability, which severely limit bioappliction and clinical research. Especially, aggregation derived from poor water solubility, seriously inhibits ROS generation and further reduces PDT efficiency.[60] To address these problems, many materials are employed as carries to encapsulate PS, including inorganic nanomaterials, polymer, liposome, hydrogel and etc.[61-63] Nevertheless, the new problems will also arise, for example, low loading efficiency, easy leak, systemic toxicity, extra inflammatory and immune response derived from the synthetic components. These problems seriously hinder clinical benefits of PDT. The development of self/co-assembled nanotechnology effectively improves loading rate of PS and therapeutic effect. Yan' group design a simple peptide-tuned nanodrugs via self-assembly for PDT against cancer.[21] In this work, Chlorin e6 (Ce6) as hydrophobic PS, Cationic diphenylalanine (CDP) and 9-Fluorenylmethoxycarbonyl-l-lysine (Fmoc-l-Lys) as amphiphilic peptides are co-assembled via hydrophobic and π–π interactions, due to that pyrrole groups of Ce6 interacted with the aromatic residues derived from CDP and Fmoc groups derived from Fmoc-l-Lys (Figure 1.7a). As-prepared FCNPs and CCNPs possess high drug-loading efficiency and low cytotoxicity that ascribes to PS and peptides as direct building blocks. *In vivo* results demonstrate that fabricated nanoparticles are easily swallowed by tumor cells, and further inhibit tumor cells (Figure 1.7b). This study provides a potential strategy that peptide-regulated nanodrugs through self-assembly method.

Next, Yan's group designs spherical metallo-nano-drugs for PDT. In this work, fluorenylmethoxycarbonyl-L-histidine (Fmoc-H) and N-benzyloxycarbonyl-L-histidine-L-phenylalanine (Z-HF) as metal-binding building blocks are selected to assemble with PS and metal ions via strong coordination interactions. As-obtained nanoparticles are employed for PDT, achieving high efficiency against tumor cells.

These assembled nanodrugs exhibit many advantages, such as robust integration for

long blood circulation, targeted burst release, simple and readily manufacturing process, increased encapsulation efficiencies. Especially, the assembly approaches are susceptible to environmental variations because of the dynamic flexibility, such as pH, resulting in targeted release in tumor site. It provides a new strategy to fabricate smart nanomedicines for effectively improve therapeutic effects (Figure 1.7c).

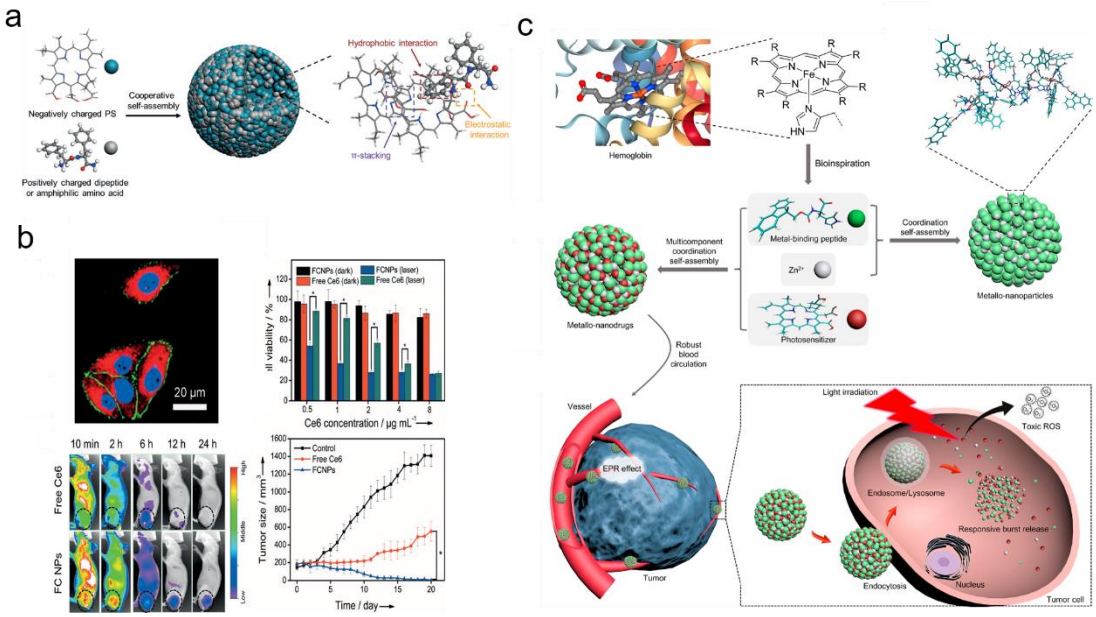


**Figure 1.7** (a) Preparation process of photosensitizer drugs.[21] (b) Fluorescent images of cell internalization *in vitro* and tumor-bearing nude mice *in viv*o treated by the assembled NPs. The evaluation of FCNPs cytotoxicity compared with free Ce6 with or without irradiation. The survival curve of animal experiment. (c) Schematic illustration that from preparation process of supramolecular metallo-nanodrugs to antitumor PDT *in vivo*.[60]

It is well known that immunotherapy as one of the anti-tumor methods is capable of detecting and eliminating tumor cells through autogenic immune system. However, primary tumors are hard to eradicate by the immune system. PDT can supply a robust ROS generation for remarkably enhancing therapeutic efficacy. Therefore, the integration of immunotherapy and PDT as a synergistic therapy method is possible for against malignant cancers. It has been reported that antigen proteins Ovalbumin (OVA) and indocyanine green (ICG) as PS are assembled to OVA-ICG nanovaccines. Assembled OVA-ICG nanovaccines with high biocompatibility and loading efficiency were able to generate robust ROS and track dendritic cells for synergistic therapy of PDT and immunotherapy.[63] The directedly synthesis strategy for more multifunctional nanovaccines or nanomedicine creates possibilities in various therapeutic method.

### 1.4.6.2 Sonodynamic therapy (SDT)

SDT efficacy depends on ultrasound, sonosensitizers and tissue oxygen, and has the same mechanism with PDT.[64] Importantly, SDT overcomes the limitation of penetration depth.[65] Therefore, SDT is worthy of regarding as a promising treatment

for tumor therapy. The targeted-nuclear sonosensitizer is designed by Zhang's group. A model cell-penetrating peptide TAT is coupled with fluorescence dyes IR780 (TAT-IR780), and Nrf2-siRNA is encapsulated for fabricating TIR@siRNA, exhibiting augmented-gene targeted-nuclear SDT for treating colorectal cancer.[66] The results demonstrate that TIR@siRNA as SDT agent can effectively treat colorectal cancer. Moreover, boosted DPPA-1 peptide is brought for anti-PD-L1 therapy, and combined with SDT to achieve a synergistic therapy of immunotherapy and SDT. *In vivo* results exhibit that the strategy effectively eradicates the primary CT26 tumor and suppresses the tumor metastases.

In addition, to improve therapeutic effect, chemotherapy is combined with SDT for tumor therapy. Hydrophobic organic dye Ce6, hydrophilic organic dye IR783 and broad spectral chemical drug Paclitaxel are used to fabricate nanoscale sonosensitizers (Ce6-PTX@IR783), which is reported by Chen's team.[67] Ce6 exerted a sonodynamic effect, PTX performed a chemotherapeutic effect and IR783 as cancer diagnosis are constructed nanoparticles by the hydrophilic–hydrophobic self-assembly strategy, avoiding introduced system toxicity of extra nanomaterials and improving therapeutic biosafety. This designed all-in-one nanosystem improve utilization efficacy of hydrophobic drugs, simplified preparation process. Importantly, results demonstrate tumor diagnosis and synergistic therapy of SDT and chemotherapy, even further exhibit potential clinical translation.

#### 1.4.6.3 Microwave dynamic therapy (MDT)

As an electromagnetic spectrum, microwave (MW) performs many fulfilling advantages, including deep penetration depth, negligible side effects, highly efficient MW-to-heat energy conversion.[68] It has received increasing attention for effectively ablating tumors. The generation mechanism ROS in MDT is similar to PDT and SDT, which depends on MW, microwave sensitizers and tissue oxygen. Meng's group has reported that supernanoparticles as microwave sensitizers can generate ROS under MW irradiation, further applicate for tumor therapy.[69] In this work, the supernanoparticles containing liquid metal with eutectic gallium−indium alloy are prepared as microwave sensitizers. During MDT, the generation of OH and·$O_2$ derived from the electron transfer from Ga to oxygen and water under MW irradiation. It is first reported that the microwave dynamic effect is applied for tumor therapy.

#### 1.4.6.4 Radiation therapy (RT)

RT as one of therapeutic modalities against tumor in the clinic, has advantages of high-intensity ionizing radiation and no penetration depth obstruction.[70] RT can tremendously suppress tumor proliferation through cell apoptosis induced by considerable ROS generation after the ionizing surrounding water.[71] X-ray with high energy is the most commonly used in clinical RT. However, therapeutic effect of X-ray is restricted owing to low energy absorption coefficient at tumor tissue. Moreover, the high-energy X-ray radiation also induces serious damage for normal tissue. To address these shortcomings, RT-based nanomedicines are reported for improved therapeutic efficacy. Reported CuS and $Bi_2S_3$ nanorods, Au nanoparticles, nanomaterials based on

carbon are used as radiosensitizers to enhance ionizing radiation energy for inhibiting tumors with lower RT dose. Zhao's group reports $WO_{2.9}$-$WSe_2$-PEG NPs (WSP NPs) to effectively suppress local and metastatic tumors.[72] WSP NPs as radiosensitizers have X-ray irradiation response because of high Z element. Additionally, WSP NPs can strongly absorbing the near-infrared spectrum for high photothermal conversion efficacy, which is used for photothermal therapy (PTT). In addition to this, based on tumor cells sensitized by PTT and RT, checkpoint blockade immunotherapy (CBT) is further employed. As a result, WSP NPs have performed huge potential of multifunctional nanosystem for eliminating primary and distance tumors via triple-synergistic therapy of RT/PTT/CBT.

Additionally, Kai Yang and his colleagues design polyoxomolybdate nanoclusters (POMo NCs) as remarkable radiosensitizers, resulting augmented X-ray for RT.[73] Next, POMo@CS–RB are prepared by chitosan (CS) loading POMo NCs and rose Bengal (RB). The scintillating properties from POMo NCs under X-ray irradiation facilitate transduced energy to stimulate RB to generate cytotoxic $_1O^2$, causing the damage of DNA and further cell apoptosis. Finally, to improve biocompatible, polyethylene glycol (PEG) was used to modify POMo@CS–RB to obtain PEGylated POM@CS–RB. Importantly, this study provides a favorable method to eliminate tumor cells with low dose X-ray, deserves further consideration for clinical cancer treatment.

### 1.4.6.5 Chemodynamic therapy (CDT)

CDT was termed as Fenton reaction from locally activated tumor microenvironment (TME) for cancer therapy in 2016. In contrast to PDT, SDT, RT under exogenous physical irradiations for treating cancer, CDT just takes advantage of endogenously elevated $H_2O_2$ to convert ROS generation in TME.[74] CDT displays many advantages, such as no damage to normal tissues and no limit of penetration depth compared with PDT, SDT, RT.[75] Thus, CDT is regarded as an ideal therapeutic method due to its high therapeutic efficiency and tumor selectivity. There have been reported that designed CDT-based nanoparticles were applied for cancer treatment, such as $FePS_3$, $Fe_3O_4$, $FeS_2$. Nevertheless, $Fe^{II}$ is unstable and easily converts into $Fe^{III}$, hindering the therapeutic effect of the CDT during the Fenton reaction. To address this shortcoming, $Fe^{II}$ and natural epigallocatechin gallate (EGCG) are co-assembled to metal-polyphenolic nanoparticles (FeEP-NPs) in precentce of poly(vinylpyrrolidone) (PVP).[76] Notably, $Fe^{II}$ can coordinate with EGCG, resulting stronger light absorption to photothermal therapy (PTT) with high photothermal conversion. It facilitates therapeutic efficiency of CDT due to positively correlating with temperature of the tumor area. The introduced EGCG further inhibits heat shock proteins during PTT. FeEP-NPs employ an all-in-one strategy for treating tumor through photoacoustic imaging-guided mild PTT-augmented CDT.

Moreover, elevated $H_2O_2$ in TME compared with normal tissues is still insufficient for burst generation of ROS, and is impossible to effectively eradicate tumor cells via CDT.[77] To solve this problem, it has been reported that β-lapachone (β-Lap) is further used to generate extra $H_2O_2$ by β-Lap cyclic reaction. It was reported that Banoxantrone dihydrochloride (AQ4N) organic ligands and 1,4,5,8-tetrahydroxyanthraquinone (THQ)

were assembled in the presence of $Cu^{2+}$ as nodes to prepare Cu-THQ/AQ4N.[78] β-Lap was loaded into Cu-THQ/AQ4N to fabricate Cu–OCNP/Lap. After uptake of Cu-THQ/AQ4N by tumor cells, $Cu^{2+}$ was reduced to $Cu^{+}$ by excessive glutathione in tumor cells, causing Cu–OCNP/Lap degraded. Released $Cu^{+}$ and β-Lap further triggered intracellular cyclic reaction to generate higher levels of $H_2O_2$, which benefited for enhancing CDT efficacy. Additionally, Cu–OCNP/Lap had high photothermal conversion efficiency for increased temperature of tumor location, amplifying CDT efficacy again. This work supported new insight to optimally amplify CDT efficacy.
In the section, various cancer therapeutic modalities of PDT, SDT, MDT, RT and CDT were discussed, they have common characteristic of large quantities of ROS generation for eliminating tumor cells. Virous ROS-upregulating nanomedicines are developed for antineoplastic therapy based on advanced progress of ROS science.

### 1.5. Research contents

The physiological actions and features of ROS at the lesion site have been deemed as a therapeutic target. Increasing number of special nanomaterials as nanomedicines for dealing with different diseases. Notedly, thanks to all-in-one development of ROS biology, ROS chemistry and ROS nanotechnology, ROS-regulating nanomaterials have made greater medical advances. However, many intractable problems need to be overcame, which are worth to ameliorate for leap-forward development of ROS-related therapeutics. In this work, the areas we strive to improve are as follows:

(1) Many small-molecule bioactive compounds, such as flavonoid and curcumin, have drawn wide attention for antioxidant and anti-inflammatory effects for disease treatment. However, their bioapplication and clinical translation are restricted owing to low bioavailability and poor water solubility. Additionally, peptides and proteins derived from biological systems should be strived to develop, such as antioxidative and immune proteins, peptides and enzymes. Nevertheless, peptides and proteins easily suffer from enzyme hydrolysis, causing low bioavailability. Nowadays, to solve these problems, different nanocarriers are developed, including polymer, liposome and inorganic nanomaterials. But there are still new problems arising, for example, induced systemic toxicity, low loading efficiency, immunoreaction and other drawbacks seriously, which limit clinical applications. Based on this problem, myricetin (Myr) as one of small-molecule bioactive compounds and glutathione (GSH) as a cellular antioxidant are chose. To overcome the disadvantages of Myr and GSH, we chose $Zn^{2+}$to effectively bond Myr and GSH via coordination interaction to prepare MZG nanoparticles, which are employed for cellular antioxidant (In chapter 2).

(2) Because of high convenience, low cost, and simple preservation process, oral delivery is the most preferred strategy compared with other drug administration Nevertheless, there are harsh pH/enzymatic conditions in the gastrointestinal tract, leading to rapid enzymatic degradation and lower delivery efficiency of the bioactive substances. Especially, if peptide antioxidants are taken for oral delivery, their efficacy has been hampered by the harsh conditions in inflamed colon. To address this problem, covalent-assembly strategy is employed for preparing

nanodrugs. In chapter3, antioxidative peptide casein phosphopeptide (CPP) and iridoid Genipin as building blocks are selected to covalently-assemble robust GCPP nanoparticles via covalent interactions, and further apply for inflammatory bowel disease (In chapter 3).

(3) PDT as a noninvasive and lower side effect manner, has exhibited satisfactory therapeutic efficacy toward neoplastic diseases, such as skin, lung cancer. Importantly, PS play a significant role in therapeutic effect. However, frequently-used PS have many disadvantages, such as poor water solubility and low bioavailability, which severely limit therapeutic effect of PDT. To solve this shortcoming, proteins with muti-functional and structure are applied as hydrophobic drug delivery. In chapter 4, ovalbumin as a drug carry is chose to assemble with photosensitive drug pheophorbide a at the presence of $Zn^{2+}$. As prepared nanodrugs are further use for PDT *in vitro* and *in vivo,* which can selectively accumulate at tumor site, exhibiting the potential for further diagnosis and treatment *in vivo* (In chapter 4).

(4) Due to the fact that the drug carriers still exist many problems, including manufacturing cost, low loading efficiency and systemic toxicity, thus assembly nanotechnology has received wide attention because of the self-assembly phenomenon derived from natural phenomena. Nowadays, assembly nanotechnology has gradually developed for achieving good therapeutic effect. Firstly, assembly nanotechnology is simple manufacturing process. Secondly, assembly nanotechnology possesses multiple noncovalent coordination and noncovalent interactions for fabricating nanomedicines, achieving robust construct for long blood circulation and susceptible response to environmental variations for targeted burst release. Thirdly, assembly nanotechnology possesses high encapsulation efficiency that is ascribe to directly assemble building blocks. In chapter 2, 3 and 4, nanodrugs are prepared by assembly nanotechnology. (In chapter 2, 3 ,4).

In this work, with the advance of science and technology, we design coordination-assembled and covalent-assembled peptide and protein nanomedicine for antioxidant, anti-inflammatory and anti-tumor therapy.

## 1.6 References


1. Palmer, R., Nitric oxide release account for the biological activity of endothelium-derived relaxing factor. *Nature* **1987,** *327*.

2. Sen, S.; Chakraborty, R., The Role of Antioxidants in Human Health. *Acs Symposium* **2011,** *1083*, 1-37.

3. Zou, S.; Guo, F.; Wu, L.; Ju, H.; Sun, M.; Cai, R.; Xu, L.; Gong, Y.; Gong, A.; Zhang, M.; Du, F., One-pot synthesis of cerium and praseodymium co-doped carbon quantum dots as enhanced antioxidant for hydroxyl radical scavenging. *Nanotechnology* **2020,** *31*, 165101.

4. Mao, X.; Gu, C.; Chen, D.; Yu, B.; He, J., Oxidative stress-induced diseases and tea polyphenols. *Oncotarget* **2017,** *8*, 81649-81661.

5. Yang, B.; Chen, Y.; Shi, J., Reactive Oxygen Species (ROS)-Based Nanomedicine. *Chem. Rev.*

**2019,** *119*, 4881-4985.
6. Whitesides, G. M.; Grzybowski, B., Self-assembly at all scales. *Science* **2002,** *295*, 2418-21.
7. Zhao, L.; Zou, Q.; Yan, X., Self-Assembling Peptide-Based Nanoarchitectonics. *Bull. Chem. Soc. Jpn.* **2019,** *92*, 70-79.
8. Murphy, M. P., How mitochondria produce reactive oxygen species. *Biochem. J.* **2009,** *417*, 1-13.
9. Gross, E.; Sevier, C. S.; Heldman, N.; Vitu, E.; Fass, D., Generating disulfides enzymatically: Reaction products and electron acceptors of the endoplasmic reticulum thiol oxidase ERO1P. *PNAS* **2006,** *103*, 299-304.
10. Lambeth; David, J., NOX enzymes and the biology of reactive oxygen. *Nat. Rev. Immunol.* **2004,** *4*, 181-189.
11. Winterbourn, C. C., Reconciling the chemistry and biology of reactive oxygen species. *Nat. Chem. Biol.* **2008,** *4*, 278-286.
12. Dickinson, B. C.; Chang, C. J., Chemistry and biology of reactive oxygen species in signaling or stress responses. *Nat. Chem. Biol.* **2011,** *7*, 504-11.
13. Nosaka, Y.; Nosaka, A. Y., Generation and Detection of Reactive Oxygen Species in Photocatalysis. *Chem. Rev.* **2017,** *117*, 11302-11336.
14. Gianni, D.; Taulet, N.; DerMardirossian, C.; Bokoch, G. M., c-Src–Mediated Phosphorylation of NoxA1 and Tks4 Induces the Reactive Oxygen Species (ROS)–Dependent Formation of Functional Invadopodia in Human Colon Cancer Cells. *Mol. Biol. Cell.* **2010,** *21* , 4287-4298.
15. Dickinson, B. C.; Peltier, J.; Stone, D.; Schaffer, D. V.; Chang, C. J., Nox2 redox signaling maintains essential cell populations in the brain. *Nat. Chem. Biol.* **2011,** *7*, 106-112.
16. Ishikawa, K.; Takenaga, K.; Akimoto, M.; Koshikawa, N.; Yamaguchi, A.; Imanishi, H.; Nakada, K.; Honma, Y.; Hayashi, J. I., ROS-Generating Mitochondrial DNA Mutations Can Regulate Tumor Cell Metastasis. *Science* **2008,** *320*, 661-664.
17. Fujishima, A.; Honda, K., Electrochemical Photolysis of Water at a Semiconductor Electrode. *Nature* **1972,** *238*, 37-38.
18. Li, J.; Xing, R.; Bai, S.; Yan, X., Recent advances of self-assembling peptide-based hydrogels for biomedical applications. *Soft Matter* **2019,** *15*, 1704-1715.
19. Quinn, J. R.; Zimmerman, S. C.; Bene, J.; Shavitt, I., Does the A.T or G.C base-pair possess enhanced stability? Quantifying the effects of CH...O interactions and secondary interactions on base-pair stability using a phenomenological analysis and ab initio calculations. *J. Am. Chem. Soc.* **2007,** *129*, 934-941.
20. Ma, X.; Xing, R.; Yuan, C.; Ogino, K.; Yan, X., Tumor therapy based on self-assembling peptides nanotechnology. *VIEW* **2020,** *1*, 20200020.
21. Liu, K.; Xing, R.; Zou, Q.; Ma, G.; Mohwald, H.; Yan, X., Simple Peptide-Tuned Self-Assembly of Photosensitizers towards Anticancer Photodynamic Therapy. *Angew. Chem. Int. Ed. Engl.* **2016,** *55*, 3036-9.
22. Sun, H.; Chang, R.; Zou, Q.; Xing, R.; Qi, W.; Yan, X., Supramolecular Protein Nanodrugs with Coordination- and Heating-Enhanced Photothermal Effects for Antitumor Therapy. *Small* **2019,** *15*, 1905326.
23. Qing, S.; Lyu, C.; Zhu, L.; Pan, C.; Wang, S.; Li, F.; Wang, J.; Yue, H.; Gao, X.; Jia, R.; Wei, W.; Ma, G., Biomineralized Bacterial Outer Membrane Vesicles Potentiate Safe and Efficient Tumor Microenvironment Reprogramming for Anticancer Therapy. *Adv. Mater.* **2020,** *32*, 2002085.
24. Meyer, E. A.; Castellano, R. K.; Diederich, F., Interactions with Aromatic Rings in Chemical

and Biological Recognition. *Angew. Chem. Int. Ed. Engl.* **2003,** *42*, 1210-1250.
25. De, S.; Mahata, K.; Schmittel, M., Metal-coordination-driven dynamic heteroleptic architectures. *Chem. Soc. Rev.* **2010,** *39*, 1555-1575.
26. Zou, Q.; Abbas, M.; Zhao, L.; Li, S.; Shen, G.; Yan, X., Biological Photothermal Nanodots Based on Self-Assembly of Peptide-Porphyrin Conjugates for Antitumor Therapy. *J. Am Chem. Soc.* **2017,** *139*, 1921-1927.
27. Zhang, H.; Liu, K.; Li, S.; Xin, X.; Yuan, S.; Ma, G.; Yan, X., Self-Assembled Minimalist Multifunctional Theranostic Nanoplatform for Magnetic Resonance Imaging-Guided Tumor Photodynamic Therapy. *ACS Nano* **2018,** *12*, 8266-8276.
28. Zhang, J.; Fu, Y.; Yang, P.; Liu, X.; Li, Y.; Gu, Z., ROS Scavenging Biopolymers for Anti-Inflammatory Diseases: Classification and Formulation. *Adv. Mater. Interfaces* **2020,** 7, 2000632.
29. Semwal, D. K.; Semwal, R. B.; Combrinck, S.; Viljoen, A., Myricetin: A Dietary Molecule with Diverse Biological Activities. *Nutrients* **2016,** *8*, 90.
30. Chung, C. H.; Jung, W.; Keum, H.; Kim, T. W.; Jon, S., Nanoparticles Derived from the Natural Antioxidant Rosmarinic Acid Ameliorate Acute Inflammatory Bowel Disease. *ACS Nano* **2020,** *14*, 6887-6896.
31. Hoivik, M. L.; Moum, B.; Solberg, I. C.; Cvancarova, M.; Hoie, O.; Vatn, M. H.; Bernklev, T.; Group, f. t. I. S., Health-related quality of life in patients with ulcerative colitis after a 10-year disease course: Results from the IBSEN study. *Inflamm. Bowel Dis.* **2012,** *18*, 1540-1549.
32. Zhao, S.; Li, Y.; Liu, Q.; Li, S.; Cheng, Y.; Cheng, C.; Sun, Z.; Du, Y.; Butch, C. J.; Wei, H., An Orally Administered CeO2@Montmorillonite Nanozyme Targets Inflammation for Inflammatory Bowel Disease Therapy. *Adv. Funct. Mater.* **2020,** *30*, 2004692.
33. Le, Z.; He, Z.; Liu, H.; Liu, L.; Liu, Z.; Chen, Y., Antioxidant Enzymes Sequestered within Lipid-Polymer Hybrid Nanoparticles for the Local Treatment of Inflammatory Bowel Disease. *ACS Appl. Mater. Interfaces* **2021,** *13*, 55966-55977.
34. Xue, F.; Wang, Y.; Zhang, Q.; Han, S.; Zhang, F.; Jin, T.; Li, C.; Hu, H.; Zhang, J., Self-assembly of affinity-controlled nanoparticles via host-guest interactions for drug delivery. *Nanoscale* **2018,** *10*, 12364-12377.
35. Hoffmann, T. W.; Pham, H.-P.; Bridonneau, C.; Aubry, C.; Lamas, B.; Martin-Gallausiaux, C.; Moroldo, M.; Rainteau, D.; Lapaque, N.; Six, A.; Richard, M. L.; Fargier, E.; Le Guern, M.-E.; Langella, P.; Sokol, H., Microorganisms linked to inflammatory bowel disease-associated dysbiosis differentially impact host physiology in gnotobiotic mice. *The ISME Journal* **2016,** *10*, 460-477.
36. Schwach-Abdellaoui, K.; Vivien-Castioni, N.; Gurny, R., Local delivery of antimicrobial agents for the treatment of periodontal diseases. *Eur. J. Pharm. Biopharm.* **2000,** *50*, 83-99.
37. Yang, Z.; He, S.; Wu, H.; Yin, T.; Wang, L.; Shan, A., Nanostructured Antimicrobial Peptides: Crucial Steps of Overcoming the Bottleneck for Clinics. *Front. Microbiol.* **2021,** 12, 710199.
38.Dumitrescu, A., *Antibiotics and Antiseptics in Periodontal Therapy*. **2011**, 1-288.
39. Koch, F.; Ekat, K.; Kilian, D.; Hettich, T.; Germershaus, O.; Lang, H.; Peters, K.; Kreikemeyer, B., A Versatile Biocompatible Antibiotic Delivery System Based on Self-Assembling Peptides with Antimicrobial and Regenerative Potential. *Adv Healthc. Mater.* **2019,** *8*, 1900167.
40. Xi, Y.; Wang, Y.; Gao, J.; Xiao, Y.; Du, J., Dual Corona Vesicles with Intrinsic Antibacterial and Enhanced Antibiotic Delivery Capabilities for Effective Treatment of Biofilm-Induced Periodontitis. *ACS Nano* **2019,** *13*, 13645-13657.
41. Singer, M.; Deutschman, C. S.; Seymour, C. W.; Shankar-Hari, M.; Annane, D.; Bauer, M.;

Bellomo, R.; Bernard, G. R.; Chiche, J.-D.; Coopersmith, C. M.; Hotchkiss, R. S.; Levy, M. M.; Marshall, J. C.; Martin, G. S.; Opal, S. M.; Rubenfeld, G. D.; van der Poll, T.; Vincent, J.-L.; Angus, D. C., The Third International Consensus Definitions for Sepsis and Septic Shock (Sepsis-3). *JAMA* **2016,** *315*, 801-810.

42. Andrades, M. É.; Morina, A.; Spasić, S.; Spasojević, I., Bench-to-bedside review: Sepsis - from the redox point of view. *Crit. Care* **2011,** *15*, 230.

43. Zhang, C. Y.; Gao, J.; Wang, Z., Bioresponsive Nanoparticles Targeted to Infectious Microenvironments for Sepsis Management. *Adv. Mater.* **2018,** *30*, 1803618.

44. Chen, G.; Deng, H.; Song, X.; Lu, M.; Zhao, L.; Xia, S.; You, G.; Zhao, J.; Zhang, Y.; Dong, A.; Zhou, H., Reactive oxygen species-responsive polymeric nanoparticles for alleviating sepsis-induced acute liver injury in mice. *Biomaterials* **2017,** *144*, 30-41.

45. Libby, P.; Bornfeldt, K. E.; Tall, A. R., Atherosclerosis Successes, Surprises, and Future Challenges. *Circ. Res.* **2016,** *118*, 531.

46. Wang, Y.; Li, L.; Zhao, W.; Dou, Y.; An, H.; Tao, H.; Xu, X.; Jia, Y.; Lu, S.; Zhang, J.; Hu, H., Targeted Therapy of Atherosclerosis by a Broad-Spectrum Reactive Oxygen Species Scavenging Nanoparticle with Intrinsic Anti-inflammatory Activity. *ACS Nano* **2018,** *12*, 8943-8960.

47. Kang, C.; Gwon, S.; Song, C.; Kang, P. M.; Park, S. C.; Jeon, J.; Hwang, D. W.; Lee, D., Fibrin-Targeted and H2O2-Responsive Nanoparticles as a Theranostics for Thrombosed Vessels. *ACS Nano* **2017,** *11*, 6194-6203.

48. LaFerla, F. M., Calcium dyshomeostasis and intracellular signalling in alzheimer's disease. *Nat Rev. Neurosci.* **2002,** *3*, 862-872.

49. Li, M.; Xu, C.; Wu, L.; Ren, J.; Wang, E.; Qu, X., Self-assembled peptide-polyoxometalate hybrid nanospheres: two in one enhances targeted inhibition of amyloid beta-peptide aggregation associated with Alzheimer's disease. *Small* **2013,** *9*, 3455-61.

50. Li, M.; Zhao, C.; Ren, J.; Qu, X., Chiral Metallo-Supramolecular Complex Directed Enantioselective Self-Assembly of beta-Sheet Breaker Peptide for Amyloid Inhibition. *Small* **2015,** *11*, 4651-5.

51. Gailit, J.; Colflesh, D.; Rabiner, I.; Simone, J.; Goligorsky, M. S., Redistribution and dysfunction of integrins in cultured renal epithelial cells exposed to oxidative stress. *Am.J. physiol.* **1993,** *264*, 149-57.

52. Russo, V.; Young, S.; Hamilton, A.; Amsden, B. G.; Flynn, L. E., Mesenchymal stem cell delivery strategies to promote cardiac regeneration following ischemic injury. *Biomaterials* **2014,** *35*, 3956-3974.

53. Hao, T.; Li, J.; Yao, F.; Dong, D.; Wang, Y.; Yang, B.; Wang, C., Injectable Fullerenol/Alginate Hydrogel for Suppression of Oxidative Stress Damage in Brown Adipose-Derived Stem Cells and Cardiac Repair. *ACS Nano* **2017,** *11*, 5474-5488.

54. Markey, A.; Workman, V. L.; Bruce, I. A.; Woolford, T. J.; Derby, B.; Miller, A. F.; Cartmell, S. H.; Saiani, A., Peptide hydrogel in vitro non-inflammatory potential. *J. Pept. Sci.* **2017,** *23*, 148-154.

55. Wychowaniec, J.; Smith, A.; Ligorio, C.; Mykhaylyk, O. O.; Saiani, A., Role of Sheet-Edge Interactions in Beta-sheet Self-Assembling Peptide Hydrogels – Supporting Information. *Biomacromolecules* **2020,** *21*, 2285-2297.

56. Burgess, K. A.; Frati, C.; Meade, K.; Gao, J.; Castillo Diaz, L.; Madeddu, D.; Graiani, G.; Cavalli, S.; Miller, A. F.; Oceandy, D.; Quaini, F.; Saiani, A., Functionalised peptide hydrogel for

the delivery of cardiac progenitor cells. *Mater. Sci. Eng. C Mater. Biol. Appl.* **2021,** *119*, 111539.
57. Liu, D.; Cornel, E. J.; Du, J., Renoprotective Angiographic Polymersomes. *Adv. Funct. Mater.* **2021,** *31*, 2007330.
58. Moore, C. M.; Pendse, D.; Emberton, M., Photodynamic therapy for prostate cancer--a review of current status and future promise. *Nat. Clin. Pract. Urol.* **2009,** *6*, 18-30.
59. Van Straten, D.; Mashayekhi, V.; De Bruijn, H. S.; Oliveira, S.; Robinson, D. J., Oncologic Photodynamic Therapy: Basic Principles, Current Clinical Status and Future Directions. *Cancers* **2017,** *9* , 19.
60. Li, S.; Zou, Q.; Li, Y.; Yuan, C.; Xing, R.;Yan, X., Smart Peptide-Based Supramolecular Photodynamic Metallo-Nanodrugs Designed by Multicomponent Coordination Self-Assembly. J.Am.Chem.Soc. 2018, 140 , 10794-10802.
61. Zhao, H.; Xu, J.; Li, Y.; Guan, X.; Han, X.; Xu, Y.; Zhou, H.; Peng, R.; Wang, J.; Liu, Z., Nanoscale Coordination Polymer Based Nanovaccine for Tumor Immunotherapy. *ACS Nano* **2019,** *13* , 13127-13135.
62. Zhang, L.; Wu, S.; Qin, Y.; Fan, F.; Zhang, Z.; Huang, C.; Ji, W.; Lu, L.; Wang, C.; Sun, H.; Leng, X.; Kong, D.; Zhu, D., Targeted Codelivery of an Antigen and Dual Agonists by Hybrid Nanoparticles for Enhanced Cancer Immunotherapy. *Nano Lett.***2019,** *19*, 4237-4249.
63. Pan, J.; Wang, Y.; Zhang, C.; Wang, X.; Wang, H.; Wang, J.; Yuan, Y.; Wang, X.; Zhang, X.; Yu, C.; Sun, S.-K.; Yan, X.-P., Antigen-Directed Fabrication of a Multifunctional Nanovaccine with Ultrahigh Antigen Loading Efficiency for Tumor Photothermal-Immunotherapy. *Adv. Mater.* **2018,** *30*, 1704408.
64. Costley, D.; Ewan, C. M.; Fowley, C.; Mchale, A. P.; Atchison, J.; Nomikou, N.; Callan, J. F., Treating cancer with sonodynamic therapy: A review. *Int J Hyperthermia* **2015,** *31*, 107-117.
65. Zhang, Y.; Khan, A. R.; Yang, X.; Shi, Y.; Zhao, X.; Zhai, G., A sonosensitiser-based polymeric nanoplatform for chemo-sonodynamic combination therapy of lung cancer. *J. Nanobiotechnology* **2021,** *19*, 57.
66. Wan, G.; Chen, X.; Wang, H.; Hou, S.; Wang, Q.; Cheng, Y.; Chen, Q.; Lv, Y.; Chen, H.; Zhang, Q., Gene augmented nuclear-targeting sonodynamic therapy via Nrf2 pathway-based redox balance adjustment boosts peptide-based anti-PD-L1 therapy on colorectal cancer. *J Nanobiotechnology* **2021,** *19*, 347.
67. Dong, C.; Jiang, Q.; Qian, X.; Wu, W.; Wang, W.; Yu, L.; Chen, Y., A self-assembled carrier-free nanosonosensitizer for photoacoustic imaging-guided synergistic chemo-sonodynamic cancer therapy. *Nanoscale* **2020,** *12*, 5587-5600.
68. Long, D.; Liu, T.; Tan, L.; Shi, H.; Liang, P.; Tang, S.; Wu, Q.; Yu, J.; Dou, J.; Meng, X., Multisynergistic Platform for Tumor Therapy by Mild Microwave Irradiation-Activated Chemotherapy and Enhanced Ablation. *ACS Nano* **2016,** *10*, 9516-9528.
69. Wu, Q.; Xia, N.; Long, D.; Tan, L.; Rao, W.; Yu, J.; Fu, C.; Ren, X.; Li, H.; Gou, L.; Liang, P.; Ren, J.; Li, L.; Meng, X., Dual-Functional Supernanoparticles with Microwave Dynamic Therapy and Microwave Thermal Therapy. *Nano Lett.* **2019,** *19*, 5277-5286.
70. Mao, F.; Wen, L.; Sun, C.; Zhang, S.; Wang, G.; Zeng, J.; Wang, Y.; Ma, J.; Gao, M.; Li, Z., Ultrasmall Biocompatible $B_{i2}Se_3$ Nanodots for Multimodal Imaging-Guided Synergistic Radiophotothermal Therapy against Cancer. *ACS Nano* **2016**, 11145-11155.
71. Song, G.; Liang, C.; Yi, X.; Zhao, Q.; Cheng, L.; Yang, K.; Liu, Z., Perfluorocarbon-Loaded Hollow Bi2Se3 Nanoparticles for Timely Supply of Oxygen under Near-Infrared Light to Enhance

the Radiotherapy of Cancer. *Adv. Mater.* **2016,** *28*, 2716-2723.
72. Dong, X.; Cheng, R.; Zhu, S.; Liu, H.; Zhou, R.; Zhang, C.; Chen, K.; Mei, L.; Wang, C.; Su, C.; Liu, X.; Gu, Z.; Zhao, Y., A Heterojunction Structured WO2.9-WSe2 Nanoradiosensitizer Increases Local Tumor Ablation and Checkpoint Blockade Immunotherapy upon Low Radiation Dose. *ACS Nano* **2020,** *14*, 5400-5416.
73. Maiti, D.; Zhong, J.; Zhang, Z.; Zhou, H.; Xion, S.; Dong, Z.; Kumar, S.; Liu, Z.; Yang, K., Polyoxomolybdate (POM) nanoclusters with radiosensitizing and scintillating properties for low dose X-ray inducible radiation-radiodynamic therapy. *Nanoscale Horiz.* **2020,** *5*, 109-118.
74. Fu, S.; Yang, R.; Zhang, L.; Liu, W.; Du, G.; Cao, Y.; Xu, Z.; Cui, H.; Kang, Y.; Xue, P., Biomimetic CoO@AuPt nanozyme responsive to multiple tumor microenvironmental clues for augmenting chemodynamic therapy. *Biomaterials* **2020,** *257*, 120279.
75. Sang, Y.; Cao, F.; Li, W.; Zhang, L.; You, Y.; Deng, Q.; Dong, K.; Ren, J.; Qu, X., Bioinspired Construction of a Nanozyme-Based H2O2 Homeostasis Disruptor for Intensive Chemodynamic Therapy. *J. Am. Chem. Soc.* **2020,** *142* , 5177-5183.
76. Yu, H.; Ma, M.; Liang, K.; Shen, J.; Lan, Z.; Chen, H., A self-assembled metal-polyphenolic nanomedicine for mild photothermal-potentiated chemodynamic therapy of tumors. *Appl. Mater. Today* **2021,** *25*, 101235.
77. Yang, B.; Shi, J., Ascorbate Tumor Chemotherapy by An Iron-Engineered Nanomedicine-Catalyzed Tumor-Specific Pro-Oxidation. *J. Am. Chem. Soc.***2020,** *142*, 21775-21785.
78. He, Y.; Guo, S.; Zhang, Y.; Liu, Y.; Ju, H., NIR-II reinforced intracellular cyclic reaction to enhance chemodynamic therapy with abundant H2O2 supply. *Biomaterials* **2021,** *275*, 120962.

# Chapter 2 Coordination-assembled Myricetin Nanoarchitectonics for Sustainably Scavenging Free Radicals


## Abstract

Oxidative stress can lead to permanent and irreversible damage to cellular components and even cause cancer and other diseases. Therefore, the development of antioxidative reagents is an important strategy to alleviate chronic diseases and maintain the redox balance in cells. Small-molecule bioactive compounds have exhibited huge therapeutic potential as antioxidants and anti-inflammatory agents. Myricetin (Myr), a well-known natural flavonoid, has drawn wide attention because of its high antioxidant, anti-inflammatory, antimicrobial, and anticancer efficacy. Especially regarding antioxidation, Myr is capable of not only chelating intracellular transition metal ions for removing reactive oxygen species, but also of activating antioxidant enzymes and related signal pathways and, thus, of sustainably scavenging radicals. However, Myr is poorly soluble in water, which limits its bioavailability for biomedical applications, and even its clinical therapeutic potential. The antioxidant peptide glutathione (GSH) plays a role as antioxidant in cells and possesses good hydrophilicity and biocompatibility. However, it is easily metabolized by enzymes. To take advantages of their antioxidation activity and to overcome the abovementioned limitations, GSH, $Zn^{2+}$, and Myr were selected to co-assemble into Myr-$Zn^{2+}$-GSH nanoparticles (NPs) or nanoarchitectonics. This study offers a new design to harness stable, sustainable antioxidant NPs with high loading capacity, high bioavailability, and good biocompatibility as antioxidants.



**Keywords:** antioxidant; co-assembly; glutathione; myricetin; nanoarchitectonics

## 2.1 Introduction

Oxidative stress, caused by an imbalance between antioxidative and oxidative systems, leads to permanent and irreversible damage of cellular components, such as proteins, lipids, and nucleic acids.[1] Furthermore, oxidative stress leads to diseases including Alzheimer's disease,[2] cardiac disease,[3] atherosclerosis,[4] kidney disease,[5] sepsis,[6] cancer,[7] and inflammatory diseases (e.g., periodontal disease and inflammatory bowel disease).[8,9] Therefore, the development of antioxidative reagents is a crucial strategy to alleviate chronic diseases and maintain the redox balance.

Increasingly efficient antioxidant materials are used for effectively scavenging multiple ROS. Metal-based nanomaterials, such as $CeO_2$ and $Fe_3O_4$, have been widely applied for antioxidant therapy.[10] In addition, bioactive small-molecule compounds, such as bilirubin and curcumin, and antioxidant peptides such as glutathione (GSH) and casein phosphopeptides, exhibited huge therapeutic potential in antioxidant treatments.[11-13] Nevertheless, a plenty of disadvantages restrict biomedical applications, namely low biocompatibility of the metal-based nanomaterials, low bioavailability of hydrophobic small-molecule compounds, and easy degradation of antioxidant peptides by proteases. The combination of liposomes or polymers with different payload materials has been reported, for example, PEG-modified liposomes loaded with resveratrol, layer-by-layer-coated gelatin nanoparticles, or Gelucire-based solid lipid and polymeric micelles.[14-19] However, low loading efficiency, systemic toxicity, and tedious preparation processes hinder biomedical applications.

Myricetin (Myr), a well-known natural flavonoid, has drawn wide attention because of its high antioxidant, anti-inflammatory, antimicrobial, and anticancer efficacy.[16] Myr is capable of not only chelating intracellular transition metal ions for removing reactive oxygen species (ROS),[20] but also of activating antioxidant enzymes and the AMPK/NRF2 signal pathway,[21] yielding sustainable scavenging of radicals. Myr can inherently increase body resistance to carcinogens, viruses, and allergens.[17] In spite of the tremendous potential, Myr possesses the same shortcomings as many hydrophobic small molecules, namely low bioavailability, poor water solubility and rapid degradation at pH > 6.8, which limits its clinical therapeutic potential.[22] GSH consists of glycine, cysteine, and glutamic acid. The cysteine residue plays a pivotal role in protecting the body from oxidation damage; however, GSH is easily metabolized by enzymes.[23] In this work, we employed a facile co-assembly strategy to design hybrid nanoparticles as antioxidants.[24-31] Myr, $Zn^{2+}$, and GSH were co-assembled to Myr-$Zn^{2+}$-GSH (MZG) nanoparticles (NPs). The obtained MZG NPs exhibit high loading capacity as well as good bioavailability and biocompatibility, leading to stable antioxidant effects.

## 2.2 Experimental section

### 2.2.1 Materials and Instruments

**Materials:** Myricetin (95%) was bought from Thermo Fisher Scientific. L-Glutathione (reduced) was obtained from Solarbio. Zinc (II) chloride ($ZnCl_2$) (98%) was purchased from Beijing Chemical Works. 2,2′-Azinobis-(3-ethylbenzthiazoline-6-sulfonate) was

bought from Innochem (Beijing). 2′,7′-Dichlorodihydrofluorescein diacetate (DCFH-DA) was got from MedChemexpress. Dulbecco's Modified Eagle Medium (DMEM), fetal bovine serum (FBS), penicillin/streptomycin, and trypsin-EDTA were bought from BioLegend.

**Instruments:** TEM images of NPs were exhibited by a model JEM-1011 transmission scanning electron microscope (JEM-1011, JEOL, Japan). The size distribution and zeta potential of NPs were measured by a Malvern DLS instrument (Zetasizer Nano ZS ZEN3600). UV/vis absorption spectra were tested by a Shimadzu UV-2600 spectrophotometer. Fourier transform infrared (FTIR) spectra were obtained by a TENSOR 27 FTIR spectrometer (BRUKER). The cell viability was evaluated using methyl thiazolyl tetrazolium (MTT) assay, in which the absorbance was measured by a microplate reader (Multiskan FC, Thermo Fisher Scientific). Confocal laser scanning microscopy (CLSM) images of cells were captured by CLSM (Olympus FV1000). Inductively coupled plasma-optical emission spectroscopy (ICP-OES, Prodigy, Leeman, USA) was used for evaluating concentration of $Zn^{2+}$ in quantitative component analysis of MZG.

### 2.2.2 Synthesis of MZG

10 mg·mL$^{-1}$ of Myr was dispersed in 0.1 M NaOH, 10 mg·mL$^{-1}$ of GSH was dispersed in deionized water, and 100 mM solution of $Zn^{2+}$ was prepared. MZG NPs were produced by adding 100 μL of Myr into a mixed solution of 200 μL of GSH solution, 15.7 μL of $Zn^{2+}$ solution and 684 μL of water. The Myr solution should be freshly prepared for use due to precipitation. The freshly prepared MZG NPs were aged for 24 h at room temperature and placed in the dark. As-prepared NPs were concentrated, purified by centrifugation, and used for further experiments.

### 2.2.3 Quantitative analysis of MZG

The precipitates of MZG were collected after centrifuging and washing with water and, subsequently, dissolved in 0.1 M NaOH solution. The concentrations of Myr and GSH were determined by UV/vis spectroscopy. The concentration of $Zn^{2+}$was measured by ICP-OES.

### 2.2.4 Evaluation of ROS scavenging activity

First, a solution of 2,2′-azino-bis (3-ethylbenzothiazoline-6-sulfonic acid) radical cations ($ABTS^{\cdot+}$) solution was prepared. 7 mM of ABTS solution was mixed with 2.45 mM of potassium persulfate solution and kept for 12 h in the dark. The UV/vis absorption intensity of a 0.7 mM ABTS solution diluted in phosphate-buffered saline (PBS) was 0.7 ± 0.02. A certain volume of diluted $ABTS^{\cdot+}$ solution was added to different concentrations of Myr, GSH, and MZG. A UV/vis spectrophotometer was used to record the absorption intensity of $ABTS^{\cdot+}$ at 734 nm. The radical scavenging rate was calculated according to the following equation:

$$\text{scavenging rate} = \frac{\text{Abs734 nm, control} - \text{Abs 734nm, sample}}{\text{Abs734 nm, control}} \cdot 100\%$$

MZG NPs and Myr/GSH complex were dispersed in $H_2O$ for 5 days. Diluted $ABTS^{\cdot+}$

solution was added with the same concentration of MZG and Myr/GSH complex (equiva- lent concentration of Myr and GSH: 4 μg·mL$^{-1}$ and 8 μg·mL$^{-1}$, respectively) every day. The UV/vis absorption intensity of ABTS$^{\cdot+}$ at 734 nm was measured, and the radical scavenging rate was calculated.

1 mL of MZG suspension (equivalent concentration of Myr and GSH: 4 μg·mL$^{-1}$ and 8 μg·mL$^{-1}$, respectively) and 1 mL of water as control were added to the same volume of ABTS$^{\cdot+}$ solution. UV/vis spectra and the absorption intensity at 734 nm were recorded. The absorption intensity of ABTS$^{\cdot+}$ at 734 nm was measured again after 24 h. Then, the same volume of ABTS$^{\cdot+}$solution was added to the abovementioned MZG suspension and $H_2O$, and UV/vis spectra and the absorption intensity at 734 nm were recorded. Before adding the same volume of ABTS$^{\cdot+}$ solution, UV/vis spectra and the absorption intensity at 734 nm were recorded. This was repeated for 5 days.

The as-prepared MZG NPs were acquired by centrifugation. Then MZG NPs were incubated with different concentrations of $H_2O_2$ (0.01, 0.1, 1, 10, and 100 mM). UV/vis spectrophotometry and dynamic light scattering (DLS) were used to record absorption spectra and size change.

### 2.2.5 Cytotoxicity experiment *in vitro*

The cytotoxicity of the as-prepared MZG NPs was assessed against 3T3 cells. 3T3 cells were cultivated with DMEM containing 10% (v/v) FBS and 1% (v/v) penicillin/streptomycin. 3T3 cells at a density of 1 ×10$^5$ cells per well were incubated with different concentrations of MZG (equivalent concentration of Myr: 0, 10, 20, 40, 80, and 100 μM) for 24 h. The cell viability was tested with MTT assay.

### 2.2.6 Evaluation of ROS scavenging in cells

First, the median lethal dose ($LD_{50}$) value of $H_2O_2$ was evaluated. 3T3 cells at a density of 2 × 10$^5$ cells per well were incubated with $H_2O_2$ at different concentrations (0, 10, 20, 40, 60, 80, 100, 150, and 200 μM). Second, the ROS scavenging activity of MZG was evaluated. After the treatment of 3T3 cells with different concentrations of MZG for 24 h, 100 μM of $H_2O_2$ was used to treat the 3T3 cells. The capability of protecting cells from damage was accessed by the cell viability assay. After that, DCFH-DA dye was used to incubate these cells for 5 min and the fluorescence intensity of the cells was recorded via CLSM.

## 2.3 Results and Discussion

### 2.3.1 Synthesis and characterization of MZG

We chose $Zn^{2+}$, a typical essential metal, to effectively bond Myr and GSH via coordination interaction (Myr/GSH =1:2).[32-34] The NPs were formed by coordination self-assembly of $Zn^{2+}$, Myr, and GSH (Figure 2.1a). They were expected to show good antioxidant activity to protect cells from the ROS-induced damage (Figure 2.1b). The TEM image in Figure 2a shows spherical MZG NPs. Size and zeta potential value of the MZG NPs were 44.6 ± 26.5 nm and −23.1 ± 3.4 mV, respectively, measured by DLS (Figure 2.2b) and consistent with the TEM results. Importantly, the co-assembly

mechanism was further revealed through quantitative stoichiometry analysis. The quantitative component analysis by UV/vis and ICP-OES proved that the molar ratio of Myr/GSH/$Zn^{2+}$ was close to 1:1:1 (Table S2.1 and Figure S2.1).

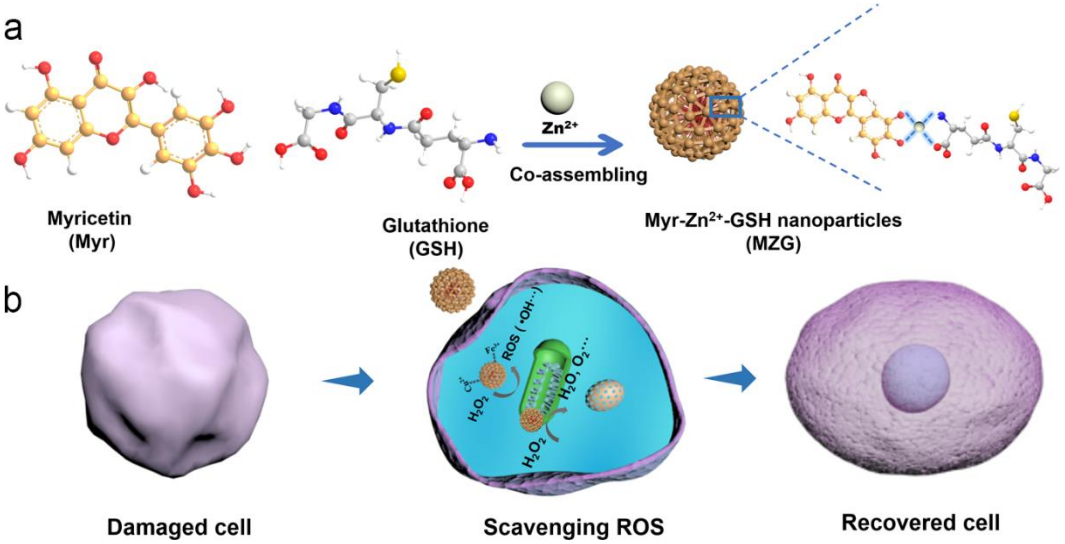


**Figure 2.1** Schematic illustration of preparing MZG NPs (a) and (b) antioxidation mechanism in cells. MZG NPs afford the antioxidant activity for maintaining redox homeostasis in cells.

The UV/vis absorption spectra of pure Myr dispersed in 0.1 M NaOH (pH 13), Myr/$Zn^{2+}$ complex (pH 5.5), and MZG NPs (pH 5.5) were measured. The UV/vis absorption spectrum of MZG NPs exhibited a blue shift at 550 nm, compared with Myr/$Zn^{2+}$, which was assigned to the charge transfer between GSH and $Zn^{2+}$ (Figure 2.2c). These results demonstrated that $Zn^{2+}$ as the coordination component co-assembles with Myr and GSH. FTIR spectra were used to further confirm the self-assembly of the MZG NPs. In Figure 2.2d, the two bands at 2522 $cm^{-1}$ and 3350 $cm^{-1}$ were assigned to the mercapto group (–SH) and the stretching vibration of the amino group (–$NH_2$) of GSH. The band at 1619 $cm^{-1}$ was assigned to the C=C group of Myr. In addition, the band at 3417 $cm^{-1}$ was assigned to the phenolic hydroxy group. The two bands of phenolic hydroxy and amino groups shifted to lower wavenumbers, compared with the corresponding bands of Myr and GSH, suggesting that these groups coordinated to $Zn^{2+}$.

The co-assembly approach mitigates the poor water solubility of Myr and improves its bioavailability for further biomedical applications. The stability of the co-assembled NPs is important for antioxidant application. The DLS profiles were used to evaluate the stability of the MZG NPs. The MZG NPs (0.5 $mg \cdot mL^{-1}$) were either dispersed in water or diluted 10-fold (v/v) in DMEM containing 10% (v/v) FBS at 37 °C for 24 h to investigate the stability. The change of DLS was recorded at different time points (0, 2, 4, 8, 24, 48, and 72 h), showing that the average size and size distribution did not change over time (Figure 2.2e, f). The results indicated that MZG NPs were stable in water and culture medium. Although noncovalent interactions are relatively weak compared to covalent interactions, the metal coordination interaction is the strongest noncovalent interaction.[4] Hence, this interaction assured the stability of assembled NPs in

physiological conditions.

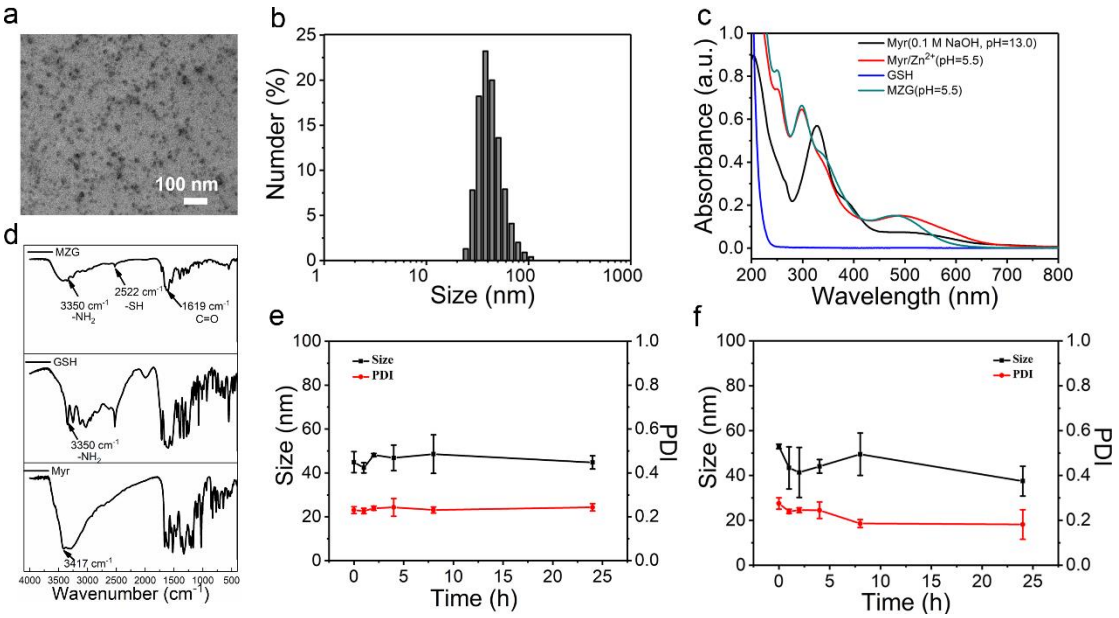


**Figure 2.2** Physicochemical characterization of MZG NPs. (a) TEM image. (b) DLS profile of MZG NPs. (c) UV/vis absorbance spectra of Myr dissolved in (0.1 M NaOH), Myr/$Zn^{2+}$ complex, GSH, and MZG (equivalent concentration of Myr: 20 μg·$mL^{-1}$). (d) FTIR spectra of MZG, GSH, and Myr. (e) Stability evaluation of MZG NPs during incubation in aqueous solution at 37 °C for 24 h. (f) Stability evaluation of MZG NPs during incubation in the mixture medium of water containing 9% DMEM and 1% FBS (v/v) at 37 °C for 24 h (equivalent concentration of Myr: 0.5 mg·$mL^{-1}$).

### 2.3.2 Evaluation of ROS scavenging activity

Myr possesses excellent antioxidant activity to scavenge ROS, which has impact on chelate metal ions such as $Fe^{2+}$ and $Cu^{2+}$, inhibits glutathione reductase activity, and regulates PI3K/Akt and MAPK signal pathways to avoid oxidative stress-induced apoptosis.[20,35-37] Also, GSH acts as an important antioxidant in the body owing to the –SH group, which can be reduced. GSH is a non-enzymatic antioxidant molecule, which is necessary for cell redox homeostasis and survival.[38] In this work, the ABTS assay was employed to evaluate the radical scavenging activity.[39] The UV/vis absorption intensity of $ABTS^{\cdot+}$ solution (0.7 mM) was 0.7 ± 0.02 in phosphate-buffered saline (PBS). The diluted $ABTS^{\cdot+}$ solution was incubated with GSH, Myr, and MZG for accessing the radical scavenging activity. The diluted $ABTS^{\cdot+}$ solution was incubated with different concentrations of Myr (0.5, 1, 2, 3, and 4 μg·$mL^{-1}$) for 5 min. The color of the diluted $ABTS^{\cdot+}$solution gradually disappeared with increasing Myr concentration (Figure S2.2a). The scavenging rate of pure Myr at 4 μg·$mL^{-1}$ was up to 94.0% (Figure S2b). In the same way, the scavenging rate of GSH was evaluated. The $ABTS^{\cdot+}$solution was treated with different concentrations of GSH (1, 2, 4, 6, and 8 μg·$mL^{-1}$), and the color gradually disappeared (Figure S2.2c). Figure S2.2d shows that the scavenging rate of GSH at 8 μg·mL−1 was up to 93.3%. Figure 2.3a showed that the UV/vis absorbance of diluted $ABTS^{\cdot+}$ solution incubated with different concentrations of MZG NPs (equivalent concentration of Myr: 0.25, 0.5, 1, 1.5, and 2 μg·$mL^{-1}$, equivalent

concentration of GSH: 1, 2, 3, and 4 μg·mL$^{-1}$) gradually decreased, suggesting that MZG NPs scavenged radicals. When the concentration of MZG NPs was equivalent to 2 μg·mL$^{-1}$ of Myr and 4 μg·mL$^{-1}$ of GSH, the scavenging rate of MZG was up to 93.5% (Figure 2.3b). This demonstrated that the scavenging effect of co-assembled MZG NPs was identical to that of the Myr/GSH complex, indicating that co-assembly did not affect the ROS scavenging activity of Myr and GSH. However, as MZG NPs could not only scavenge ROS, but also overcome the poor water solubility of Myr, the co-assembly was effective to enhance the bioavailability of both Myr and GSH, especially regarding a sustainable antioxidant efficacy. The stable radical scavenging activity of MZG was further assessed. As shown in Figure 2.3c, the radical scavenging activity of the Myr/GSH complex was lower than that of MZG NPs at the same concentration over 5 days, which demonstrated that MZG NPs were more stable to scavenge radicals than the Myr/GSH complex. Next, we explored whether the as-prepared MZG NPs possessed the sustainability of radical scavenging activity due to the co-assembly that might have enhanced the stability of Myr and GSH. As shown in Figure 2.3d, ABTS$^{\cdot+}$ solution was persistently added to 1 mL of MZG nanoparticle suspension or water for 5 days. The result revealed that MZG NPs exhibited prolonged activity for scavenging ABTS$^{\cdot+}$compared with water. It demonstrated that the as-prepared MZG NPs exhibited stable and sustainable radical scavenging activity. ROS-responsive disruption of MZG NPs during ROS scavenging was further explored. While MZG NPs were incubated with different concentrations of $H_2O_2$ (0.01, 0.1, 1, 10, and 100 mM), UV/vis absorption spectra and the size of the MZG NPs were measured. The UV–vis absorbance of MZG NPs from 300 to 400 nm (Figure 2.3e) decreased with the increase of $H_2O_2$ concentration. Also, the size of MZG NPs was tested by DLS. The result showed that the size also decreased dramatically with the increase of $H_2O_2$ concentration. The UV/vis absorbance and size of MZG NPs obviously changed at 1 mM of $H_2O_2$, indicating that there was a ROS-responsive disassembly of MZG NPs (Figure 2.3f).

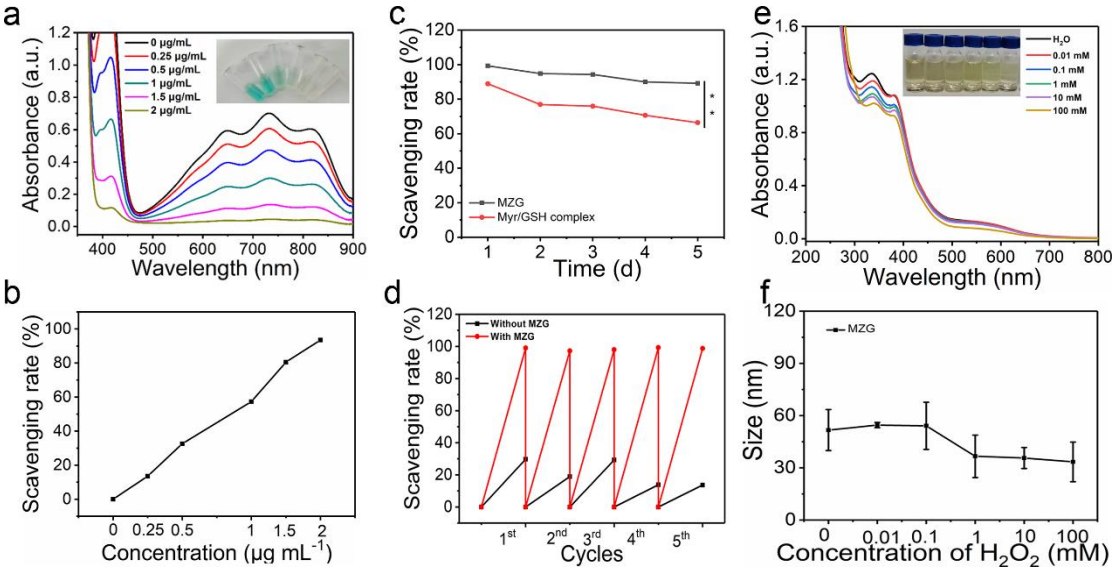


**Figure 2.3** Measurement of ROS scavenging. (a) UV/vis absorption spectra of ABTS$^{\cdot+}$solution incubated with different concentrations of MZG NPs for 5 min (a sample picture is shown in the inset, equivalent concentration of Myr: 0.25, 0.5, 1, and

2 μg·mL$^{-1}$). (b) The scavenging rate of MZG NPs as fitted by the maximum UV/vis absorption at 734 nm. (c) Stably scavenging radical activity evaluation of MZG NPs and Myr/GSH complex (equivalent concentration of Myr: 4 μg·mL$^{-1}$, ** indicates $p < 0.01$). (d) Evaluation of the sustainable radical scavenging activity of MZG NPs (equivalent concentration of Myr: 4 μg·mL$^{-1}$). (e) UV/vis absorption spectra of MZG NPs treated with different concentrations of $H_2O_2$ (equivalent concentration of Myr: 20 μg·mL$^{-1}$). (f) Size of MZG NPs treated with different concentrations of $H_2O_2$ (equivalent concentration of Myr: 0.5 mg·mL$^{-1}$).

### 2.3.3 Cell experiments

The cytotoxicity of antioxidants is of importance for biomedical applications. Therefore, the cytotoxicity of MZG NPs was assessed by incubating 3T3 cells and determining the cell viability via MTT assay.[40] 3T3 cells were treated with different concentrations of MZG NPs (equivalent concentration of Myr: 10, 20, 40, 80, and 100 μM) for 24 h. The lowest cell viability was approximately 80% at the highest tested concentration of MZG NPs (Figure 2.4a). The result indicates that MZG NPs did not affect the growth of 3T3 cells.

The antioxidant activity of MZG NPs was also examined using 3T3 cells and the MTT assay. $H_2O_2$ can produce ROS, and a high level of ROS can cause damage to cellular functions and components.[41,42] To explore the antioxidative effect of MZG NPs the $LD_{50}$ value of $H_2O_2$ against 3T3 cells was measured by the MTT assay. The cell viability of 3T3 cells decreased with increasing $H_2O_2$ concentration (Figure 2.4b). The $LD_{50}$ concentration of $H_2O_2$

against 3T3 cells was 100 μM. Next, cell recovery due to the antioxidant activity of MZG NPs was demonstrated by the MTT assay. After incubating with different concentrations of MZG NPs (equivalent concentration of Myr: 2.5, 5, 10, 20, 40, and 80 μM) for 24 h, 3T3 cells were further incubated with 100 μM of $H_2O_2$ for 24 h. The cell viability gradually increased with increasing MZG concentration (Figure 2.4c).

This observation indicated that MZG could scavenge ROS to effectively protect cells from damage. DCFH-DA was used to probe ROS in cells, which showed no fluorescence signal without ROS, while it turned to highly fluorescent 2′7′-dichlorofluorescein after interacting with ROS in cells. As shown in the CLSM images, the fluorescence intensity of cells treated with $H_2O_2$ and MZG NPs was weaker than that of cells only treated with $H_2O_2$ (Figure 2.4e). The fluorescence intensity of cells was further measured, indicating that the fluorescence intensity of cells treated with a combination of MZG NPs and $H_2O_2$ was lower than that of cells treated with $H_2O_2$, suggesting that MZG NPs were capable of scavenging ROS in cells (Figure 4d).

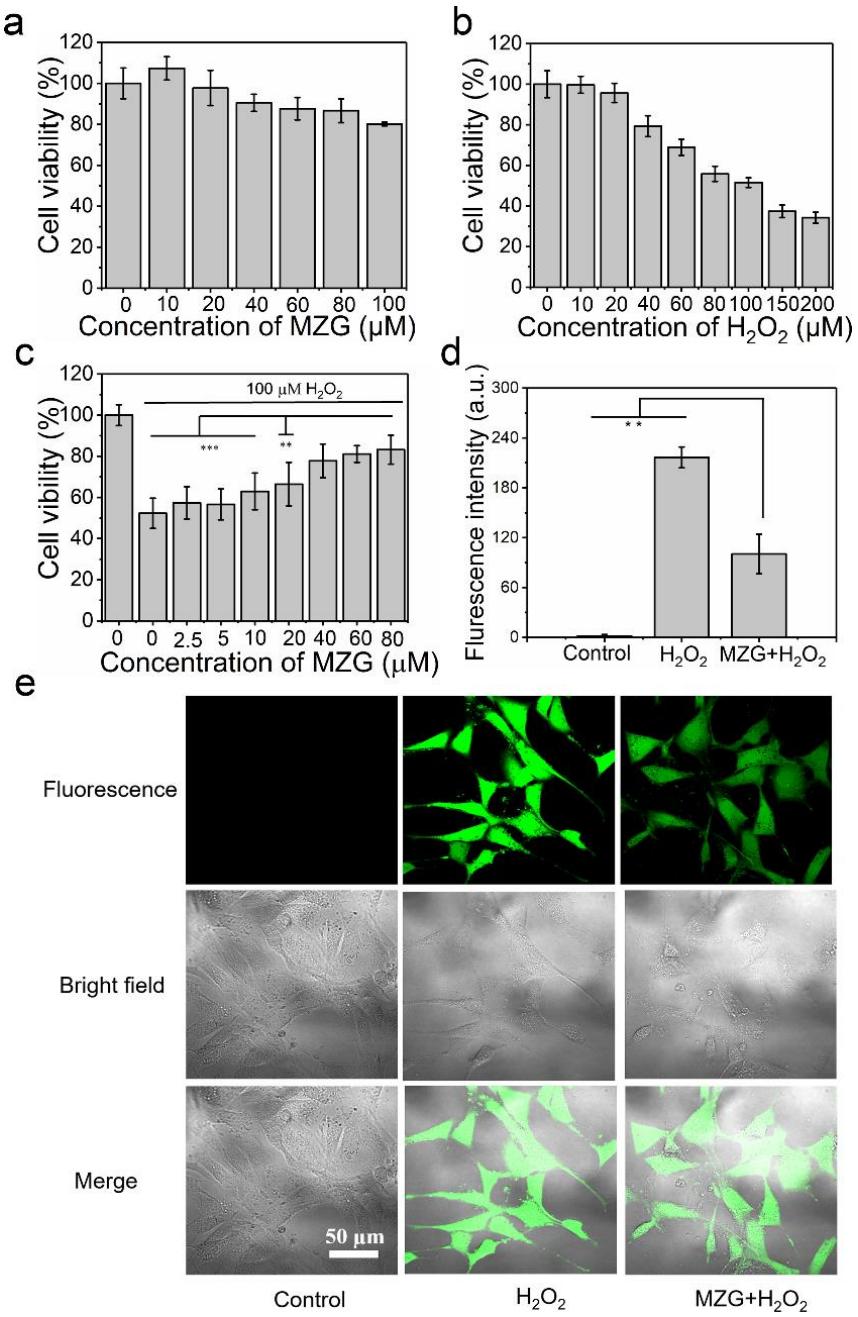


**Figure 2.4** Antioxidant activity evaluation in cells. (a) Cytotoxicity evaluation of MZG NPs by incubating 3T3 cells with different concentrations of MZG NPs (equivalent concentration of Myr: 10, 20, 40, 80, and 100 μM). (b) $H_2O_2$-induced oxidative stress by incubating 3T3 cells with different concentrations of $H_2O_2$. (c) Antioxidant activity evaluation of MZG NPs using 3T3 cells under $H_2O_2$-induced oxidative stress (** indicates $p < 0.01$, *** indicates $p < 0.001$). (d) Fluorescence intensity of ROS probed by DCFH-DA in cells after incubating with $H_2O_2$ and a combination of MZG NPs and $H_2O_2$ (** indicates $p < 0.01$). (e) CLSM images of 3T3 cells probed by DCFH-DA after incubating with MZG NPs and $H_2O_2$ (the first row shows fluorescence images, the second row shows bright-field images, and the third row shows the merged images).

## 2.4 Conclusions

We have prepared antioxidant MZG NPs by co-assembly of the naturally occurring flavonoid Myr and GSH in the presence of $Zn^{2+}$. The resulting MZG NPs overcame the disadvantages of water-insoluble Myr and GSH that is quickly metabolized, improving their bioavailability. Importantly, the as-prepared MZG NPs exhibited robust stability and sustainable ROS scavenging activity, protecting cells from ROS damage. The MZG NPs provide an alternative opportunity for optimizing the antioxidation capability ofconventional drugs and present great potential for further biomedical applications.


## Acknowledgements

This work was financially supported by the Innovation Research Community Science Fund of China (No. 21821005), National Natural Science Foundation of China (Project Nos. 22072154 and 21977095), the Key Research Program of Frontier Sciences of Chinese Academy of Sciences (CAS, Grant No. QYZDB-SSWJSC034), and the National Natural Science Foundation of Hebei Province (No. B2020103025).


## 2.5 Supporting information

| Component | Myr | GSH | $Zn^{2+}$ |
|---|---|---|---|
| Feeding concentration (mM) | 3 | 6 | 1.57 |
| Measured concentration (mM) | 1.5 | 1.5 | 1.3 |

Table 2.1. Component analysis of MZG NPs.

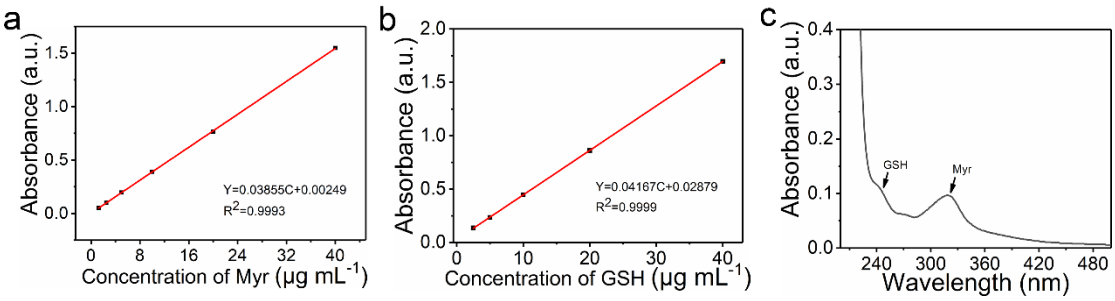

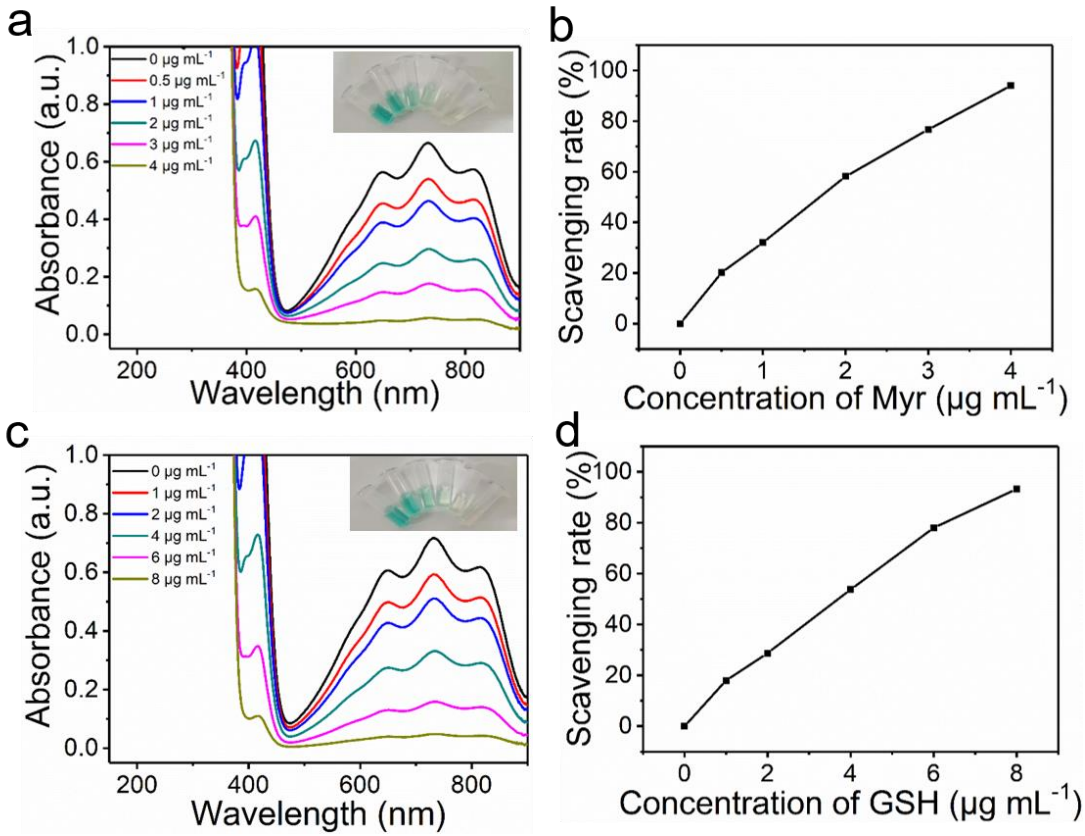


**Figure S2.1** (a) The standard curve of Myr in 0.1 M NaOH. (b) The standard curve of GSH in 0.1 M NaOH. GSH dissolved in 0.1 M NaOH has an UV/vis absorption peak at ca. 240 nm. (c) The UV/vis absorption spectrum of diluted MZG NPs (2000-fold) in 0.1 M NaOH.

## 2.6 References


1. Wei, Z.; Wang, L.; Tang, C.; Chen, S.; Wang, Z.; Wang, Y.; Bao, J.; Xie, Y.; Zhao, W.; Su, B.; Zhao, C., Metal-Phenolic Networks Nanoplatform to Mimic Antioxidant Defense System for Broad-Spectrum Radical Eliminating and Endotoxemia Treatment. *Adv. Funct. Mater.* **2020,** *30*, 2002234.

2. Herring, A.; Blome, M.; Ambrée, O.; Sachser, N.; Paulus, W.; Keyvani, K., Reduction of Cerebral Oxidative Stress Following Environmental Enrichment in Mice with Alzheimer-Like Pathology. *Brain Pathol.* **2010,** *20*, 166-175.

3. Han, J.; Kim, Y. S.; Lim, M. Y.; Kim, H. Y.; Kong, S.; Kang, M.; Choo, Y. W.; Jun, J. H.; Ryu, S.; Jeong, H. Y.; Park, J.; Jeong, G. J.; Lee, J. C.; Eom, G. H.; Ahn, Y.; Kim, B. S., Dual Roles of Graphene Oxide To Attenuate Inflammation and Elicit Timely Polarization of Macrophage Phenotypes for Cardiac Repair. *ACS Nano* **2018,** *12*, 1959-1977.

4. Wang, Y.; Li, L.; Zhao, W.; Dou, Y.; An, H.; Tao, H.; Xu, X.; Jia, Y.; Lu, S.; Zhang, J.; Hu, H., Targeted Therapy of Atherosclerosis by a Broad-Spectrum Reactive Oxygen Species Scavenging Nanoparticle with Intrinsic Anti-inflammatory Activity. *ACS Nano* **2018,** *12*, 8943-8960.

5. Liu, D.; Cornel, E. J.; Du, J., Renoprotective Angiographic Polymersomes. *Adv. Funct. Mater.* **2021,** *31*, 2007330.

6. Soh, M.; Kang, D. W.; Jeong, H. G.; Kim, D.; Kim, D. Y.; Yang, W.; Song, C.; Baik, S.; Choi, I. Y.; Ki, S. K.; Kwon, H. J.; Kim, T.; Kim, C. K.; Lee, S. H.; Hyeon, T., Ceria-Zirconia NPs as an Enhanced Multi-Antioxidant for Sepsis Treatment. *Angew. Chem. Int. Ed. Engl.* **2017,** *56*, 11399-11403.
7. Zhao, L.; Zou, Q.; Yan, X., Self-Assembling Peptide-Based Nanoarchitectonics. *Bull. Chem. Soc. Jpn.* **2019,** *92*, 70-79.
8. Bao, X.; Zhao, J.; Sun, J.; Hu, M.; Yang, X., Polydopamine NPs as Efficient Scavengers for Reactive Oxygen Species in Periodontal Disease. *ACS Nano* **2018,** *12*, 8882-8892.
9. Nishiguchi, A.; Taguchi, T., Oligoethyleneimine-Conjugated Hyaluronic Acid Modulates Inflammatory Responses and Enhances Therapeutic Efficacy for Ulcerative Colitis. *Adv. Funct. Mater.* **2021,** *31*, 2100548.
10. Zhao, S.; Li, Y.; Liu, Q.; Li, S.; Cheng, Y.; Cheng, C.; Sun, Z.; Du, Y.; Butch, C. J.; Wei, H., An Orally Administered CeO2@Montmorillonite Nanozyme Targets Inflammation for Inflammatory Bowel Disease Therapy. *Adv. Funct. Mater.* **2020,** *30*, 2004692.
11. Kitts, D. D., Antioxidant properties of casein-phosphopeptides. *Trends Food Sci. Technol.* **2005,** *16*, 549-554.
12. Chung, C. H.; Jung, W.; Keum, H.; Kim, T. W.; Jon, S., NPs Derived from the Natural Antioxidant Rosmarinic Acid Ameliorate Acute Inflammatory Bowel Disease. *ACS Nano* **2020,** *14*, 6887-6896.
13. Li, Y.; Zou, Q.; Yuan, C.; Li, S.; Xing, R.; Yan, X., Amino Acid Coordination Driven Self-Assembly for Enhancing both the Biological Stability and Tumor Accumulation of Curcumin. *Angew. Chem. Int. Ed. Engl.* **2018,** *57*, 17084-17088.
14. Ahmadi, Z.; Mohammadinejad, R.; Ashrafizadeh, M., Drug delivery systems for resveratrol, a non-flavonoid polyphenol: Emerging evidence in last decades. *J. Drug Delivery Sci. Technol.* **2019,** *51*, 591-604.
15. Shutava, T. G.; Balkundi, S. S.; Vangala, P.; Steffan, J. J.; Bigelow, R. L.; Cardelli, J. A.; O'Neal, D.; Lvov, Y. M., Layer-by-Layer-Coated Gelatin NPs as a Vehicle for Delivery of Natural Polyphenols. *ACS Nano* **2009,** *3*, 1877-85.
16. Sun, F.; Zheng, Z.; Lan, J.; Li, X.; Li, M.; Song, K.; Wu, X., New micelle myricetin formulation for ocular delivery: improved stability, solubility, and ocular anti-inflammatory treatment. *Drug Deliv.* **2019,** *26*, 575-585.
17. Gaber, D. M.; Nafee, N.; Abdallah, O. Y., Myricetin solid lipid NPs: Stability assurance from system preparation to site of action. *Eur. J. Pharm. Sci.* **2017,** *109*, 569-580.
18. Battista, S.; Campitelli, P.; Galantini, L.; Köber, M.; Vargas-Nadal, G.; Ventosa, N.; Giansanti, L., Use of N-oxide and cationic surfactants to enhance antioxidant properties of (+)-usnic acid loaded liposomes. *Colloids Surf. A* **2020,** *585*, 124154.
19. Chatzidaki, M.; Kostopoulou, I.; Kourtesi, C.; Pitterou, I.; Avramiotis, S.; Xenakis, A.; Detsi, A., β-Cyclodextrin as carrier of novel antioxidants: A structural and efficacy study. *Colloids Surf. A* **2020,** *603*, 125262.
20. Gupta, G.; Siddiqui, M. A.; Khan, M. M.; Ajmal, M.; Ahsan, R.; Rahaman, M. A.; Ahmad, M. A.; Arshad, M.; Khushtar, M., Current Pharmacological Trends on Myricetin. *Drug Res. (Stuttg)* **2020,** *70*, 448-454.

21. Kan, X.; Liu, J.; Chen, Y.; Guo, W.; Xu, D.; Cheng, J.; Cao, Y.; Yang, Z.; Fu, S., Myricetin protects against H2 O2 -induced oxidative damage and apoptosis in bovine mammary epithelial cells. *J. Cell Physiol.* **2021,** *236*, 2684-2695.
22. Yao, Y.; Lin, G.; Yan, X.; Ma, P.; Wu, T., Preformulation studies of myricetin: A natural antioxidant flavonoid. *Pharmazie* **2014,** *69*, 19-26.
23. Sharma, A.; Kharb, S.; Chugh, S. N.; Kakkar, R.; Singh, G. P., Effect of glycemic control and vitamin E supplementation on total glutathione content in non-insulin-dependent diabetes mellitus. *Ann. Nutr. Metab.* **2000,** *44*, 11-13.
24. Ariga, K.; Shionoya, M., Nanoarchitectonics for Coordination Asymmetry and Related Chemistry. *Bull. Chem. Soc. Jpn.* **2021,** *94*, 839-859.
25. Ariga, K.; Shrestha, L. K., Intelligent Nanoarchitectonics for Self-Assembling Systems. *Adv. Intell. Syst.* **2020,** *2*, 1900157.
26. Xing, R.; Yuan, C.; Li, S.; Song, J.; Li, J.; Yan, X., Charge-Induced Secondary Structure Transformation of Amyloid-Derived Dipeptide Assemblies from beta-Sheet to alpha-Helix. *Angew. Chem. Int. Ed. Engl.* **2018,** *57*, 1537-1542.
27. Xing, R.; Zou, Q.; Yuan, C.; Zhao, L.; Chang, R.; Yan, X., Self-Assembling Endogenous Biliverdin as a Versatile Near-Infrared Photothermal Nanoagent for Cancer Theranostics. *Adv. Mater.* **2019,** *31*, 1900822.
28. Cao, M.; Xing, R.; Chang, R.; Wang, Y.; Yan, X., Peptide-coordination self-assembly for the precise design of theranostic nanodrugs. *Coord. Chem. Rev.* **2019,** *397*, 14-27.
29. Liu, Y.; Zhao, L.; Shen, G.; Chang, R.; Zhang, Y.; Yan, X., Coordination self-assembly of natural flavonoids into robust NPs for enhanced in vitro chemo and photothermal cancer therapy. *Colloid. Surf. A* **2020,** *598*, 124805.
30. Sun, H.; Li, S.; Qi, W.; Xing, R.; Zou, Q.; Yan, X., Stimuli-responsive NPs based on co-assembly of naturally-occurring biomacromolecules for in vitro photodynamic therapy. *Colloid. Surf. A* **2018,** *538*, 795-801.
31. Xing, R.; Yuan, C.; Li, S.; Song, J.; Li, J.; Yan, X., Charge-Induced Secondary Structure Transformation of Amyloid-Derived Dipeptide Assemblies from β-Sheet to α-Helix. *Angew. Chem. Int. Ed. Engl.* **2018,** *57*, 1537-1542.
32. Azhar, A.; Li, Y.; Cai, Z.; Zakaria, M. B.; Masud, M. K.; Hossain, M. S. A.; Kim, J.; Zhang, W.; Na, J.; Yamauchi, Y.; Hu, M., Nanoarchitectonics: A New Materials Horizon for Prussian Blue and Its Analogues. *Bull. Chem. Soc. Jpn.* **2019,** *92*, 875-904.
33. Chang, X.; Zhou, Z.; Shang, C.; Wang, G.; Wang, Z.; Qi, Y.; Li, Z.-Y.; Wang, H.; Cao, L.; Li, X.; Fang, Y.; Stang, P. J., Coordination-Driven Self-Assembled Metallacycles Incorporating Pyrene: Fluorescence Mutability, Tunability, and Aromatic Amine Sensing. *J. Am. Chem. Soc.* **2019,** *141*, 1757-1765.
34. Dickinson, B. C.; Chang, C. J., Chemistry and biology of reactive oxygen species in signaling or stress responses. *Nat. Chem. Biol.* **2011,** *7*, 504-11.
35. Yahfoufi, N.; Alsadi, N.; Jambi, M.; Matar, C., The Immunomodulatory and Anti-Inflammatory Role of Polyphenols. *Nutrients* **2018,** *10*, 1618.
36. Semwal, D. K.; Semwal, R. B.; Combrinck, S.; Viljoen, A., Myricetin: A Dietary Molecule with Diverse Biological Activities. *Nutrients* **2016,** *8*, 90.
37. Li, X.; Mai, W.; Chen, D., Chemical Study on Protective Effect Against Hydroxyl-induced DNA Damage and Antioxidant Mechanism of Myricitrin. *J. Am. Chem. Soc.* **2014,** *61*, 383-390.

38. Gorrini, C.; Harris, I. S.; Mak, T. W., Modulation of oxidative stress as an anticancer strategy. *Nat. Rev. Drug Discov.* **2013,** *12*, 931-47.
39. Yim, D.; Lee, D. E.; So, Y.; Choi, C.; Son, W.; Jang, K.; Yang, C. S.; Kim, J. H., Sustainable Nanosheet Antioxidants for Sepsis Therapy via Scavenging Intracellular Reactive Oxygen and Nitrogen Species. *ACS Nano* **2020,** *14*, 10324-10336.
40. Sies, H.; Jones, D. P., Reactive oxygen species (ROS) as pleiotropic physiological signalling agents. *Nat. Rev. Mol. Cell Biol.* **2020,** *21*, 363-383.
41. Yang, B.; Chen, Y.; Shi, J., Reactive Oxygen Species (ROS)-Based Nanomedicine. *Chem. Rev.* **2019,** *119*, 4881-4985.
42. Mujagic, A.; Marushima, A.; Nagasaki, Y.; Hosoo, H.; Hirayama, A.; Puentes, S.; Takahashi, T.; Tsurushima, H.; Suzuki, K.; Matsui, H.; Ishikawa, E.; Matsumaru, Y.; Matsumura, A., Antioxidant nanomedicine with cytoplasmic distribution in neuronal cells shows superior neurovascular protection properties. *Brain Res.* **2020,** *1743*, 146922.

# Chapter 3 Orally Administered Covalent-assembled Antioxidative Peptide NPs for Inflammatory Bowel Disease Therapy


## Abstract

Inflammatory bowel disease (IBD) as a chronic inflammation disease, still exists many challenges, such as antibiotic resistance and side effects caused by long-term use of antibiotics. Therefore, development of highly efficient, biocompatible, conveniently administered nanomaterials for treating IBD is urgently required. Casein phosphopeptide (CPP) possesses antioxidative properties due to the existence of phosphate groups, which is capable of chelating transition metal ions to prevent from reactive oxygen species (ROS) generation. The CPP has high biocompatibility and tissue permeability, but it easily suffers from hydrolysis or enzymatic degradation, which limits further clinical application. Additionally, Genipin, derived from iridoid, can interact with other compounds to fabricate nanoarchitecture through covalent interaction. Herein, CPP and Genipin were combined to covalently assemble robust GCPP NPs (NPs). As-prepared GCPP NPs show antioxidant property for scavenging ROS. GCPP NPs remain stable enough to overcome easy degradation of CPP in the molecular form, which are adapted for oral administration. Meanwhile, nanoscale GCPP NPs can passively accumulate and retain at inflamed sites. In DSS-induced colitis model, the body weight and colon length of DSS-induced colitis mice treated by GCPP NPs perform rehabilitation trend. The obtained results demonstrated that GCPP NPs exhibited potential as therapeutic nanomedicine for anti-inflammatory therapy including IBD.



**Keywords:** Inflammatory bowel disease, Antioxidant peptides, Covalent assembly, Oral administration, Anti-inflammation therapy

## 3.1 Introduction

Inflammatory bowel disease (IBD) as a chronic inflammation disease, severely decreases the life quality of IBD patients and increases the risk of developing colon cancer.[1-4] Current anti-inflammatory therapeutics, such as antibiotics, small-molecular bioactive drugs, anti-TNF agents, corticosteroids and surgery, still exist many shortcomings and difficult to completely eliminate IBD.[5-7] Long-term application of these anti-inflammatory treatments will cause many side effects, including dysregulated gut commensal bacteria, increased risk of intestinal diseases, antibiotic resistance, and potential systemic toxicity.[8,9] The additional problem attributes to the lack of specificity drugs for treating IBD. Because a large amount of immune-related cells, including dendritic cells and macrophages, and positively charged proteins are enriched at the inflammatory site, leading to uptake small particles.[10-13] Thus, it has been be deemed be as a target for purpose of substantial and passive accumulation of nanodrugs with negative charge in inflamed tissue. It is of great significance to design special drugs with minimizing side effects for effective IBD treatment.

Bioactive peptides can be derived from active parent proteins though enzymatic hydrolysis.[14] These bioactive peptides perform various physiological functions, such as antioxidative, antimicrobial, immunomodulatory and antihypertensive function.[15-18] In particular, antioxidative bioactive peptides have received increasing attention on oxidative stress injury. There have been reported that antioxidant properties of bioactive peptides are hydrolysates that are widely sourced from plants or animals. Therefore, naturally occurring antioxidant peptides intrinsically perform good superiorities of high biocompatibility and tissue permeability, especially, relatively low side effects for long-run administration in comparison with other drugs.[19,20] However, bioactive peptides easily suffer from hydrolysis or enzymatic degradation in hostile environments containing different kinds of enzymes. To address these limitations, encapsulation approach has been further adopted and made great advances. Nevertheless, the encapsulation strategy still causes other problems, e.g. systemic toxicity, low drug loading efficiency.

Iridoids as a kind of natural compounds, exist in a wide range of plants and animals.[21] It has been reported that as-prepared nanomaterials by peptides and iridoid Genipin display high biocompatibility, especially, high stability through covalent interaction.[22-25] This strategy provides a new insight for designing and fabricating new types of nanomedicine for treatment of many diseases.

Herein, antioxidative peptide casein phosphopeptides (CPP) and iridoid Genipin as building blocks are selected to covalent-assemble robust GCPP NPs (NPs) via covalent interactions (Scheme 3.1a). Amino groups of CPP can occur anucleophilic reaction with the olefinic carbon atom at C-3 of deoxyloganin aglycone of Genipin to form CPP-Genipin compounds.[23] Obtained intermediate compounds can be further assembled to construct GCPP NPs. As-prepared GCPP NPs retain antioxidative activity from the CPP component. GCPP NPs possess stable nanostructures, which exhibit structural and functional resistance in the gastrointestinal tract (e.g. strong acidic and enzymatic environment) during oral delivery. *In vivo* results substantiate that GCPP NPs are capable of preferentially accumulating at inflamed sites for scavenging ROS,

promoting crypt regeneration, alleviating inflammation, and realizing specific and effective IBD treatment (Scheme 3.1b). GCPP NPs provide a novel insight of the covalent-assembly peptide nanomedicine for treating diseases via oral administration.

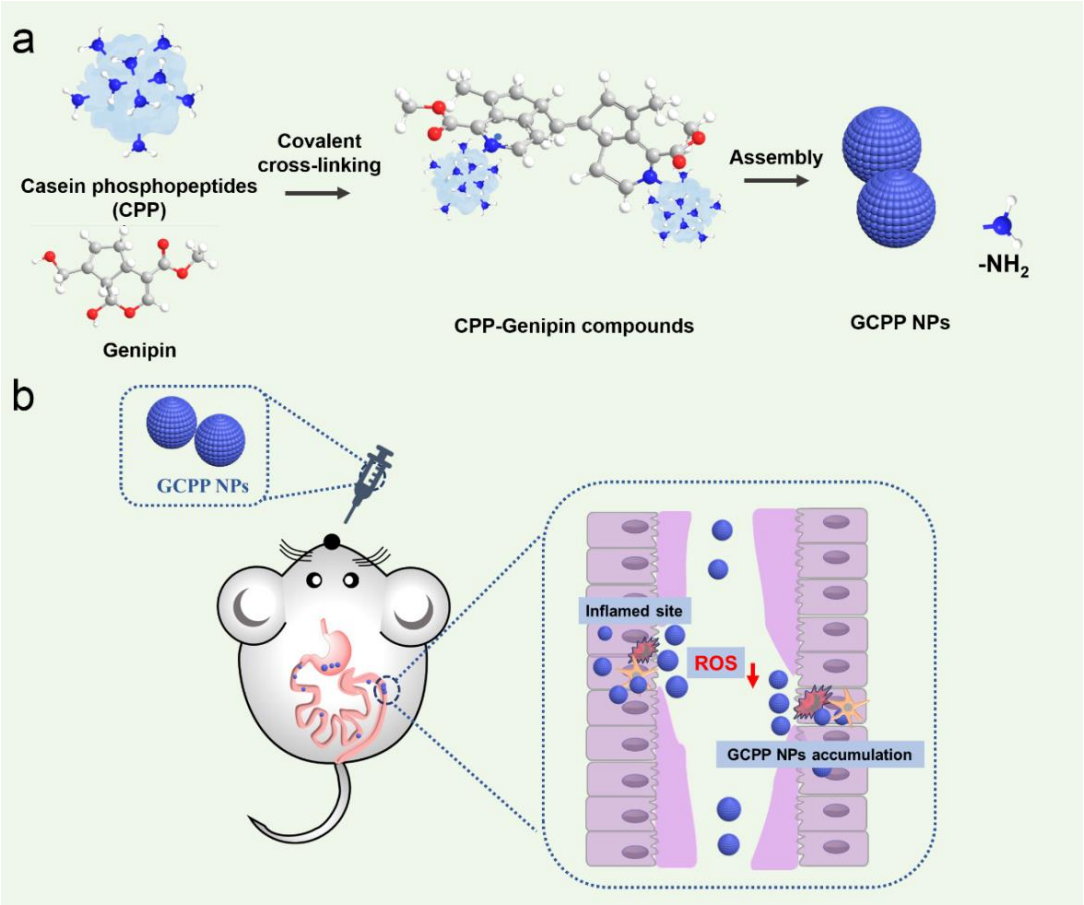


**Scheme 3.1** Schematic illustration. (a) The preparing process of GCPP NPs through covalent cross-linking of CPP and Genipin. (b) Covalently assembled GCPP NPs preferentially accumulated at inflamed site at colon for scavenging ROS, realizing specific and effective IBD treatment.

## 3.2. Experimental section

### 3.2.1 Materials and instruments

**Materials:** Casein phosphopeptide (99%) was bought from Xi'an Binghe Biological Technology Co., Ltd.. Genipin (97%) was bought from Tci (Shanghai) Development Co., Ltd.. 2,2'-azinobis-3-ethylbenzothiazoline-6-sulfonic acid (ABTS) (98%) was purchased from Beijing Innochem Science & Technology Co., Ltd.. 2',7'-Dichlorodihydrofluorescein diacetate (DCFH-DA) was got from MedChemexpress Co., Fetal bovine serum (FBS), Penicillin-Streptomycin Solution (100X) and Methylthiazolyldiphenyl-tetrazolium bromide (MTT) (98%), phosphate-buffered saline solution (PBS), and Dulbecco's Modified Eagle Medium (DMEM) were brought from Beijing Solarbio Science &Technology Co.,Ltd.. Dextran sulfate sodium salt (DSS, MW 40,000) was obtained from Shanghai Macklin Biochemical Co.,Ltd.. Indocyanine green (ICG, 90%) was brought from J&K Scientific Co.,Ltd.. DSPE-PEG2K-CY5 was brought from Xi'an ruixi Biological Technology Co.,Ltd.. IR806

(90%) was obtained from Sigma-Aldrich Co.,Ltd. All chemicals were used as provided unless further stated.

**Instruments:** Transmission scanning electron microscope (TEM) image of GCPP NPs was captured by a JEOL JEM-1011 and operated at an acceleration voltage of 100 kV Transmission scanning electron microscope (SEM) image of GCPP NPs was captured by a JEOL S-4800, and operated at an acceleration voltage of 10 kV. The dynamic light scattering (DLS) and zeta potential measurements of GCPP NPs were measured by a Malvern instrument (Zetasizer Nano ZS ZEN3600). The hydrodynamic diameter (denote as size in the following contexts) of GCPP NPs was obtained by multi-exponential fitting using a spherical model. Ultraviolet/visible (UV/vis) absorbance spectra were tested by a Shimadzu UV-2600 spectrophotometer. Fourier transform infrared spectroscopy (FTIR) spectra were obtained by a TENSOR 27 FTIR spectrometer (BRUKER) with the spectral resolution of 2 $cm^{-1}$. The cell viability was evaluated by using the MTT assay, the absorbance at 490 nm of MTT was measured by a microplate reader (Multiskan FC, Thermo Fisher Scientific). Confocal laser scanning microscopy (CLSM) images of cells were captured by an Olympus FV1000 instrument. The fluorescence images were captured by an *in vivo* imaging system (PerkinElmer, IVIS Spectrum).

### 3.2.2 Synthesis of GCPP NPs

50 μL of CPP dissolved in water (10 mg $mL^{-1}$) and 50 μL of Genipin dissolved in water (5 mg $mL^{-1}$) were mixed in 900 μL of water. After sonicate for 1 min, the mixture was placed in a water bath at a constant temperature of 60 ℃ for 75 h. During incubation, the mixture gradually underwent color change from achromatic color to dark blue color, indicating production of GCPP NPs accompanied by deposition of particles. Before characterization and other bioapplications, GCPP NPs were purified by ultracentrifugation for 10 min, followed by redispersion in water and refrigerated at 4 ℃.

### 3.2.3 Stability of GCPP NPs

Firstly, the simulated gastric fluid was prepared with 50 mM of NaCl and 3.2 mg $mL^{-1}$ of pepsin at pH 1.2±0.3. The simulated intestinal fluid was obtained with 12.5 mg $mL^{-1}$ of bile salt and 8 mg $mL^{-1}$ trypsin from porcine pancreas in phosphate-buffered saline (10 mM, pH 7.4). Secondly, GCPP NPs were incubated in the simulated gastric fluid and the simulated intestinal fluid for 4 h and 24 h, respectively.[26,27] Meanwhile, the UV/vis absorbance intensity of GCPP NPs incubated with the simulated intestinal fluid and the intestinal fluid at 37 ℃ for 72 h were recorded by a UV/vis spectrophotometer. Thirdly, 10-fold (v/v) dilution of GCPP NPs suspension was made with water, PBS (pH 7.4) and DMEM with 10% (v/v) FBS and incubated at 37 ℃ for 72 h. The DLS profile was applied to test the change of average size and size distribution.

### 3.2.4 ROS scavenging activity of GCPP NPs

ABTS dissolved in water (7 mM) and potassium persulfate dissolved in water (2.45 mM) were equivalently mixed and kept for 12 h in the dark to obtain the ABTS radical

cations ($ABTS^{\cdot+}$) stock solution. The $ABTS^{\cdot+}$ stock solution was diluted by PBS for guaranteeing the absorbance intensity of $ABTS^{\cdot+}$ at 734 nm being 0.7±0.02 by the UV/vis spectrophotometer. Next, the diluted $ABTS^{\cdot+}$ stock solution was treated with the different concentrations of GCPP NPs, and the UV/vis spectrophotometer was used to record the absorbance intensity of $ABTS^{\cdot+}$ at 734 nm after 5 min incubation at the room temperature. ROS scavenging ratio was calculated according to the following equation:

$$Scavenging\ ratio\ (\%) = \frac{\text{Abs@734nm, control} - \text{Abs@734nm, sample}}{\text{Abs@734nm, control}} * 100\% \quad (1)$$

### 3.2.5 Cytotoxicity evaluation *in vitro*

The mouse embryonic fibroblast (3T3) cell line was chosen to assess the cytotoxicity of GCPP NPs. 3T3 cells were cultivated with 10 mL of DMEM medium containing 10% (v/v) of FBS, 1% (v/v) of Penicillin-Streptomycin Solution (100X). 3T3 cells were subcultured every three days. Cells at a density of $1 \times 10^5$ cells $well^{-1}$ were seeded in 96-well plates overnight. Then 3T3 cells were treated with different concentrations of GCPP NPs (10, 20, 40, 60, 80, and 100 μg $mL^{-1}$) for 24 h. Afterwards, cells were incubated with MTT (5 mg $mL^{-1}$) for 4 h, followed by calculating cell viabilities using a Microplate Reader under absorbance of 570 nm.

### 3.2.6 ROS scavenging activity evaluation of GCPP NPs in cells

Firstly, different concentrations of $H_2O_2$ (0, 10, 20, 40, 60, 80, 100, 150, 200 μM) were incubated with 3T3 cells at a density of $1 \times 10^5$ cells $well^{-1}$. The median lethal dose ($LD_{50}$) value of $H_2O_2$ was determined to be 100 μM. Secondly, 3T3 cells at a density of $1 \times 10^4$ cells $well^{-1}$ were incubated with different concentrations of GCPP NPs (10, 20, 40, 60, 80, and 100 μg $mL^{-1}$) for 24 h, cells continued to be treated with fresh medium (control) and 100 μM of $H_2O_2$. After incubation for another 24 h, the cell viability was tested by the MTT assay.

### 3.2.7 Detection of ROS in cells

3T3 cells were equably seeded in petri dishes ($2\times10^5$ cells) and cultured overnight. After incubating 3T3 cells with 20 μg $mL^{-1}$ of GCPP NPs for 24 h, 1 mL of $H_2O_2$ dispersed cell culture (100 μM) was used to continue incubate cells for 24 h to mimic the oxidation environment. Then 3T3 cells were co-incubated with 10 μM of DCFH-DA as the oxidant-sensing probe for 5 min before captured by a CLSM (excitation wavelength at 488 nm).

### 3.2.8 Preferential localization of GCPP NPs to the inflamed colon

All animal experiments were approved by the Institution Animal Care and Use Committee in compliance with Chinese law for experimental animals. Female C57BL/6 mice were brought from Vital Animal Technology Co. Ltd.. Fifteen female C57BL/6 mice were DSS-fed mice with drinking water containing 3% (w/v) DSS for 5 days. 50 μL of indocyanine green (ICG) solution (10 mg $mL^{-1}$) and 1 mL of GCPP NPs (3 mg $mL^{-1}$) were mixed and stirred for 24 h. After washing with deionized water once, ICG-

loaded GCPP NPs were obtained. Firstly, three female C57BL/6 mice were explored for *in vivo* fluorescence imaging over time. Before imaging, DSS-induced colitis mice were fasted overnight. The *in vivo* fluorescence images of DSS-induced colitis mice fed by ICG-loaded GCPP NPs, were captured by the imaging system for 5 min, 2 h, 6 h, 10 h, and 24 h, respectively. Then twelve female C57BL/6 mice were randomly divided into three groups. After oral delivery for 6 h, liver, heart, lung, spleen, kidneys, and colon were collected and imaged by the imaging system, then corresponding fluorescence intensity was measured.[8] Similar procedures have been employed using the DSPE-PEG2K-CY5 (50 μL of 20 mg $mL^{-1}$) and the IR806 (100 μL of 5 mg $mL^{-1}$) fluorescence dyes to label 1 mL of 3 mg $mL^{-1}$ GCPP NPs. After labeling for 24 h, fluorescence labeling GCPP NPs were washed by deionized water. DSPE-PEG2K-CY5 modified GCPP NPs and IR806-loaded GCPP NPs were orally delivered to DSS-induced colitis mice. After 6 h, liver, heart, lung, spleen, kidneys, and colon were collected. The fluorescence images were captured by an *in vivo* imaging system.

### 3.2.9 Anti-inflammatory effect of GCPP NPs *in vivo*

Twenty-four female C57BL/6 mice with average weight of 16-20 g were acclimatized for one week. Except for the six mice were fed with pure water in the control group, the other mice were DSS-fed mice with drinking water containing 3% (w/v) DSS for 5 days. After drinking DSS for 5 days, their drinking water was replaced by pure water. Either CPP or GCPP NPs (30 mg $kg^{-1}$) were orally administrated every other day until the $14^{th}$ day. After 14 days, colon length was measured. Major organs (liver, heart, lung, spleen, kidneys, and colon) were collected from all mice, and histological assessed via a hematoxylin and eosin (H&E) staining method.

## 3.3. Results and discussion

### 3.3.1 Synthesis and characterization of GCPP NPs

It has been reported that CPP contains multiple components and the critical sequence of -Ser(P)-Ser(P)-Ser(P)-Glu-Glu- (P denotes phosphate groups), which has antioxidant activity to scavenge ROS via chelating multivalent cations.[28,29] To overcome these drawbacks of rapid hydrolysis or enzymatic degradation and rapid metabolism during therapy, CPP were covalent-assembled with Genipin to fabricate GCPP NPs by covalent interaction.[22] According to reported covalent interaction associated with Genipin, amide groups could occur nucleophilic reaction with olefinic carbon atom at C-3 during attacking on deoxyloganin aglycone of Genipin. Accompanied by opening the dihydropyran ring, N-heterocyclic intermediates were produced, and were dimerized to from π-conjugated compounds under oxygen radicals (Figure S3.1).[30] GCPP NPs were obtained by mixing CPP with Genipin at 60 ℃ for 75 h. The solution color of the CPP and Genipin mixture gradually transformed from transparent to blue. During this process, the molar ratio of CPP/Genipin was close to 1:5. In addition, the reaction ratio of Genipin was up to 98% by the standard curve of Genipin and UV/vis absorption at 241 nm of Genipin dispersed in transparent supernatant solution after ultrahigh centrifugation (Figure S3.2a, b). Based on excess Genipin, CPP could be completely covalent cross-linked to form blue compounds. As Figure 3.1a, b showed

that as-obtained GCPP NPs exhibited spherical particles by TEM and SEM images. As illustrated by Figure S3.3a and b, the size distribution of GCPP NPs was 95±20 nm by particle-size statistic from TEM and SEM images. The particle size (hydrodynamic diameter) and the surface charge of GCPP NPs were 116±20 nm and -22.3 mV determined by DLS profile (Figure 3.1c) and Zeta potential measurements. In comparison with particle-size statistics from TEM and SEM images, the size distributions of GCPP NPs from DLS profile were close to 120 nm due to surface hydration of the amphiphilic nanoparticles dispersed in water. As UV/vis spectra shown, as-obtained GCPP had a UV/vis absorbance at 600 nm compared with either CPP or Genipin, suggesting that GCPP NPs were synthesized through generation of new covalent bond (Figure 3.1d). FTIR spectra was further employed to confirm the covalent reaction of GCPP. Figure 1e exhibited the disappearance of C−O−C stretching signal at 1100 $cm^{-1}$ and hydroxyl group at 3248 $cm^{-1}$ and appearance of C=C stretching of cycloolefin at 1623 $cm^{-1}$, indicating that dihydropyran ring of Genipin was opened and cycloolefin was formed.[31] The disappearance of amide I signal at 1650 $cm^{-1}$ from CPP and the appearance of pyridine signal at 1608 $cm^{-1}$ appeared suggested that the amino groups was reacted.[32,33] In addition, the signal at 1630 $cm^{-1}$ represented the conjugated alkenes signal from GCPP NPs.[22] These results indicated that CPP and Genipin can undergo a covalently-triggered assembly way to form well-defined GCPP NPs.

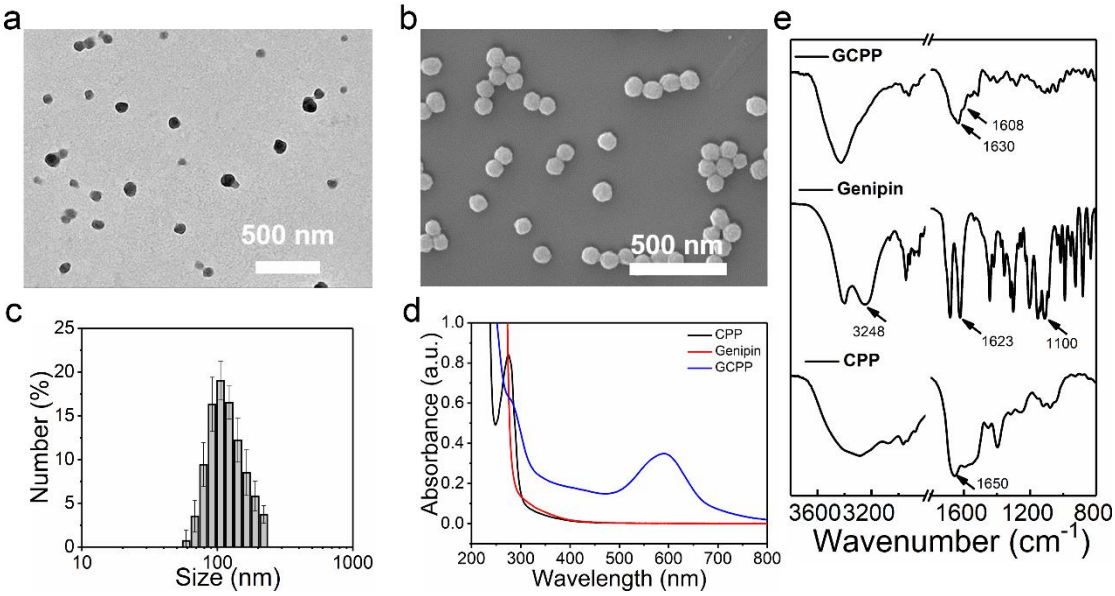


**Figure 3.1** Structural and spectral characterizations of GCPP NPs. (a) TEM and (b) SEM images of GCPP NPs. (c) DLS size profile of GCPP NPs. (d) UV/vis absorbance spectra of CPP, Genipin and GCPP NPs. (e) FTIR spectra of CPP, Genipin and GCPP NPs.

### 3.3.2 The stability evaluation of GCPP NPs

Oral delivery is the most preferred strategy compared with other drug administration owing to high convenience, low cost, and simple preservation process.[34-36] Nevertheless,

there are harsh pH/enzymatic conditions in the gastrointestinal tract, leading to rapid enzymatic degradation and lower delivery efficiency of the bioactive substances.[37,38] Therefore, the stability evaluation of GCPP NPs was necessary to get through the oral delivery route. First, we tested the zeta potential of GCPP NPs in simulated gastrointestinal fluid with different pH conditions. the average zeta potentials of GCPP NPs in the simulated gastric fluid (pH 1.2), neutral physiological solution (pH 7.4) (pH 7.4) and the simulated intestinal fluid (pH 8.1) were -7.61, -24.4 and -26.3, respectively (Fig.S3.4). Based on retaining negatively charged property, it indicated that GCPP NPs possessed good stability under various pH conditions. Next, the stability of GCPP NPs further was accessed by TEM. GCPP NPs were incubated with simulated gastric fluid (pH 1.2±0.3) at 37 ℃ for 72 h. As shown in Figure 3.2a, the morphology of GCPP was not obviously altered at different time points (0, 4, 8, 24, 48, 72 h), which demonstrated that the nanostructure of GCPP NPs were stable in the acidic gastric fluid with the existence of pepsin at low pH. Additionally, UV/vis UV-2600 spectrophotometer was used to test the change of absorption peak of covalent bond at 600 nm. The UV/vis absorbance intensity (at 600 nm) of GCPP NPs dispersed in the simulated gastric fluid did not remarkably reduce for 72 h (Figure 3.2b). These results implied that GCPP had minimized enzymatic degradation upon passing through the stomach. Simultaneously, GCPP NPs were treated with the simulated intestinal fluid (pH 7.4) at 37 ℃ for 72 h. The nanostructure of GCPP maintained integrity (Figure 3.2c). After incubating with the simulated intestinal fluid for 72 h, the UV/vis absorbance intensity at 600 nm of GCPP exhibited slightly increased due to their further aggregation during long-term incubation (Figure 3.2d). This result was consistent with the TEM image at 72 h, in which the size of GCPP NPs slightly increased. The results revealed that GCPP NPs were favorable for oral administration based on their good stability in simulated gastrointestinal fluid. After passing through the epithelial barrier, GCPP NPs might perform intravasation. Therefore, the stability of GCPP NPs need to be further investigated under other physiological conditions. 10-fold (v/v) dilutions of GCPP NPs were created with water at 37 ℃ for 72 h, the unaltered average sizes and size distributions of GCPP NPs indicated that GCPP NPs possessed good stability **(**Figure 3.2e). Then 10-fold (v/v) dilutions of GCPP NPs were created with PBS (pH 7.4) and DMEM medium supplemented with 10% (v/v) FBS and incubated at 37 ℃ for 72 h. As shown in Figure 3.2f, g, the average sizes and size distributions of GCPP NPs remained unchanged, suggesting GCPP NPs were stable enough under these physiological conditions.

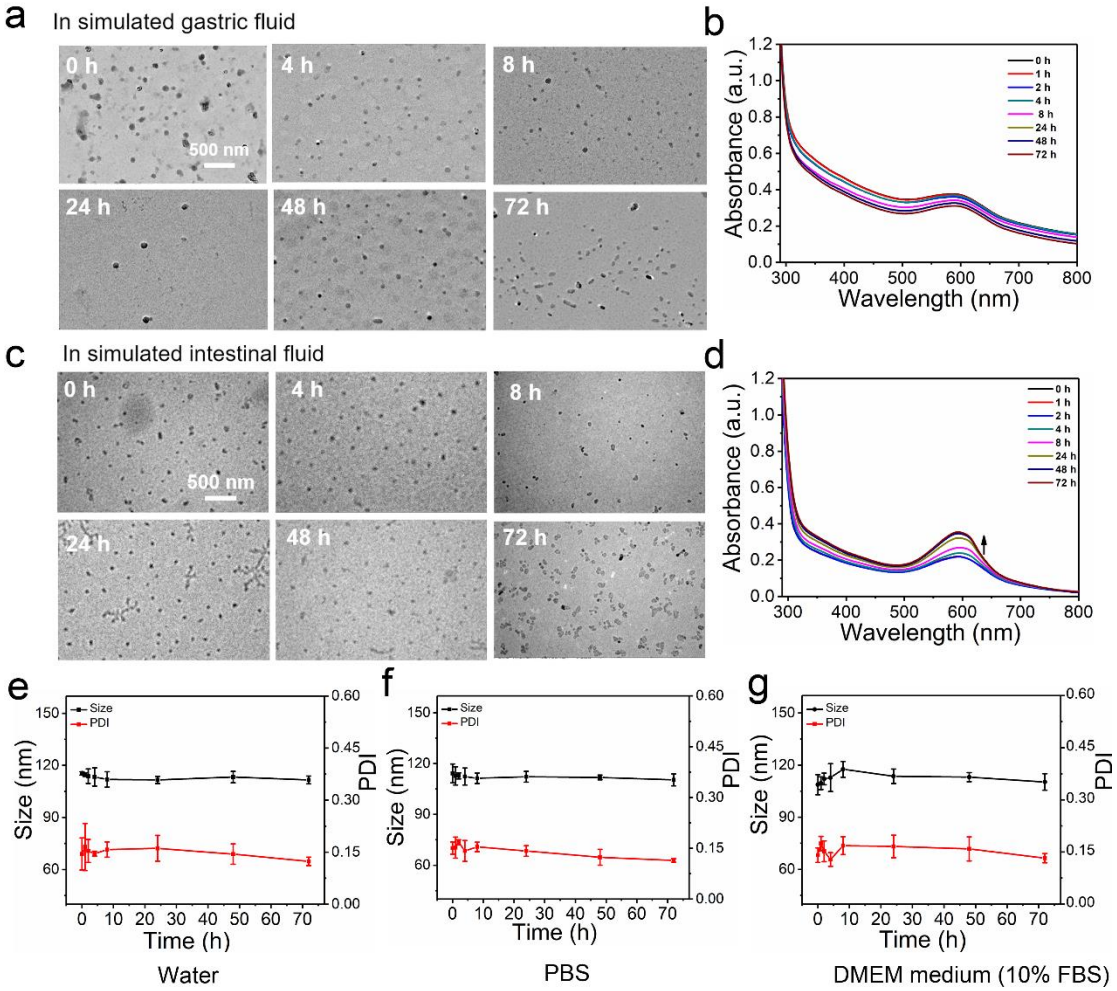


**Figure 3.2** The stability evaluation of GCPP NPs. (a) TEM images of GCPP NPs incubated with the simulated gastric fluid at 37 ℃ for 72 h. (b) The UV/vis absorbance intensity of GCPP NPs treated with the simulated gastric fluid. (c) TEM images of GCPP NPs incubated with the simulated intestinal fluid at 37 ℃ for 72 h. (d) The UV/vis absorbance intensity of GCPP NPs incubated with the simulated intestinal fluid at 37 ℃ for 72 h. Dilute stability evaluation of GCPP NPs incubated with water (e), PBS (F) and DMEM media containing 10% (v/v) FBS (f) at 37 °C for 24 h, respectively. repeated experiments=3).

### 3.3.3 ROS scavenging activity evaluation of GCPP NPs *in vitro.*

CPP possesses antioxidant property through chelating metal ions such as $Ca^{2+}$, $Fe^{2+}$, $Cu^{+}$, and $Zn^{2+}$ to function as divalent metal catalysts and eliminate oxidation reactions.[28] The antioxidant ability of GCPP NPs were measured via the ABTS assay. The prepared $ABTS^{\cdot+}$solution was incubated with different concentrations of CPP solutions (0, 0.04, 0.08, 0.12, 0.16 and 0.20 mg $mL^{-1}$) for 5 min, showing that the absorbance peak of $ABTS^{\cdot+}$ at 734 nm gradually decreased (Figure S5a). Next, the ROS scavenging ratio of CPP was calculated, reaching up to 94.7% at 0.20 mg $mL^{-1}$ of CPP (Figure 3.3a). The ROS scavenging activity of GCPP NPs was assessed through the same method. Because the absorbance intensity of $ABTS^{\cdot+}$ at 734 nm was elevated due to the UV/vis absorbance of GCPP NPs at 600 nm, especially at high concentration of GCPP NPs

(Figure S3.5b). Therefore, the ROS scavenging ratio of GCPP NPs at low concentration was further investigated. The ROS scavenging ratio of GCPP NPs at 0.04 mg $mL^{-1}$ was assessed by compared with CPP at 0.04 mg $mL^{-1}$. Figure 3.3b showed that the ROS scavenging ratio of CPP and GCPP NPs were 51.8% and 54.5%, respectively. The result indicated that the covalent reaction between CPP and Genipin for formation of GCPP NPs did not reduce the ROS scavenging activity of CPP. This ensured the feasibility of subsequent oral administration of GCPP NPs for disease treatment.

Next, ROS-responsive disruption of GCPP NPs was further explored to test whether it disintegrated or disrupted under oxidation. The UV/vis absorbance spectra and size of GCPP NPs (equivalent concentration of CPP: 50 μg $mL^{-1}$) were measured after incubating with different concentrations of $H_2O_2$ (0.01, 0.1, 1,10, 100, 1000 mM). As the concentration of $H_2O_2$ increased, UV/vis absorbance intensity of GCPP NPs at 600 nm was decreased dramatically. The color of GCPP solution gradually became lighter with the increase of $H_2O_2$ concentrations (Figure 3.3c). As Figure 3.3d shown, the size of GCPP NPs gradually decreased, which was consistent with decreased UV/vis absorbance. Above all, these results suggested that GCPP NPs could be disintegrated or disrupted in response to ROS.

Based on GCPP NPs for oral delivery, the ROS scavenging activity of GCPP NPs in the simulated gastrointestinal fluid was further assessed via the ABTS assay. GCPP NPs were incubated with the simulated gastric fluid at 37 ℃ for 4 h.[37] ROS scavenging ratio of GCPP NPs (0.04 mg $mL^{-1}$) was calculated every hour. In contrast to 49.2% of scavenging ratio in the control group, the scavenging ratio for every hour was 13.3%, 17.5%, 22.0% and 23.0%. This result demonstrated that the antioxidant performance of GCPP NPs in the simulated gastric fluid was inhibited compared with GCPP NPs in water, which attributed to form stable ABTS molecule in the presence of a large number of $H^+$ cation.[39] It was favorable for oral delivery with the purpose of controlled release and antioxidation **(**Figure 3.3e**)**. Then the ROS scavenging activity of GCPP NPs in the simulated intestinal fluid was tested using the same method. GCPP NPs (0.04 mg $mL^{-1}$) were incubated with the simulated intestinal fluid at 37 ℃ for 24 h. The scavenging ratios were not altered at different time points (1, 2, 3, 4, 6, 8 and 24 h) compared with GCPP NPs in water (Figure 3.3f). These results corroborated that GCPP NPs possessed good stability in the simulated gastric fluid and intestinal fluid, presenting high potential for oral administration. Importantly, GCPP NPs exhibited property of controlled antioxidation, which was benefit for employing IBD treatment due to sustainably effective ROS scavenging activity in the intestinal fluid.

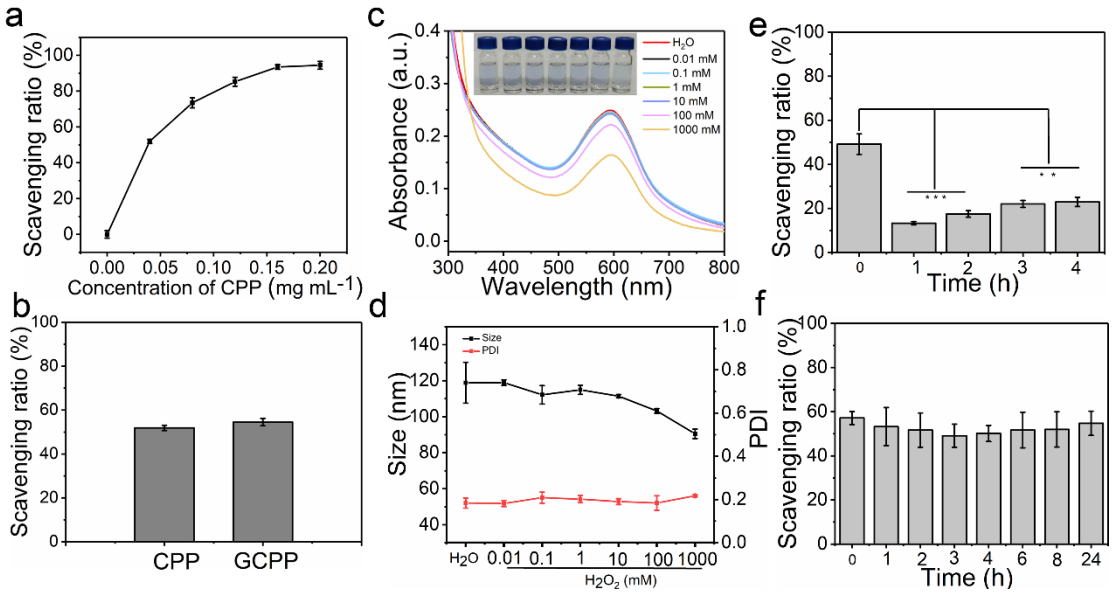


**Figure 3.3** ROS scavenging activity evaluation of GCPP NPs *in vitro*. (a) The ROS scavenging ratio of CPP at different concentrations (0, 0.04, 0.08, 0.12, 0.16 and 0.20 mg $mL^{-1}$, repeated experiments=3) (b) The contrast of ROS scavenging ratio of CPP and GCPP NPs at 0.04 mg $mL^{-1}$, repeated experiments=3) (c) UV/vis absorbance spectra of GCPP NPs (equivalent concentration of CPP: 0.5 mg $mL^{-1}$) as incubated with different concentrations of $H_2O_2$. (d) The size alteration of GCPP NPs incubated under different concentrations of $H_2O_2$ (equivalent concentration of CPP: 0.5 mg $mL^{-1}$, repeated experiments=3) (e) The ROS scavenging activity evaluation of GCPP NPs in the simulated gastric fluid (equivalent concentration of CPP: 0.04 mg $mL^{-1}$, repeated experiments=3). (f) The ROS scavenging activity evaluation of GCPP NPs in the simulated intestinal fluid (equivalent concentration of CPP: 0.04 mg $mL^{-1}$, repeated experiments=3).

### 3.3.4 Biocompatibility and ROS scavenging activity of GCPP NPs *in vitro*

The biosafety of GCPP NPs is significant for biomedical application. Thereafter, the cytotoxicity of GCPP was evaluated using 3T3 cells. The viability of 3T3 cells treated with different concentrations of GCPP NPs (10, 20, 40, 60, 80, 100 μg $mL^{-1}$) was measured by the MTT assay. Cells were viable after treating with up to 100 μg $mL^{-1}$ of GCPP NPs, and very limited cell death was observed (within error <10%) as tested by the MTT assay (Figure 3.4a).

Moreover, the oxidation toxicity of $H_2O_2$ and the antioxidation activity of GCPP NPs were further explored using 3T3 cells. To induce oxidative stress and cell damage, 3T3 cells were treated with $H_2O_2$.[40] Firstly, the $LD_{50}$ $H_2O_2$ to 3T3 cells was examined using the MTT assay. Cells were treated with different concentrations of $H_2O_2$ (10, 20, 40, 60, 80, 100, 150, 200 μM), and the $LD_{50}$ value of $H_2O_2$ was 100 μM (Figure 3.4b). Next, ROS scavenging activity of GCPP NPs was investigated parallelly using 3T3 cells. After incubating 3T3 cells with different concentrations of GCPP NPs (10, 20, 40, 60, 80, 100 μg $mL^{-1}$) for 24 h, cells continued to be incubated with 100 μM of $H_2O_2$ for 24 h. As shown in Figure 3.4c, the cell viability was elevated with the increased concentration of GCPP NPs. Thence, it indicated that the GCPP NPs could prevent cells

from $H_2O_2$ damage. Furthermore, the antioxidant effect of GCPP NPs was directly observed by CLSM. DCFH-DA as the oxidant-sensing probe was used to detect ROS generation.[41] After incubation 3T3 cells with 20 μg $mL^{-1}$ of GCPP NPs for 24 h, cells were incubated with additional 100 μM of $H_2O_2$ for 24 h. Before capture by CLSM (excited at 488 nm), 3T3 cells were co-incubated with 10 μM DCFH-DA. As the CLSM images shown, the fluorescence signal intensity of ROS from cells treated with combination of GCPP NPs and $H_2O_2$ lowered compared with that of individual $H_2O_2$, suggesting that GCPP NPs possessed antioxidant property (Figure 3.4 d, e).

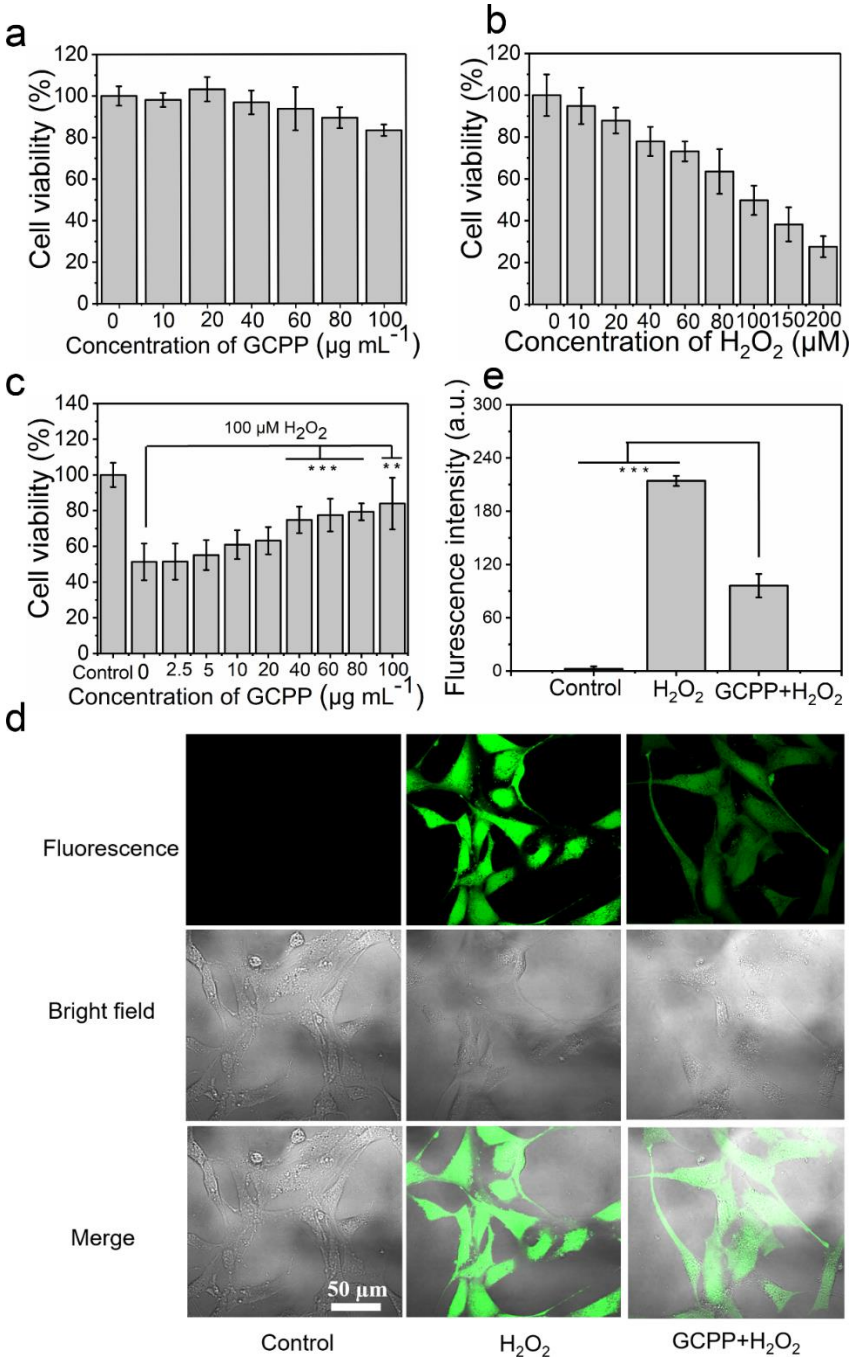


**Figure 3.4** Antioxidation evaluations of GCPP NPs *in vitro*. (a) The cytotoxicity evaluation of GCPP NPs at 3T3 cells incubated with different concentrations of GCPP NPs (equivalent concentration of CPP: 10, 20, 40, 60, 80,100 μg $mL^{-1}$, repeated

experiments=5). (b) The $LD_{50}$ determination of $H_2O_2$ at 3T3 cells incubated with different concentrations of $H_2O_2$ (repeated experiments=5). (c) Antioxidant activity evaluation of GCPP NPs pretreated 3T3 cells from $H_2O_2$-induced oxidative stress (** indicates $p<0.01$, *** indicates $p<0.001$, repeated experiments=5). (d) Fluorescence intensity of ROS probed by DCFH-DA in cells after incubating with $H_2O_2$, the combination of GCPP NPs and $H_2O_2$ (** indicates $p<0.01$, repeated experiments=3). (e) CLSM images of 3T3 cells probed by DCFH-DA after incubating with individual $H_2O_2$, the combination of GCPP NPs and $H_2O_2$ (equivalent concentration of CPP: 40 $\mu g\ mL^{-1}$).

### 3.3.5 GCPP NPs preferentially localizing to the inflamed colon

In comparison with normal intestinal tissue, the inflamed colon has high tissue permeability and accumulated inflammatory cells and enriched charged proteins,[42-44] which benefits for NPs to more preferentially localize in such tissue than small molecules.[11,45,46] The next, anionic GCPP NPs were investigated whether or not to preferentially localized to the inflamed colon. Here, GCPP loaded with ICG were used for exploring biodistribution in the DSS-induced acute colitis model of mice. After centrifugation at 6000 rpm for 10 min, the ICG-loaded GCPP NPs were collected in the sediment. Fluorescence emission at 778 nm of the ICG/GCPP mixture suggested that ICG was successfully loaded into GCPP NPs **(**Figure S3.6**)**. Firstly, after oral delivery of ICG-loaded GCPP NPs, the fluorescence images of DSS-induced colitis mice were captured by *in viv*o imaging system at 5 min, 2 h, 6 h, 10 h, 24 h (Figure 3.5a). A quantitative analysis of fluorescence intensities of colitis mice abdomens exhibited a strong fluorescence signal at colitis mice abdomens after oral administration for 6 h. With the extension of observation time, the fluorescence signals at colitis mice abdomens gradually decreased, but were still obverted at 24 h (Figure 3.5b). In order to directly observe ICG-loaded GCPP NPs accumulated at in the inflamed colon, after oral delivery of ICG, the mixture of CPP and ICG, and the ICG-loaded GCPP NPs for 6 h, major organs (liver, heart, lung, spleen, kidneys, and colon) were collected from the DSS-induced colitis mice.[8] As shown in the fluorescence images, ICG and the ICG/CPP mixture could be obverted in the liver, while ICG-loaded GCPP NPs were considerably localized in the inflamed colon compared with other groups (Figure 3.5c). As shown in Figure 3.5d**,** a quantitative analysis of fluorescence intensity further confirmed that ICG-loaded GCPP NPs favorably accumulated in the inflamed colon, with less accumulation in the liver compared with ICG, the mixture of CPP and ICG. In addition, the DSPE-PEG2K-CY5) and the IR806 fluorescence dyes to label GCPP NPs. DSPE-PEG2K-CY5/GCPP NPs IR806/GCPP NPs were orally delivered to DSS-induced colitis mice. After 6 h, liver, heart, lung, spleen, kidneys, and colon were collected, resulting that GCPP NPs could preferentially localize in inflammation site (Figure S3.7) Collectively, the above results demonstrated that GCPP NPs were capable of passively accumulating in the inflamed colon, which achieved satisfactory therapeutic effect. The passive accumulation effect is closely related to the inflammation severity of the ulcerated regions and NPs with small size of less 100 nm.[12,45] Thus, GCPP NPs were further employed for IBD treatment.

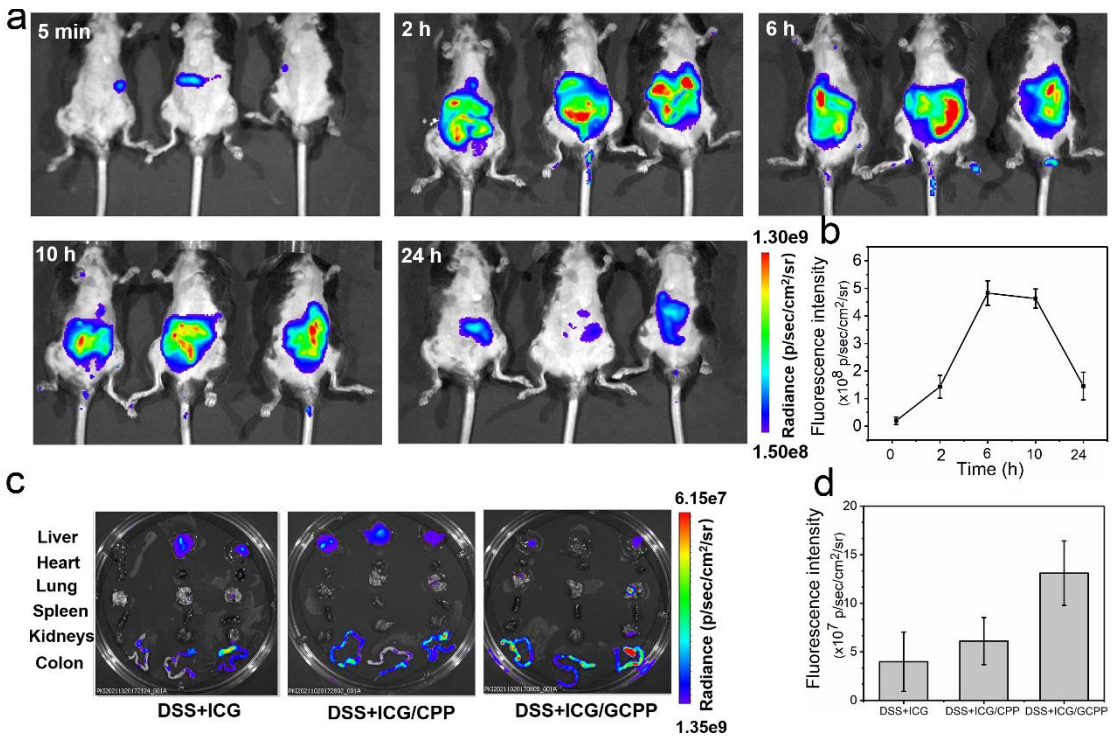


**Figure 3.5** GCPP NPs preferentially localizing to the inflamed colon. (a) Fluorescence images of 3% DSS-induced colitis mice at different time points after oral delivery of ICG-loaded GCPP NPs (n=3, excited at 745 nm). (d) Fluorescence intensity curve of colitis mice abdomens at various time points. (c) The fluorescence biodistribution images of ICG, the mixture of CPP and ICG, and ICG-loaded GCPP NPs in 3% DSS-induced colitis mice (n=3) after oral delivery for 6 h. (d) The quantitative analysis from the fluorescence imaging results of ICG, the mixture of CPP and ICG, and the ICG-loaded GCPP NPs in the inflamed colon.

### 3.3.6. Anti-inflammatory effect of GCPP NPs *in vivo*

GCPP NPs have exhibited remarkable advantages in scavenging ROS activity to protect cells and preferentially localize in the inflamed colon. Then the therapeutic efficacy of GCPP NPs was further evaluated in 3% DSS-induced colitis mice model. Twenty-four female C57BL/6 mice with average weight of 16-20 g were randomly divided into four groups, i.e. 6 mice in each group. These included a control group as mice treated by water and three DSS-induced acute colitis groups as mice treated by 3% DSS. The later three DSS-fed groups were orally administered by water (DSS group), CPP (DSS+CPP group), and GCPP NPs (DSS+GCPP NPs group) every other day for up to 14 days (Figure 3.6a), respectively. During the treatment period, the mice were observed daily. After drinking water containing 3% DSS for 5 days, DSS-induced acute colitis mice treated with water (DSS group) and CPP (DSS+CPP group) developed symptoms of diarrhea and bloody stools. DSS-induced acute colitis mice treated with GCPP NPs (DSS+GCPP NPs group) did not obviously develop symptoms of diarrhea and bloody stools. This observation suggested that GCPP NPs had good therapeutic effects in curing the IBD disease (Figure 3.6b). The body weight of all mice was recorded daily, the body weight of normal mice was stable in the control group. After treating for 7

days, the body weight of the colitis mice treated GCPP NPs gradually increased compared with other colitis mice. The body weight change of colitis mice treated with GCPP NPs was significantly lower than the other colitis mice treated with CPP or water, effectively alleviating inflammation through accumulating in inflamed colon and scavenging ROS (Figure 3.6c). As a key index, colon length is commonly used for evaluating the severity of DSS-induced acute colitis.[11] Thence, the colons were collected on the 14$^{th}$ day, and colon length were further measured. The colon length of colitis mice treated with water or CPP was 6.6±0.2 cm, 6.7±0.3 cm, respectively. Whereas the colon length of colitis mice treated by GCPP NPs was 8.3±0.8 cm, suggesting that GCPP NPs effectively attenuated colon shortening (Figure 3.6d, e). After treating for 14 days, major organs (liver, heart, lung, spleen, kidneys, and colon) were collected from normal mice and DSS-induced mice and then stained with H&E staining (Figure 3.6f). The pathological sections of major organs (liver, heart, lung, spleen, kidneys) did not exhibit obvious abnormalities in all mice, suggesting both CPP and GCPP NPs possessed high biocompatibility (Figure S3.8). In comparison with the colon histology from normal mice, colitis colons of colitis mice treated with water and CPP exhibited irregular morphology of colon (yellow arrow), edema, disruption of cryptal glands and infiltration of inflammatory cells (black arrow). Notably, the histology of colon of mice treated with GCPP NPs showed retention and regeneration of crypts (red arrow) and less infiltration of inflammatory cells, suggesting that GCPP NPs can be developed for treating the inflammation disease including IBD.

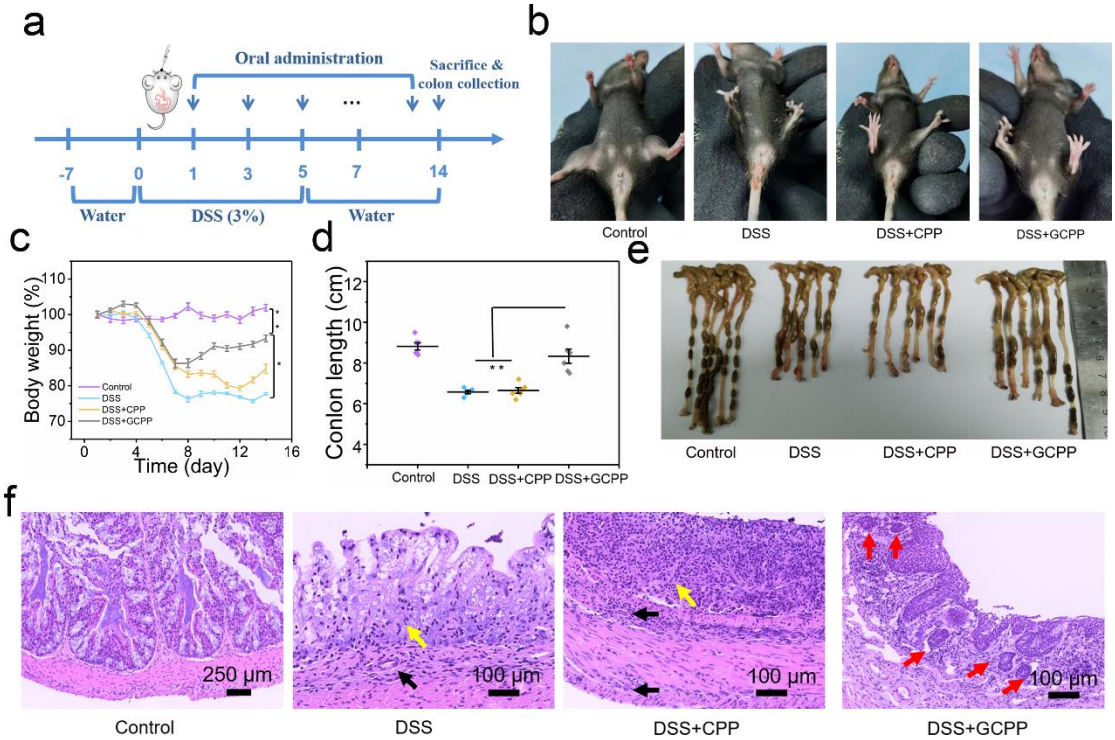


**Figure 3.6** Therapeutic efficacy of GCPP NPs in treating the DSS-induced colitis mice. (a) The experimental design of either CPP or GCPP NPs treating 3% DSS-induced acute colitis mice. The acute colitis mode was induced by drinking water containing 3% DSS for 5 days. Meanwhile, mice received water, CPP or GCPP NPs through oral

administration every other day from the first day to the 14$^{th}$ day. (b) Representative photographs of rectal areas of a normal mouse and DSS-induced acute colitis mice treated by water, CPP and GCPP NPs (on day 7) (the dotted line circle). (c) The body weight changes of normal mice, colitis mice treated with water, CPP and GCPP NPs, respectively. (d) The colon length changes and (e) photographs of colons of normal mice, colitis mice treated with water, CPP and GCPP NPs. (f) Colonic pathological sections of normal mice, colitis mice treated with water, CPP and GCPP NPs via H&E staining (black arrow: disruption of cryptal glands and infiltration of inflammatory cells, yellow arrow: irregular morphology of colon, red arrow: retention and regeneration of crypts). Scale bars: 100 or 250 μm. (n = 6; *P < 0.05, **P < 0.01)

### 3.4 Conclusions

We have designed and prepared robust peptide-based nanoparticles for IBD treatment via oral administration. An antioxidant peptide CPP is covalently assembled with iridoids Genipin to form GCPP NPs. Firstly, GCPP NPs possess robust nanostructure owing to covalent interaction enhancement, which perform good stability through harsh pH/enzymatic conditions in the simulated gastrointestinal fluids. Therefore, GCPP NPs are regarded as a promising candidate for oral administration with high compliance. Secondly, during evaluation of scavenging ROS in the simulated gastrointestinal fluid, GCPP NPs present special property of controlled antioxidation to sustainably scavenge ROS, which is conducive to treat IBD. Additionally, in vivo fluorescence profiles of various fluorescently-labeled GCPP NPs suggest that GCPP NPs preferentially accumulate at the inflamed colon site. Importantly, GCPP NPs promote crypt regeneration for effectively alleviating inflammation in the IBD model. All in all, GCPP NPs have been spotlighted as a potential peptide-based antioxidant nanoagent to treat ROS-related inflammation diseases. This study provides an alternative strategy to fabricate bioactive peptide nanoagents suitable for oral administration.

### Acknowledgements

This work was financially supported by the National Natural Science Foundation of China (Project Nos. 22025207, 22072154 and 21977095), Innovation Research Community Science Fund of China (No. 21821005), and the National Natural Science Foundation of Hebei Province (No. B2020103025). All the animal experiments in this work were conducted in accordance with protocols approved by the Animal Care and Use Committee of Institute of Process Engineering, Chinese Academy of Sciences, and in compliance with the Chinese law on experimental animals.

### 3.5 Supporting information

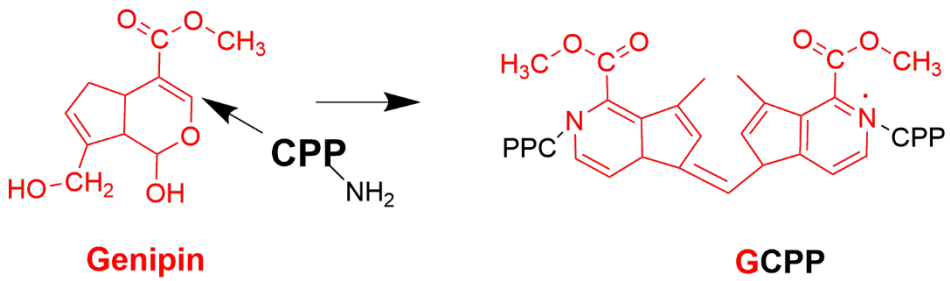


**Figure S3.1** Schematic illustration of the reaction mechanism between CPP and Genipin.

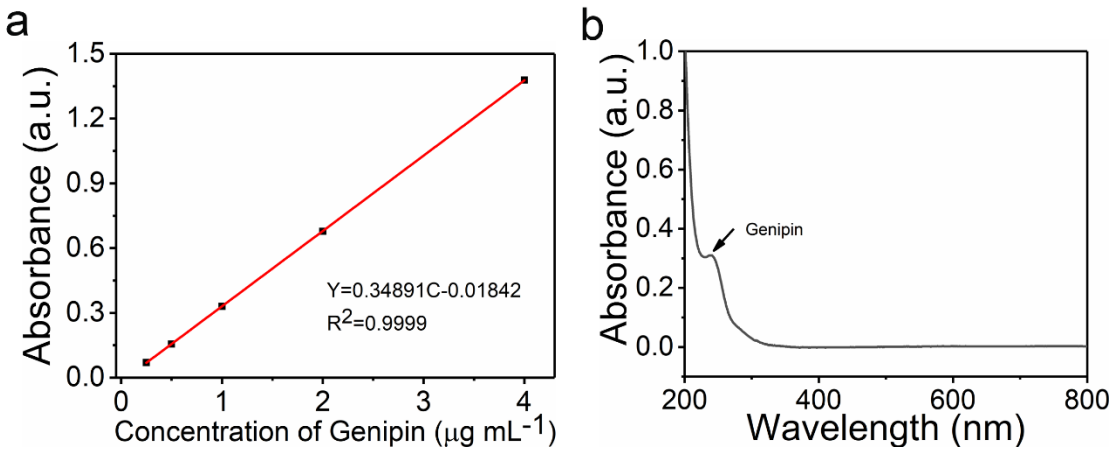


**Figure S3.2** (a) The standard curve of Genipin. (b) UV/vis absorption at 241 nm of Genipin dispersed transparent supernatant solution after ultrahigh centrifugation.

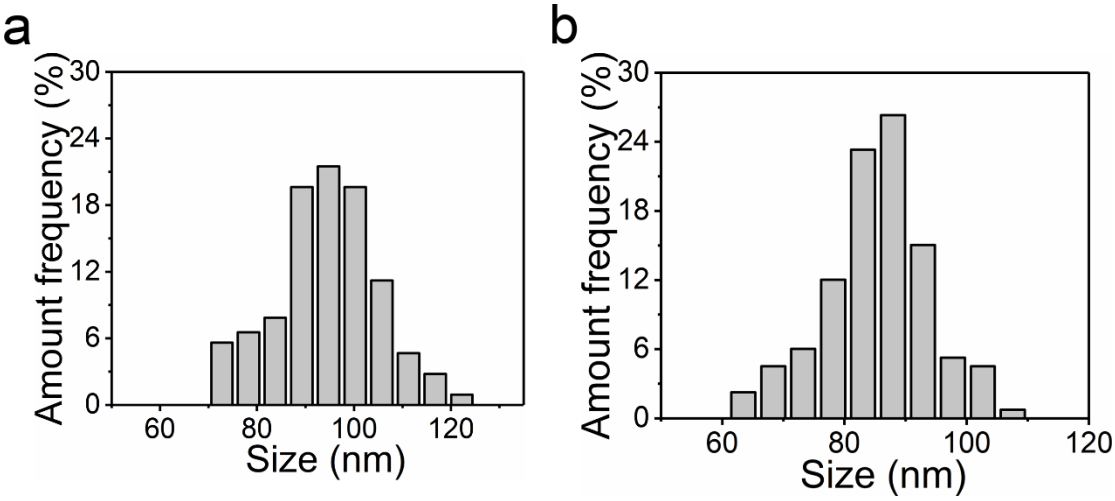


**Figure S3.3** (a) Particle-size statistics of GCPP NPs from TEM, (b) SEM images.

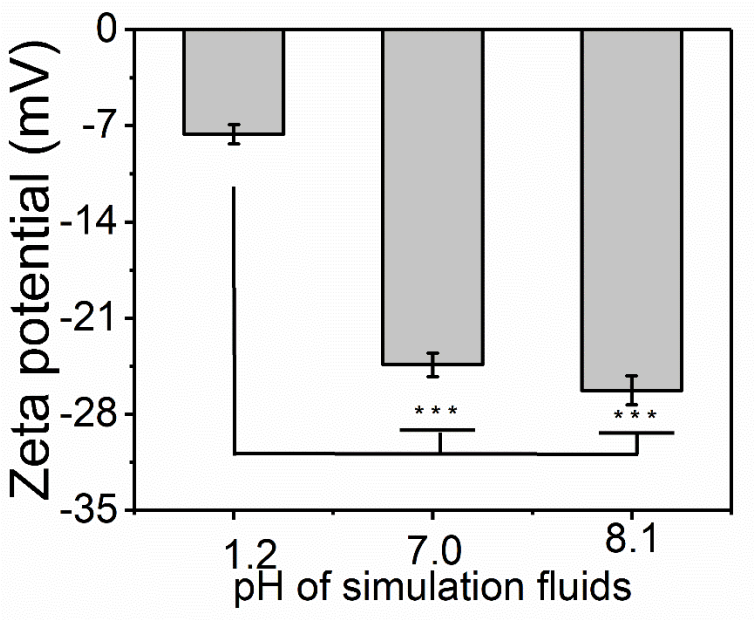


**Figure S3.4** Zeta potentials of GCPP NPs in the simulated gastric fluid (pH 1.2), neutral physiological solution (pH 7.4) and the simulated intestinal fluid (pH 8.1) (*** indicates $p<0.001$, repeated experiments=3).

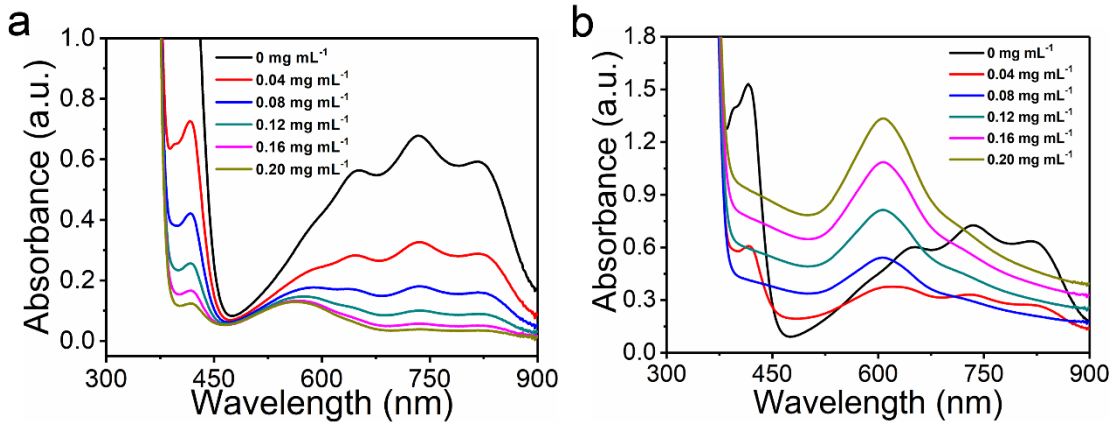


**Figure S3.5 (**a), (b) UV/vis absorbance spectra of $ABTS^{\cdot+}$ stock solution treated with CPP and GCPP with different concentrations.

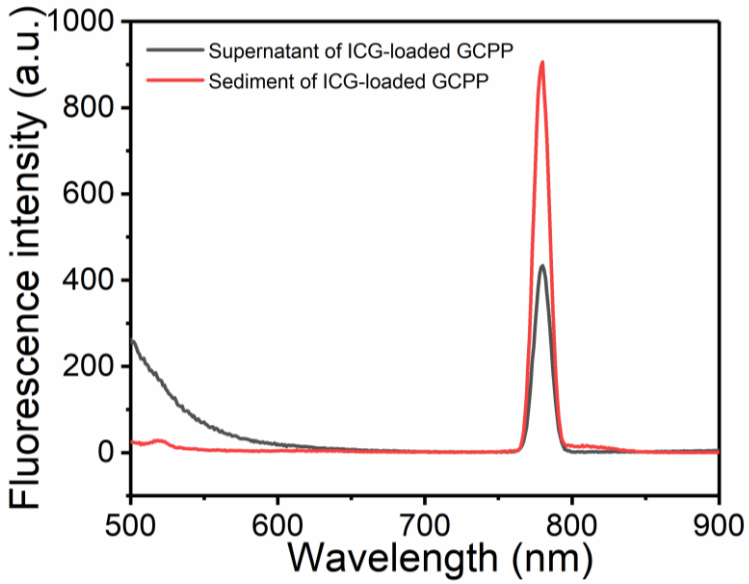


**Figure S3.6** Fluorescence emission spectra of supernatant and sediment of ICG-loaded GCPP NPs (equivalent concentration of CPP: 50 μg $mL^{-1}$, concentration of ICG: 100 μg $mL^{-1}$, excited at 778 nm).

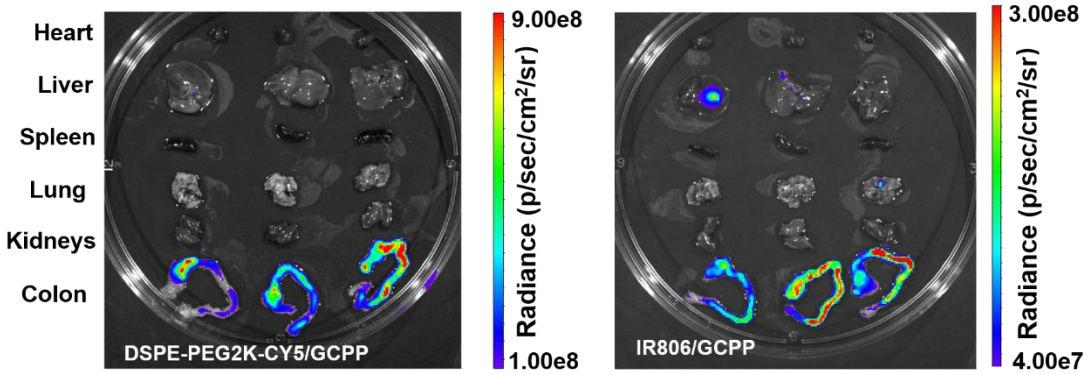


**Fig. S3.7** The fluorescence biodistribution images of DSPE-PEG2K-CY5/GCPP NPs and IR806/GCPP NPs in 3% DSS-induced colitis mice (n=3, excited at 650 nm, 745 nm)

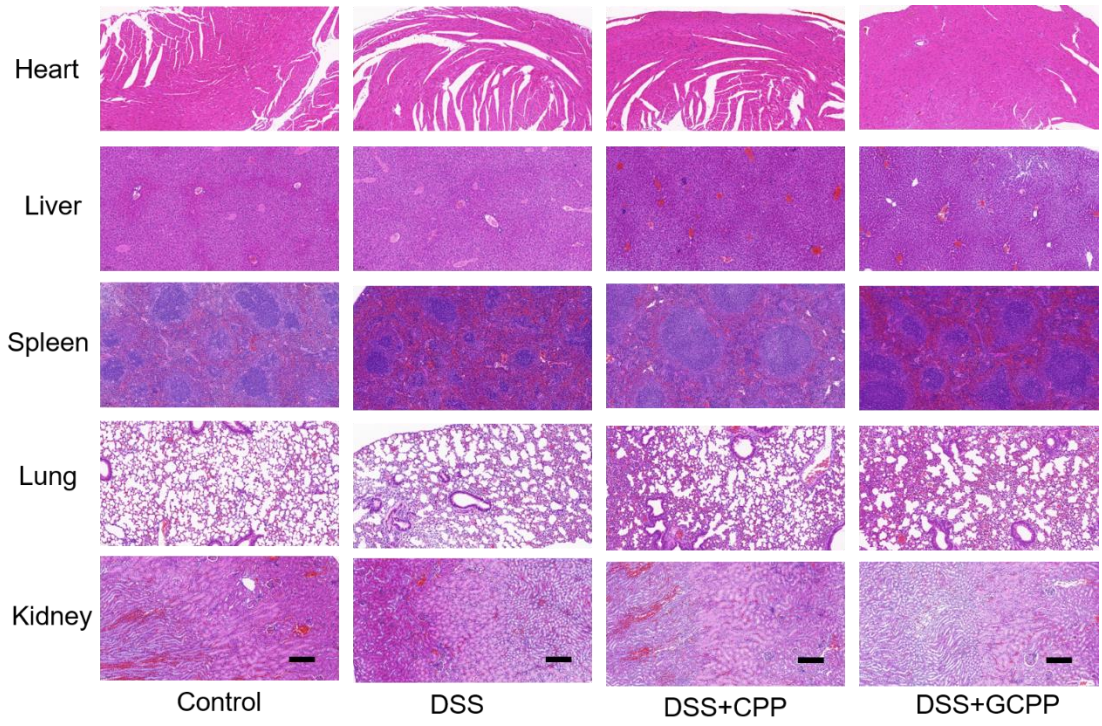


**Figure S3.8** H&E-stained sections of the major organs (heart, liver, spleen, lung, kidneys) of healthy mice and DSS-induced colitis mice treated with water and GCPP NPs (30 mg $kg^{-1}$), scale bar: 200 μm.

### 3.6 References

1. Zhang, Q.; Tao, H.; Lin, Y.; Hu, Y.; An, H.; Zhang, D.; Feng, S.; Hu, H.; Wang, R.; Li, X.; Zhang, J., A superoxide dismutase/catalase mimetic nanomedicine for targeted therapy of inflammatory bowel disease. *Biomaterials* **2016,** *105*, 206-221.

2. Chen, G.; Yu, Y.; Fu, X.; Wang, G.; Wang, Z.; Wu, X.; Ren, J.; Zhao, Y., Microfluidic encapsulated manganese organic frameworks as enzyme mimetics for inflammatory bowel disease treatment. *J Colloid Interface Sci* **2022,** *607*, 1382-1390.

3. Tu, Z.; Zhong, Y.; Hu, H.; Shao, D.; Haag, R.; Schirner, M.; Lee, J.; Sullenger, B.; Leong, K. W., Design of therapeutic biomaterials to control inflammation. *Nat. Rev. Mater.* **2022**.

4. Hu, B.; Yu, S.; Shi, C.; Gu, J.; Shao, Y.; Chen, Q.; Li, Y.; Mezzenga, R., Amyloid–Polyphenol Hybrid Nanofilaments Mitigate Colitis and Regulate Gut Microbial Dysbiosis. *ACS Nano* **2020,** *14*, 2760-2776.

5. Bernstein, C. N.; Fried, M.; Krabshuis, J. H.; Cohen, H.; Eliakim, R.; Fedail, S.; Gearry, R.; Goh, K. L.; Hamid, S.; Khan, A. G.; LeMair, A. W.; Malfertheiner; Ouyang, Q.; Rey, J. F.; Sood, A.; Steinwurz, F.; Thomsen, O. O.; Thomson, A.; Watermeyer, G., World Gastroenterology Organization Practice Guidelines for the diagnosis and management of IBD in 2010. *Inflamm Bowel Dis.* **2010,** *16*, 112-24.

6. Yuan, J.; Li, L.; Yang, Q.; Ran, H.; Wang, J.; Hu, K.; Pu, W.; Huang, J.; Wen, L.; Zhou, L.; Jiang, Y.; Xiong, X.; Zhang, J.; Zhou, Z., Targeted Treatment of Ischemic Stroke by Bioactive Nanoparticle-Derived Reactive Oxygen Species Responsive and Inflammation-Resolving Nanotherapies. *ACS Nano* **2021,** *15*, 16076-16094.

7. Xiao, B.; Ma, P.; Ma, L.; Chen, Q.; Si, X.; Walter, L.; Merlin, D., Effects of tripolyphosphate on

cellular uptake and RNA interference efficiency of chitosan-based NPs in Raw 264.7 macrophages. *J. Colloid Interface Sci.* **2017,** *490*, 520-528.
8. Lee, Y.; Sugihara, K.; Gillilland, M. G., 3rd; Jon, S.; Kamada, N.; Moon, J. J., Hyaluronic acid-bilirubin nanomedicine for targeted modulation of dysregulated intestinal barrier, microbiome and immune responses in colitis. *Nat. Mater.* **2020,** *19*, 118-126.
9. Sela-Passwell, N.; Kikkeri, R.; Dym, O.; Rozenberg, H.; Margalit, R.; Arad-Yellin, R.; Eisenstein, M.; Brenner, O.; Shoham, T.; Danon, T.; Shanzer, A.; Sagi, I., Antibodies targeting the catalytic zinc complex of activated matrix metalloproteinases show therapeutic potential. *Nat. Med.* **2012,** *18*, 143-147.
10. Zhang, S.; Ermann, J.; Succi, M.; Zhou, A.; Hamilton, M. J.; Cao, B.; Korzenik, J. R.; Glickman, J. N.; Vemula, P. K.; Glimcher, L. H., An inflammation-targeting hydrogel for local drug delivery in inflammatory bowel disease. *Sci. Transl. Med.* **2015,** *7*, 300ra128.
11. Chung, C. H.; Jung, W.; Keum, H.; Kim, T. W.; Jon, S., NPs Derived from the Natural Antioxidant Rosmarinic Acid Ameliorate Acute Inflammatory Bowel Disease. *ACS Nano* **2020,** *14*, 6887-6896.
12. Lamprecht, A., IBD: selective nanoparticle adhesion can enhance colitis therapy. *Nat. Rev. Gastro & Hepat.* **2010,** *7*, 311-2.
13. Hasani, S.; Pellequer, Y.; Lamprecht, A., Selective Adhesion of NPs to Inflamed Tissue in Gastric Ulcers. *Pharm. Res-dordr.* **2009,** *26*, 1149-1154.
14. Sarmadi, B. H.; Ismail, A., Antioxidative peptides from food proteins: a review. *Peptides* **2010,** *31*, 1949-56.
15.Torres-Fuentes, C.; Contreras, M. D. M.; Recio, I.; Alaiz, M.; Vioque, J., Identification and characterization of antioxidant peptides from chickpea protein hydrolysates. *Food Chem.* **2015,** *180*, 194-202.
16. Gauthier, S. F.; Pouliot, Y.; Saint-Sauveur, D., Immunomodulatory peptides obtained by the enzymatic hydrolysis of whey proteins - ScienceDirect. *Int. Dairy J.* **2006,** *16*, 1315-1323.
17. Shazly, A. B.; He, Z.; El-Aziz, M. A.; Zeng, M.; Zhang, S.; Qin, F.; Chen, J., Fractionation and identification of novel antioxidant peptides from buffalo and bovine casein hydrolysates. *Food Chem.* **2017,** *232*, 753-762.
18. Li, S.; Zhang, W.; Xing, R.; Yuan, C.; Xue, H.; Yan, X., Supramolecular Nanofibrils Formed by Coassembly of Clinically Approved Drugs for Tumor Photothermal Immunotherapy. *Adv. Mater.* **2021,** *33*, 2100595.
19. Liu, K.; Xing, R.; Zou, Q.; Ma, G.; Mohwald, H.; Yan, X., Simple Peptide-Tuned Self-Assembly of Photosensitizers towards Anticancer Photodynamic Therapy. *Angew. Chem. Int. Ed.* **2016,** *55*, 3036-9.
20. Cevaal, P. M.; Ali, A.; Czuba-Wojnilowicz, E.; Symons, J.; Lewin, S. R.; Cortez-Jugo, C.; Caruso, F., In Vivo T Cell-Targeting Nanoparticle Drug Delivery Systems: Considerations for Rational Design. *ACS Nano* **2021,** *15*, 3736-3753.
21.Cao, J.; Yu, H.; Wu, Y.; Wang, X., Occurrence and Biological Activities of Phenylpropionyl Iridoids. *Mini-Rev. Med. Chem.* **2019,** *19* , 292-309.
22 Liu, Y.; Shen, G.; Zhao, L.; Zou, Q.; Jiao, T.; Yan, X., Robust Photothermal Nanodrugs Based on Covalent Assembly of Nonpigmented Biomolecules for Antitumor Therapy. *ACS Appl. Mater. Interfaces* **2019,** *11* , 41898-41905.
23 Fujikawa, S.; Fukui, Y.; Koga, K.; Iwashita, T.; Komura, H.; Nomoto, K., Structure of

genipocyanin G1, a spontaneous reaction product between genipin and glycine. Tetrahedron Lett. 1987, 28, 4699-4700.
24. Ruirui Xing, Q. Z., Xuehai Yan, Peptide-based Supramolecular Colloids. *Acta Phys. -Chim. Sin.* **2020,** *36*, 1909048.
25.Zhao, L.; Li, S.; Liu, Y.; Xing, R.; Yan, X., Kinetically Controlled Self-Assembly of Phthalocyanine–Peptide Conjugate Nanofibrils Enabling Superlarge Redshifted Absorption. *CCS Chemistry* **2019,** *1*, 173-180.
26.Zhou, X.; Zhang, X.; Han, S.; Dou, Y.; Liu, M.; Zhang, L.; Guo, J.; Shi, Q.; Gong, G.; Wang, R.; Hu, J.; Li, X.; Zhang, J., Yeast Microcapsule-Mediated Targeted Delivery of Diverse NPs for Imaging and Therapy via the Oral Route. *Nano Lett.* **2017,** *17*, 1056-1064.
27. Shen, M. Y.; Liu, T. I.; Yu, T. W.; Kv, R.; Chiang, W. H.; Tsai, Y. C.; Chen, H. H.; Lin, S. C.; Chiu, H. C., Hierarchically targetable polysaccharide-coated solid lipid NPs as an oral chemo/thermotherapy delivery system for local treatment of colon cancer. *Biomaterials* **2019,** *197*, 86-100.
28. Zhang, H.; Nakamura, S.; Kitts, D. D., Antioxidant Properties of Casein Phosphopeptides (CPP) and Maillard-Type Conjugated Products. *Antioxidants* **2020,** *9*, 648.
29. Liu, F.; He, X.; Zhang, J.; Zhang, H.; Wang, Z., Employing Tryptone as a General Phase Transfer Agent to Produce Renal Clearable Nanodots for Bioimaging. *Small* **2015,** *11*, 3676-85.
30. Kanungo, I.; Fathima, N. N.; Jonnalagadda, R. R.; Unni Nair, B., Elucidation of hydration dynamics of locust bean gum–collagen composites by impedance and thermoporometry. Carbohydrate Polymers 2014, 103, 250-260.31. Tao, X. U.; Liu, Y.; Huang, Z. L., A FTIR spectroscopic study of hydroxyl in chlorinated hydroxyapatite solid solutions. *AIP Conf. Proc.* **2007,** *26*, 371-374.
32.Vonhoff, S.; Condliffe, J.; Schiffter, H., Implementation of an FTIR calibration curve for fast and objective determination of changes in protein secondary structure during formulation development. *J. Pharmaceut. Biomed.* **2010,** *51*, 39-45.
33. Wahyuni, N.; Zissis, G.; Mouloungui, Z., Characterization of acid sites on modified kaolinite by FTIR spectra of pyridine adsorbed. *AIP Conf. Proc.* **2018,** *2026*, 020042.
34. Tang, Y.; Wu, S.; Lin, J.; Cheng, L.; Zhou, J.; Xie, J.; Huang, K.; Wang, X.; Yu, Y.; Chen, Z.; Liao, G.; Li, C., NPs Targeted against Cryptococcal Pneumonia by Interactions between Chitosan and Its Peptide Ligand. *Nano Lett.* **2018,** *18*, 6207-6213.
35. Gao, Y.; He, Y.; Zhang, H.; Zhang, Y.; Gao, T.; Wang, J.-H.; Wang, S., Zwitterion-functionalized mesoporous silica NPs for enhancing oral delivery of protein drugs by overcoming multiple gastrointestinal barriers. *J. Colloid. Interface. Sci.* **2021,** *582*, 364-375.
36. Brown, T. D.; Whitehead, K. A.; Mitragotri, S., Materials for oral delivery of proteins and peptides. *Nat. Rev. Mater.* **2019,** *5*, 127-148.
37. Florek, J.; Caillard, R.; Kleitz, F., Evaluation of mesoporous silica NPs for oral drug delivery – current status and perspective of MSNs drug carriers. *Nanoscale* **2017,** *9*, 15252-15277.
38. Zhang, T.; Zhu, G.; Lu, B.; Qian, Z.; Peng, Q., Protein corona formed in the gastrointestinal tract and its impacts on oral delivery of NPs. *Med. Res. Rev.* **2021,** *41*, 1835-1850.
39. Li, X.; Mai, W.; Chen, D., Chemical Study on Protective Effect Against Hydroxyl-induced DNA Damage and Antioxidant Mechanism of Myricitrin. *J. Am. Chem. Soc.* **2014,** *61*, 383-390.
40. Zou, S.; Guo, F.; Wu, L.; Ju, H.; Sun, M.; Cai, R.; Xu, L.; Gong, Y.; Gong, A.; Zhang, M.; Du, F., One-pot synthesis of cerium and praseodymium co-doped carbon quantum dots as enhanced

antioxidant for hydroxyl radical scavenging. *Nanotechnology* **2020,** *31*, 165101.
41. Li, S.; Zou, Q.; Li, Y.; Yuan, C.; Xing, R.; Yan, X., Smart Peptide-Based Supramolecular Photodynamic Metallo-Nanodrugs Designed by Multicomponent Coordination Self-Assembly. *J. Am. Chem. Soc.* **2018,** *140*, 10794-10802.
42. Zhao, S.; Li, Y.; Liu, Q.; Li, S.; Cheng, Y.; Cheng, C.; Sun, Z.; Du, Y.; Butch, C. J.; Wei, H., An Orally Administered CeO2@Montmorillonite Nanozyme Targets Inflammation for Inflammatory Bowel Disease Therapy. *Adv. Funct. Mater.* **2020,** *30*, 2004692.
43. Zhang, S.; Ermann, J.; Succi, M. D.; Zhou, A.; Hamilton, M. J.; Cao, B.; Korzenik, J. R.; Glickman, J. N.; Vemula, P. K.; Glimcher, L. H.; Traverso, G.; Langer, R.; Karp, J. M., An inflammation-targeting hydrogel for local drug delivery in inflammatory bowel disease. *Sci. Transl. Med.* **2015,** *7*, 300ra128.
44. Dickinson, B. C.; Chang, C. J., Chemistry and biology of reactive oxygen species in signaling or stress responses. *Nat. Chem. Biol.* **2011,** *7*, 504-511.
45. Schmidt, C.; Lautenschlaeger, C.; Collnot, E.-M.; Schumann, M.; Bojarski, C.; Schulzke, J.-D.; Lehr, C.-M.; Stallmach, A., Nano- and microscaled particles for drug targeting to inflamed intestinal mucosa—A first in vivo study in human patients. *J. Control Release* **2013,** *165* , 139-145.
46. Lamprecht, A., Selective nanoparticle adhesion can enhance colitis therapy. *Nat. Rev. Gast & Hepato.* **2010,** *7*, 311-312.

# Chapter 4 Multicomponent Coassembled Nanodrugs Based on Ovalbumin, Pheophorbide a and $Zn^{2+}$ for in vitro Photodynamic Therapy


## Abstract

Photodynamic therapy (PDT) has been considered as a therapeutic method based on non-invasiveness and lower side effect. However, photosensitizers (PS), as a major component of PDT, suffer from aggregation and limit reactive oxygen species (ROS) generation in the delivery process, thus causing unsatisfactory therapeutic effect of PDT. Herein, we demonstrate a multicomponent coordination coassembly strategy based on the combination of metal-binding protein (ovalbumin, OVA), metal ions ($Zn^{2+}$) and a photosensitive drug (pheophorbide a, PheoA) for constructing supramolecular photosensitive nanodrugs towards antitumor PDT. The resulting photosensitizer nanodrugs exhibit well-defined nanorod structures, good colloidal dispersity, and high encapsulation efficiency. Most importantly, multicomponent coassembled nanorods possess favorable stability of physiological environment and on-demand release of PS in response to an acidic ambient in tumor cells. These features result in the high level of ROS generation in tumor cells, benefiting for enhanced therapeutic effect of *in vitro* PDT.



**Keywords:** multicomponent coassembly; nanorods; nanodrugs; controlled release; photodynamic therapy

## 4.1 Introduction

Photodynamic therapy (PDT), as a clinically promising therapeutic modality, has exhibited satisfactory therapeutic efficacy toward neoplastic diseases due to its spatiotemporal selectivity and noninvasive nature.[1,2] Highly reactive oxygen species (ROS) derived from PDT is capable of mediating cell apoptosis or necrosis through a series of biological events.[3] The core element of PDT is photosensitizers (PS).[4] To date, a large amount of PS have been employed for preclinical study and clinical application.[5] However, most of the available PS suffer from resultant aggregation behavior in aqueous solutions due to poor water solubility induced by highly conjugated structures, which further limits ROS generation and further reduces therapeutic effect of PDT.[6,7] Additionally, inevitable side effect, skin photosensitization caused by non-silent PS in the blood, require patients to stay out of the light for a long time after treatment.[8] Hence, a variety of drug delivery vehicles including liposomes, polymer and inorganic nanomaterials have been proposed to tailor pharmacokinetics of PS and improve blood stability of nanoengineered PS.[9,10] Nonetheless, these nanoengineered PS still have several disadvantages, such as low PS-loading capacity and premature PS release. Thence, one strategy that simultaneously integrates high loading efficiency and controlled release in single PS nanodrugs is highly appreciated.

Attributing to the functional and structural diversity of proteins, nanodrugs based on protein coassembly are expected to solve the problems of hydrophobic drug delivery.[11-14] Protein coassembly involves multiple noncovalent interactions, such as hydrophobic interaction, π-π sacking, hydrogen bonding, and electrostatic interaction.[12,15-18] These noncovalent interactions can induce coassembly of hydrophobic PS to form nanostructures, resulting in a high drug-loading capacity without redundant components. Moreover, prepared nanostructures are susceptible to complex physiological environment, leading to dynamic reversibility of coassembled protein nanostructures under suitable conditions.[2,19,20] Importantly, inspired by the metalloproteins found in natural organisms, the coordination interactions between proteins with metal ions have been employed to self-assemble proteins, constructing more stable protein-based nanodrugs.[21-25] Therefore, the enhanced stability and dynamic reversibility originated from protein-induced PS coassembly are feasible for delivery of PS, realizing enhanced PDT effect.

Herein, we construct a multicomponent nanodrug based on coassembled strategy by the combination of protein, PS, and metal ion ($Zn^{2+}$) for PDT against tumor (Scheme 4.1). Uniform and monodisperse nanorods are readily obtained by multicomponent coassembly of ovalbumin (OVA), pheophorbide a (PheoA) and $Zn^{2+}$ through a combination of coordination and noncovalent interactions. Intriguingly, the as-prepared nanorods possess robust stability in aqueous solution and physiological conditions, but controlled disassembly behavior at lower pH values in tumor cellular environments. These characteristics attribute to the robustness of coordination interaction and flexibility of multiple noncovalent interactions. Furthermore, the nanorods exhibit negligible dark toxicities and enhanced *in vitro* PDT efficiency. Taken together, our results demonstrate that multicomponent coordination coassembly is a promising strategy for fabricating PS-based delivery systems with robust physiological stability

and controlled release behavior towards enhancing PDT efficiency.

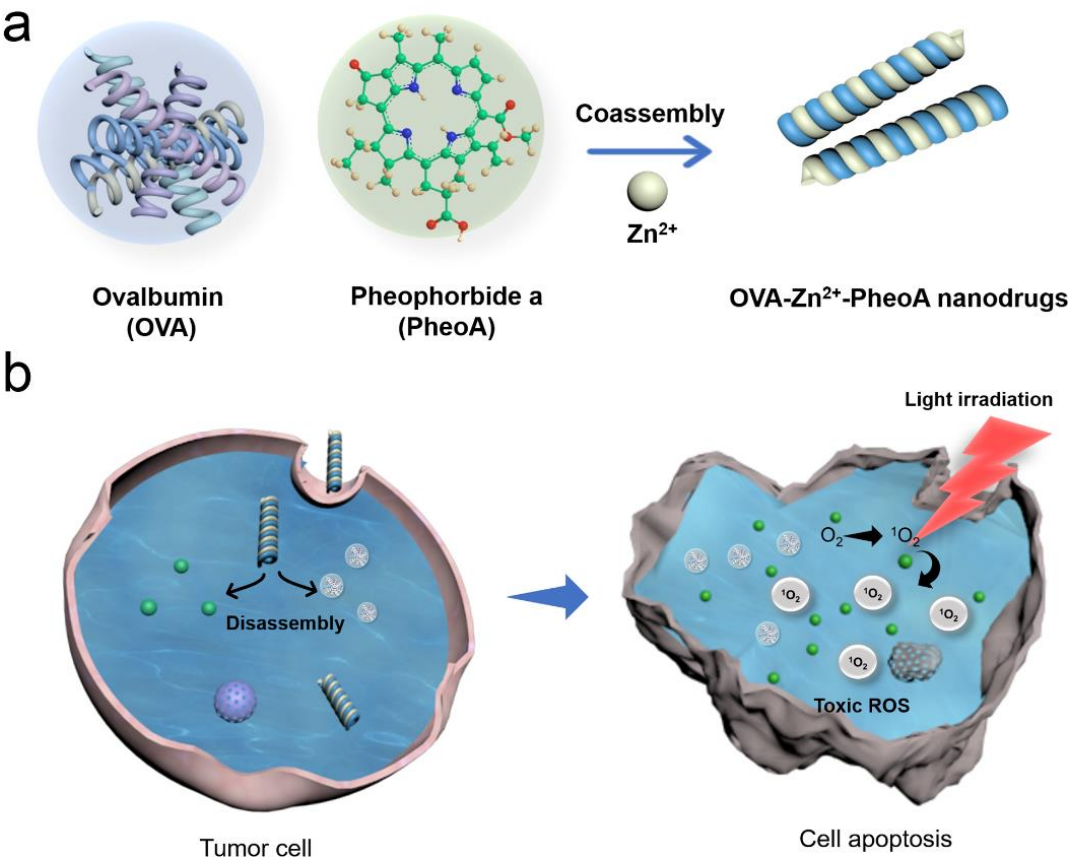


**Scheme 4.1** Schematic illustration of supramolecular nanodrugs for efficient antitumor PDT *in vitro*. (a) Supramolecular nanorods based on coordination coassembly of metal-binding OVA and PheoA in the presence of $Zn^{2+}$. (b) The process of cellular internalization of nanorods by tumor cells and release of PheoA in response to cellular environments, achieving toxic ROS generation for efficient PDT *in vitro*.

## 4.2 Experimental section

### 4.2.1 Materials and instruments

**Materials:** Albumin, from chicken egg white (98 %), Calcein-AM and propidium iodide (PI) were bought from Sigma-Aldrich (Shanghai) Trading Co. Ltd.. Pheophorbide a (mixture of diastereomers) (95%) was obtained from Frontier Scientific, Inc. Zinc (II) chloride ($ZnCl_2$) (98%) was bought from Beijing Chemical Works. Methylthiazolyldiphenyl-tetrazolium bromide (MTT) was purchased from Beijing Solarbio Science &Technology Co., Ltd.. 2',7'-Dichlorodihydrofluorescein diacetate DCFH-DA was got from MedChemexpress CO., Ltd.. Roswell Park Memorial Institute (RPMI) 1640 medium and phosphate buffer saline (PBS) were purchased from Beijing Solarbio Science & Technology Co., Ltd.. Fetal bovine serum (FBS) was got from BioLegend Co.

**Instruments:** Transmission electron microscopy (TEM) images of nanorods were exhibited by a model JEM-1011 transmission scanning electron microscope (JEM-1011, JEOL, Japan). The zeta potential of nanorods was measured by a Malvern DLS

instrument (Zetasizer Nano ZS ZEN3600). UV/vis absorption spectra were tested by a Shimadzu UV-2600 spectrophotometer. Fourier transform infrared (FTIR) spectra were obtained by a TENSOR 27 FTIR spectrometer (BRUKER). The cell viability was evaluated by using MTT assay, in which the absorbance was measured by a microplate reader (Multiskan FC, Thermo Fisher Scientific). The biodistribution of OVA-$Zn^{2+}$-PheoA nanorods *in vivo* was measured with an imaging system (PerkinElmer, IVIS Spectrum). Confocal laser scanning microscopy (CLSM) (Olympus FV1000) was used for imaging cells. 680 nm diode laser (0.3 W $cm^{-2}$, equipped within Olympus FV1000) was used for irradiating cells.

### 4.2.2 The synthesis of the OVA-$Zn^{2+}$-PheoA nanorods

The OVA-$Zn^{2+}$-PheoA nanorods were prepared by a simple method that 400 μL OVA dispersed in aqueous solution (10 mg $mL^{-1}$) and 20 μL PheoA dispersed in DMSO (10 mg $mL^{-1}$) were mixed. Then, 10 μL $ZnCl_2$ solution with the concentration of 100 mM was added into the mixed solution, then 0.1 M NaOH solution was used for adjusting the pH value of the mixtures to neutral. The final concentrations of OVA, $Zn^{2+}$ and PheoA were 4 mg $mL^{-1}$, 0.01 mM and 0.2 mg $mL^{-1}$, respectively. OVA-$Zn^{2+}$-PheoA nanorods were obtained after aging for 24 h.

### 4.2.3 Encapsulation efficiency of PheoA of OVA-$Zn^{2+}$-PheoA nanorods

OVA-$Zn^{2+}$-PheoA nanorods were placed into ultrafiltration device to centrifugate 6000 r for 10 min. The precipitates were dispersed in DMSO. Then, the concentration of PheoA was measured by UV/vis spectroscopy. The following formula was accorded to calculate the encapsulation efficiency of PheoA:

$$Encapsulation\ efficiency = \frac{weight\ of\ PheoA\ in\ the\ precipitate}{weight\ of\ PheoA\ added} * 100\%$$

### 4.2.4 The stability of OVA-$Zn^{2+}$-PheoA nanorods

The stability of OVA-$Zn^{2+}$-PheoA nanorods was evaluated by dynamic light scattering (DLS). OVA-$Zn^{2+}$-PheoA nanorods were incubated with water (pH 7.4), PBS (pH 7.4) and RPMI 1640 medium containing 10% (v/v) FBS at 37 °C for 72 h, respectively.

### 4.2.5 Release profiles of PheoA from the OVA-$Zn^{2+}$-PheoA nanorods

The PheoA release profiles *in vitro* were measured by the dialysis method. 1 mL OVA-$Zn^{2+}$-PheoA nanorods was placed into a dialysis membrane (Mw cutoff = 14 K) and incubated with 50 mL of PBS solution (pH 5.5 and 7.4) containing 0.5% (v/v) Tween 80 at 37 ℃ for 24 h. Then, 1 mL of the dialysate was collected and replaced with 1 mL of fresh PBS containing 0.5% (v/v) Tween 80 at different time points. The data was monitored by UV/vis spectrophotometry. The standard curve of PheoA dissolved in PBS solution containing 0.5% (v/v) Tween 80 see Figure S4.3.

### 4.2.6 The biocompatibility evaluation of OVA-$Zn^{2+}$-PheoA nanorods *in vitro*

Mouse melanoma cells (B16) cells were cultured in 96-well plates ($1\times10^5$ cells $well^{-1}$) for overnight. The different concentrations of the OVA- $Zn^{2+}$-PheoA were used to treat cells for 24 h. The cell viability was tested by MTT assay.

### 4.2.7 Cellular uptake

B16 cells were cultured at $5\times10^4$ cells in coverglass bottom dishes for overnight. After 24 h, B16 cells were further incubated with RPMI 1640 medium containing the nanorods (10 μg $mL^{-1}$ of PheoA) for 1, 8, 24 h. After incubation, the cells were washed with PBS, and imaged by CLSM with the excited wavelength of 635 nm.

### 4.2.8 The PDT effect of OVA-$Zn^{2+}$-PheoA nanorods *in vitro*

B16 cells were equably dispersed in 96-well plates ($1\times10^5$ cells $well^{-1}$) and incubated for overnight. Then, B16 cells were incubated with various concentrations of the OVA-$Zn^{2+}$-PheoA or PheoA for 24 h. After incubation, B16 cells were washed by PBS with three times and were incubate by fresh RPMI 1640 medium. 680 nm laser (0.3 W $cm^{-2}$) was used to illuminate tumor cells in groups needing laser. After further incubation for another 24 h, the cell viability was tested by MTT assay.

### 4.2.9 Generation and detection of ROS

B16 cells were equably dispersed in petri dishes ($5\times10^4$ cells) and cultured for 24 h. RPMI 1640 medium containing OVA-$Zn^{2+}$-PheoA (10 μg $mL^{-1}$ of PheoA) was used to replace the original medium and incubate with cells for 24 h in OVA-$Zn^{2+}$-PheoA and OVA-$Zn^{2+}$-PheoA (+Laser) groups. Before laser irradiation, B16 cells were incubated with 10 μM DCFH-DA for 0.5 h. Then, cells were irradiated by a 680 nm diode laser (0.3 W $cm^{-2}$) for 1 min. The cells in control group and OVA-$Zn^{2+}$-PheoA groups were only incubated with 10 μM DCFH-DA for 0.5 h. CLSM was used to image cells (excited at 488 nm).

### 4.2.10 Staining of living and dead cells

B16 cells were equably dispersed in petri dishes ($5\times10^4$ cells) and cultured for 24 h. RPMI 1640 medium containing OVA-$Zn^{2+}$-PheoA (10 μg $mL^{-1}$ of PheoA) was used to replace the original medium and incubate cells for 24 h in OVA-$Zn^{2+}$-PheoA group and OVA-$Zn^{2+}$-PheoA (+Laser) group. After 680 nm diode laser (0.3 W $cm^{-2}$) irradiation for 5 min, B16 cells were incubated with 50 μg $mL^{-1}$ of Calcein-AM and propidium iodide (PI) in only laser group and OVA-$Zn^{2+}$-PheoA (+Laser) group. The cells in control group and OVA-$Zn^{2+}$-PheoA group were only incubated with Calcein-AM and PI. Finally, CLSM was used to image cells (excited at 488 nm).

### 4.2.11 The biodistribution of OVA-$Zn^{2+}$-PheoA nanorods *in vivo*

10 mg $kg^{-1}$ OVA-$Zn^{2+}$-PheoA nanorods dispersed in 5% glucose solution were intravenously injected into B16 tumor-bearing mice before imaging. At predetermined time points (1, 4, 8, 24 h), the mice treated nanorods were imaged by an *in vivo* fluorescence imaging system. After the treatment for 24 h, the mice were sacrificed,

and the organs (heart, liver, spleen, lung and kidneys) as well as tumors were harvested and imaged by the fluorescence imaging system. Fluorescence intensity of different organs and tumors was obtained via the imaging system software.

## 4.3 Results and discussion

### 4.3.1 The preparation of OVA-$Zn^{2+}$-PheoA nanorods

As a model metal-binding protein, OVA was chosen as the building block for coassembling with PS. As a biologically derived PS, PheoA with biocompatibility and biodegradability could generate ROS under laser irradiation to effectively destroy tumor cells.[26,27] Nevertheless, the high hydrophobicity of PheoA restricted bioavailability and ROS generation (singlet oxygen, $^1O_2$). We investigated coassembly of OVA and PheoA in aqueous solutions with the addition of $Zn^{2+}$. TEM images of OVA and PheoA dispersed in water (Figure 4.1a, b) showed irregular morphology in OVA and aggregation of large clusters in PheoA. While TEM image of OVA-$Zn^{2+}$-PheoA (Figure 4.1c**)** exhibited spiral nanorod structures. The morphology difference between individual PheoA and OVA-$Zn^{2+}$-PheoA nanorods indicated that the presence of OVA and $Zn^{2+}$ influenced and regulated the molecular stacking patterns of PheoA though the simultaneous integration of coordination and noncovalent interactions.[24] The multicomponent coordination interaction and secondary structure of assembled nanorods was proved by FTIR spectroscopy. As shown in Figure 4.1d, the band identified at 1737 $cm^{-1}$ was due to the carboxy group of PheoA. Compared to the PheoA, corresponding band of OVA-$Zn^{2+}$-PheoA in the FTIR spectra significantly shifted to lower wavenumbers, indicating the carboxyl groups coordinated to $Zn^{2+}$.[22,28,29] The absorption band of OVA at 1651 $cm^{-1}$ (amide I) confirmed its typical α helix secondary structure.[30-31] The absorption band of typical α helix secondary structure was also present in OVA-$Zn^{2+}$-PheoA nanorods (1658 $cm^{-1}$). Circular dichroism (CD) spectroscopy was employed to further analyze the secondary structure of nanorods. As shown in Figure 4.1e, OVA-$Zn^{2+}$-PheoA exhibited a typical α helix secondary structure, performing a positive peak at 195 nm and two negative peaks at 208 nm and 222 nm, respectively.[32] This CD result was consistent with the FTIR spectra. The surface charge of OVA-$Zn^{2+}$-PheoA (-2.85 mV) was obviously more positive compared with PheoA clusters (-42.2 mV), which also demonstrated that the binding of $Zn^{2+}$occured in the formation of the OVA-$Zn^{2+}$-PheoA nanorods. (Figure 4.1f) These results suggested that the OVA-$Zn^{2+}$-PheoA nanorods were formed by coordination coassembly of the three components. Significantly, the PheoA encapsulation efficiency of OVA-$Zn^{2+}$-PheoA nanorods was higher than 94% (Figure S4.1). Such high encapsulation efficiencies indicated that PheoA acted as both a cargo and a building block to participate in the coassembly of the nanorods.

To further understand the assembly mechanism of the OVA-$Zn^{2+}$-PheoA nanorods, the interactions of three components were investigated by UV/vis absorption spectra (Figure 4.1g). Compared to the spectrum of monomeric PheoA (dispersed in DMSO), OVA-$Zn^{2+}$-PheoA nanorods showed a red-shifted Q-band at 668 nm accompanied by the widening of the peak, which suggested PheoA was in aggregated state in the assemblies. Such aggregated state was not conducive to $^1O_2$ generation.[33] As expected,

OVA-$Zn^{2+}$-PheoA nanorods totally quenched the fluorescence of monomeric PheoA due to robust nanostructure constructed by strong cooperative coordination interactions (Figure 4.1h). The significant inhibition of fluorescence was benefit for hindering photosensitization caused by non-silent PS in the blood.

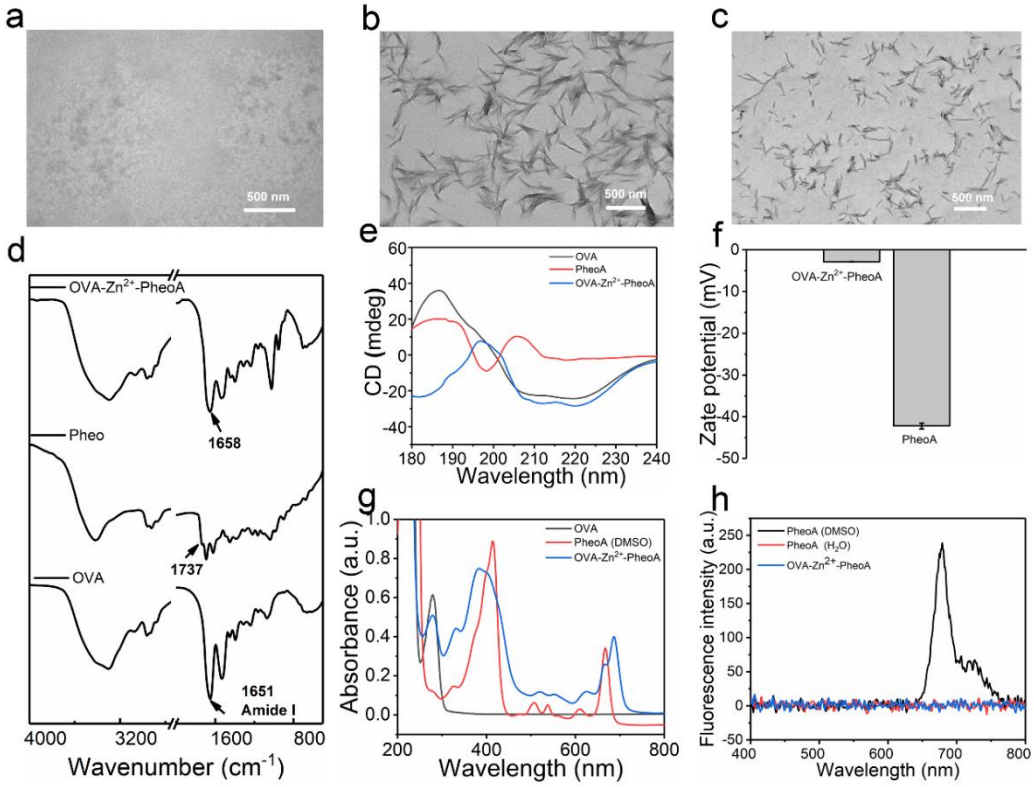


**Figure 4.1** The characterization of OVA-$Zn^{2+}$-PheoA nanorods. TEM images of (a) OVA, (b) PheoA, and (c) OVA-$Zn^{2+}$-PheoA nanorods in aqueous solution. (d) FTIR spectra and (e) CD spectra of OVA, PheoA and OVA-$Zn^{2+}$-PheoA. (f) Zeta potential of PheoA and OVA-$Zn^{2+}$-PheoA nanorods. (g) The UV/vis absorption spectra of OVA, PheoA (dispersed in DMSO) and OVA-$Zn^{2+}$-PheoA nanorods (equivalent concentration of PheoA). (h) Fluorescence emission spectra of PheoA (dispersed in DMSO), PheoA (dispersed in water) and OVA-$Zn^{2+}$-PheoA nanorods (equivalent concentration of PheoA, excited at 678 nm).

### 4.3.2 The stability evaluation of OVA-$Zn^{2+}$-PheoA nanorods

The stability of nanomaterials is highly crucial for PDT not only *in vitro* and *in vivo*. In comparison with traditional noncovalent interactions, coordination interaction is significantly stronger and its bond energy is closed to the covalent bond. Therefore, the integration of coordination interactions and noncovalent interactions is an ingenious way to design robust nanodrugs. The stability of OVA-$Zn^{2+}$-PheoA nanorods was evaluated by incubating OVA-$Zn^{2+}$-PheoA nanorods with a water, RPMI 1640 medium supplemented with 10% (v/v) fetal bovine serum (FBS), and phosphate buffer saline (PBS) (pH 7.4) at 37 °C for different times (1, 6, 24, 48, 72 h) (Figure 4.2a, b, c). The results showed that OVA-$Zn^{2+}$-PheoA nanorods were stable under such environments because their average sizes and polymer dispersity index (PDI) exhibited negligible

changes. Such good performance indicated that the nanorods constructed by multicomponent coordination coassembly were highly stable under physiological environment.

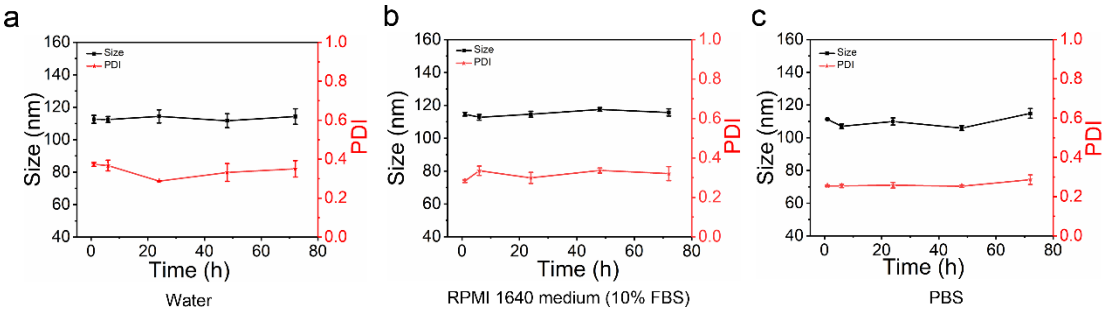


**Figure 4.2** The stability evaluation of OVA-$Zn^{2+}$-PheoA nanorods by DLS. Size and PDI of OVA-$Zn^{2+}$-PheoA nanorods during the incubation in (a) water (pH 7.4), (b) RPMI 1640 medium supplemented with 10% (v/v) FBS, and (c) PBS buffer (pH 7.4) at 37 °C for 24 h.

### 4.3.3 The pH responsiveness of OVA-$Zn^{2+}$-PheoA nanorods

It is critical that PheoA can be released from OVA-$Zn^{2+}$-PheoA nanorods for effective ROS generation under laser irradiation. Due to the dynamic flexibility of noncovalent interactions, the formed assemblies may be susceptible to environmental variations, such as pH, leading to controlled disassembly mediated by tumor acid environment. The release of PheoA from the OVA-$Zn^{2+}$-PheoA nanorods was tested by dialysis against PBS (pH 5.5 and pH 7.4) with 0.5% (v/v) Tween 80, which were used to simulate the normal physiological environment and tumor cells, respectively (Figure 4.3a). The release efficiency of PheoA from OVA-$Zn^{2+}$-PheoA nanorods in pH 5.5 PBS with 0.5% (v/v) Tween 80 was reaching up to approximately 73% at 24 h. In contrast, about 22% of the PheoA was released at 24 h in pH 7.4 PBS with 0.5% (v/v) Tween 80 because of compatibilization function of Tween 80. These results indicated that nanorods performed pH responsiveness and relative stability in normal physiological condition. It might ascribe to protonation of the carboxyl groups of PheoA, inducing weakening the electrostatic interaction and coordination interaction with $Zn^{2+}$.[34] Next, the disassembly process of OVA-$Zn^{2+}$-PheoA nanorods was directly observed by TEM. As shown in Figure 4.3b, OVA-$Zn^{2+}$-PheoA nanorods were incubated with pH 5.5 and pH 7.4 PBS with 0.5% (v/v) Tween 80 for 24 h, respectively. The morphology of OVA-$Zn^{2+}$-PheoA nanorods incubated with pH 7.4 PBS exhibited negligible changes, maintaining the integrity of the nanorods for 24 h. In contrast to unaltered morphology of OVA-$Zn^{2+}$-PheoA incubated with pH 7.4 PBS, OVA-$Zn^{2+}$-PheoA nanorods incubated with pH 5.5 PBS gradually disassembled. It was observed that a portion of the nanorods showed collapse of the rod-like structure (yellow arrow) at 8 h. After 24 h, the nanorods almost disassembled and the rod-like nanostructures completely disappeared, accompanying by aggregation of hydrophobic PheoA. These results demonstrated that OVA-$Zn^{2+}$-PheoA nanorods possessed pH responsiveness, which was suitable for controllable disassembly to achieve the release of monomeric PheoA in tumor cells.

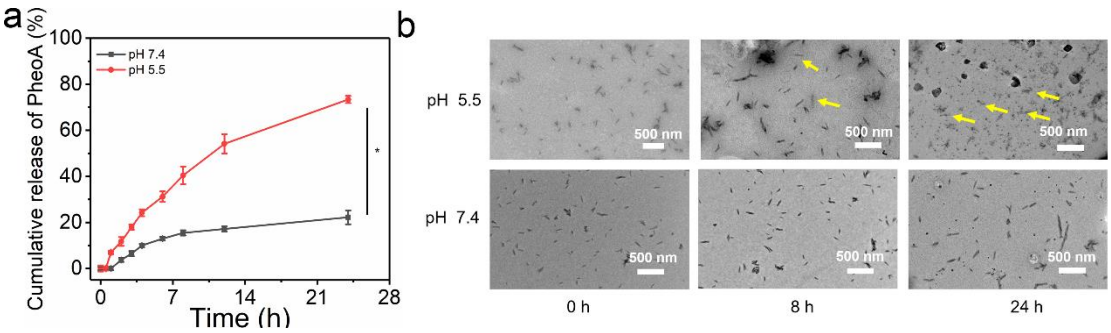


**Figure 4.3** pH responsiveness and disassembly evaluation of OVA-$Zn^{2+}$-PheoA nanorods. (a) Release profiles of PheoA from OVA-$Zn^{2+}$-PheoA nanorods in different buffer solutions with Tween 80 (pH 5.5 and pH 7.4, * indicates $p < 0.05$). (b) TEM images of OVA-$Zn^{2+}$-PheoA nanorods incubated with different buffer solutions (pH 5.5 and pH 7.4) over time.

### 4.3.4 The *in vitro* PDT effect of OVA-$Zn^{2+}$-PheoA nanorods

The biosafety of nanomaterials is priority for further biomedical applications. Hence, the biocompatibility was further investigated at the cellular level. B16 cells were chosen as the cell line to culture with OVA-$Zn^{2+}$-PheoA nanorods with different concentrations (6.25, 12.5, 25, 50, 100 μg $mL^{-1}$). As shown in Figure 4.4a, after co-incubating with nanorods for 24 h, survival rate of B16 cell was more than 90% under 50 μg $mL^{-1}$ OVA-$Zn^{2+}$-PheoA nanorods. Even at the concentration of 100 μg $mL^{-1}$, cell proliferation inhibition rate was less than 15%, indicating that OVA-$Zn^{2+}$-PheoA nanorods possessed good biocompatibility. Next, OVA-$Zn^{2+}$-PheoA nanorods were further explored for PDT *in vitro*. The images of B16 cells incubated with 10 μg $mL^{-1}$ of OVA-$Zn^{2+}$-PheoA nanorods for 1, 8, 24 h, were captured by CLSM. After incubation with cells for 8 h, the fluorescent cells could be clearly observed and the intensity increased with the prolonged incubation time (Figure 4.4b, c), indicating the uptake of OVA-$Zn^{2+}$-PheoA nanorods by cells. It is worth to note that the strong fluorescence resulting from the cells accounted for the disassembly of the nanorods and release of molecular PheoA, which is of importance for the efficient PDT. The antitumor PDT efficiency and ROS generation capacity were further investigated through MTT assay. As shown in Figure 4.4d, the B16 cells treated both the laser-free or laser alone group all showed high cell viability. The cytotoxicity of the PheoA and OVA-$Zn^{2+}$-PheoA nanorods with laser irradiation was also evaluated. The survival rate of B16 cells treated with PheoA (+Laser) and OVA-$Zn^{2+}$-PheoA (+Laser) both showed a significant decrease in a concentration-dependent manner. In addition, the OVA-$Zn^{2+}$-PheoA (+Laser) group exhibited more cytotoxicity than the PheoA (+Laser) group, especially at higher doses. These results suggested that the OVA-$Zn^{2+}$-PheoA nanorods might have better intracellular uptake and ROS generation capacity than aggregated PheoA. Furthermore, the intracellular ROS generation was detected by DCFH-DA probe that could be oxidized by generated ROS to yield fluorescent substance.[35] The OVA-$Zn^{2+}$-PheoA nanorods (+Laser) treated cells exhibited obvious fluorescence emission compared to the other control groups. It demonstrated that the PheoA could be released from the OVA-$Zn^{2+}$-PheoA nanorods in B16 cancer cells for effective ROS generation (Figure

4.4e). Calcein-AM and PI were used to stain live and dead cells.[36] As shown in Figure 4.4f, while strong red fluorescence signal of PI in B16 cells treated with OVA-$Zn^{2+}$-PheoA (+Laser) was observed by CLSM, the other groups treated with only laser or only OVA-$Zn^{2+}$-PheoA nanorods exhibited strong green fluorescence signal of Calcein-AM. The results indicated that the generated ROS from OVA-$Zn^{2+}$-PheoA nanorods under laser irradiation could effectively trigger the B16 cell apoptosis, achieving enhanced antitumor PDT effect *in vitro*.

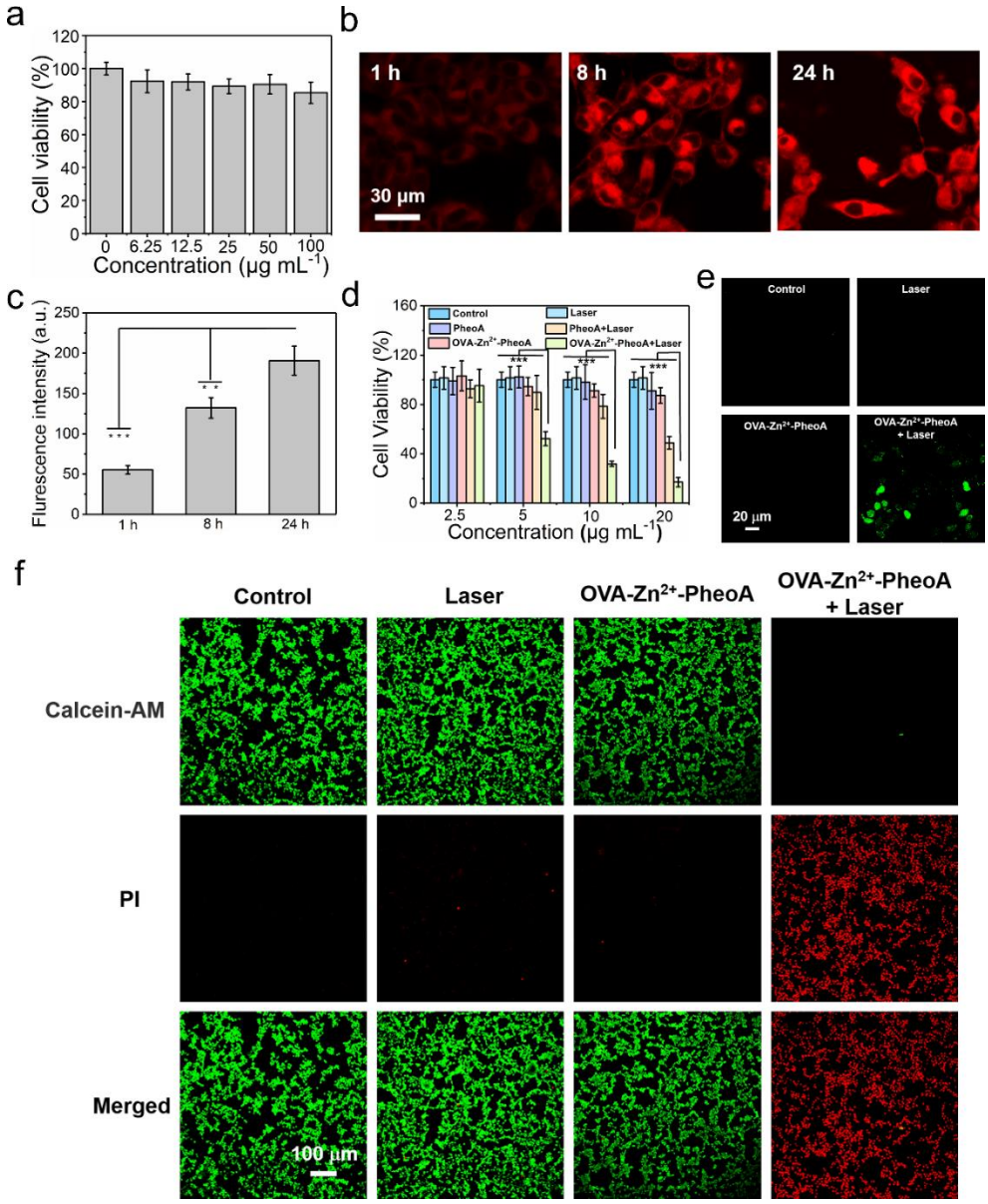


**Figure 4**.4 The biocompatibility and *in vitro* PDT effect of OVA-$Zn^{2+}$-PheoA nanorods. (a) Cell viability of B16 cells after incubation with OVA-$Zn^{2+}$-PheoA nanorods containing different concentrations. (b) CLSM images of B16 cells incubated with OVA-$Zn^{2+}$-PheoA nanorods for 1, 8, 24 h. Excited at 635 nm. (c) Fluorescence intensity analysis of cells incubated with OVA-$Zn^{2+}$-PheoA nanorods for 1, 8, 24 h. (** indicates $p < 0.01$, *** indicates $p < 0.001$) (d) Cell viability of B16 cells treated with different concentrations of OVA-$Zn^{2+}$-PheoA nanorods in the presence or absence of laser

irradiation. (680 nm, 0.3 W $cm^{-2}$, *** indicates $p < 0.001$) (e) CLSM images of B16 cells stained with DCFH-DA. Excited at 488 nm. (f) The CLSM images of B16 cells stained with Calcein-AM and PI. Excited at 488 nm and 559 nm.

### 4.3.5 The biodistribution of OVA-$Zn^{2+}$-PheoA nanorods *in vivo*

The *in vivo* distribution of the OVA-$Zn^{2+}$-PheoA nanorods was further investigated in B16 tumor-bearing mice. Before intravenous injection, the stability of OVA-$Zn^{2+}$-PheoA nanorods in physiological medium was further evaluated. As shown in Fig. S4.2, the UV/vis absorbance of nanorods after incubation with RPMI 1640 medium containing 10% (v/v) FBS for 24 h showed negligible changes, indicating the nanorods stability in the physiological medium. After the injection of OVA-$Zn^{2+}$-PheoA nanorods, the tumor site exhibited strong fluorescence signal at 1 h and showed an obvious increase at 4 h (Figure 4.5a**)**, suggesting gradual accumulation of the OVA-$Zn^{2+}$-PheoA nanorods and released PheoA at the tumor site. With the prolonging of time, the intensity of fluorescence signal gradually decreased due to metabolic clearance but remained stronger than that of other organs at 24 h (Figure 4.5b**)**. The contrast of fluorescence intensity between harvested organs and tumor sites was consistent with the fluorescence signal intensity *in vivo* **(**Figure 4.5c), suggesting that OVA-$Zn^{2+}$-PheoA nanorods still accumulated in the tumor with prolonged blood circulation time.

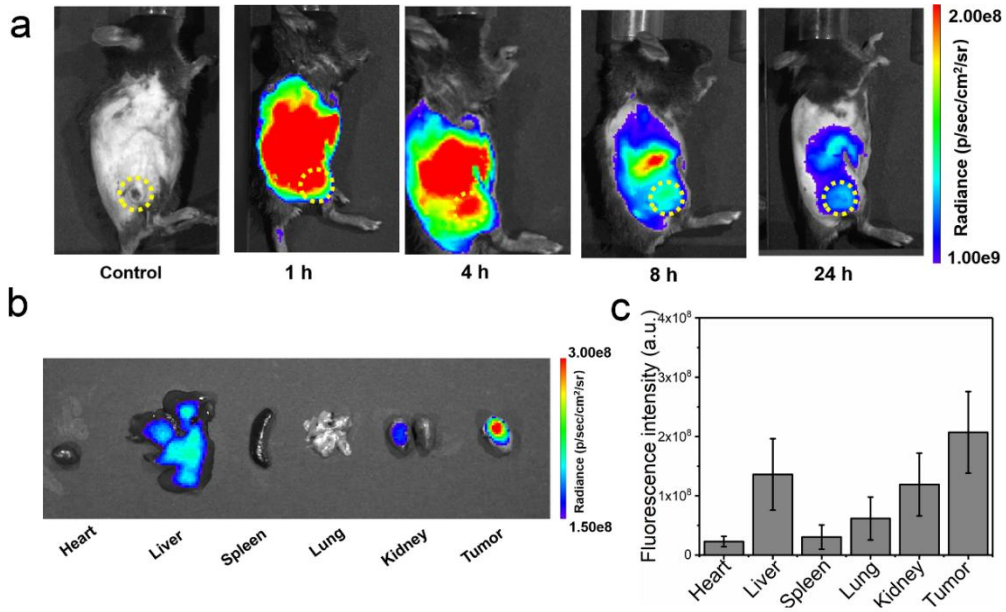


**Figure 4.5** The biodistribution of OVA-$Zn^{2+}$-PheoA nanorods *in vivo*. (a) Fluorescence images of mice injected with OVA-$Zn^{2+}$-PheoA nanorods at different time, and dashed line indicates tumor region (equivalent concentration of PheoA: 1 mg $mL^{-1}$). (b) Fluorescence images of harvested tumor and various organs. (c) The fluorescence intensity of OVA-$Zn^{2+}$-PheoA nanorods distributed in harvested tumor and various organs. Error bars denote the standard deviation (n = 3).

## 4.4 Conclusions

In summary, we have constructed supramolecular photosensitizer nanorods by

coordination coassembly based on the combination of OVA, $Zn^{2+}$ and PheoA. The as-prepared OVA-$Zn^{2+}$-PheoA nanorods exhibit good colloidal dispersity, biocompatibility and high encapsulation efficiency (>90%). Moreover, the as-prepared nanorods show favorable stability in physiological environment, but have responsiveness to acid pH in tumor cells for the controlled release of monomeric photosensitizer and corresponding generation of ROS, thus enhancing *in vitro* PDT efficiency. OVA-$Zn^{2+}$-PheoA nanorods can selectively accumulate in tumors and present the potential for further diagnosis and treatment *in vivo*. Multicomponent coordination coassembly is a versatile approach applicable for preparing various protein-photosensitizer nanodrugs, paving the way for design of multifunctional nanodrugs toward synergistic antitumor therapy.

**Acknowledgements**

This work was financially supported by the National Natural Science Foundation of China (Project Nos. 22102188 and 22072154), the Chinese Postdoctoral Science Foundation (Grand No. 2020M680674) and the National Natural Science Foundation of Hebei Province (No. B2020103025). All the animal experiments in this work were conducted in accordance with protocols approved by the Animal Care and Use Committee of Institute of Process Engineering, Chinese Academy of Sciences, and in compliance with the Chinese law on experimental animals.

**4.5 Supporting information**

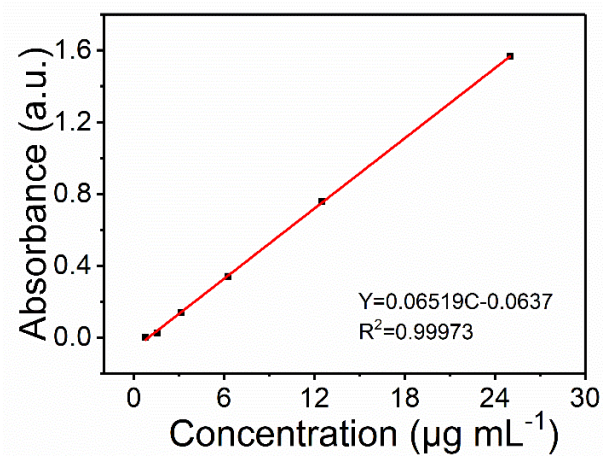


**Figure S4.1** The standard curve of PheoA dissolved in DMSO.

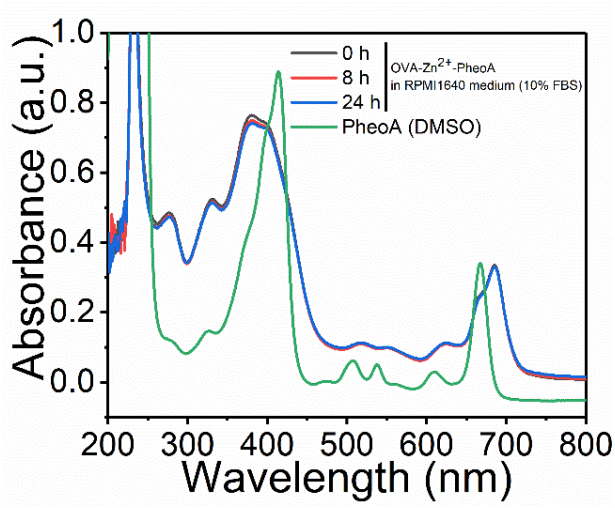


**Figure S4.2** UV/vis absorption spectra of OVA-$Zn^{2+}$-PheoA nanorods incubated with RPMI 1640 medium (10% FBS) at different points (0, 8, 24 h) and PheoA dispersed in DMSO.

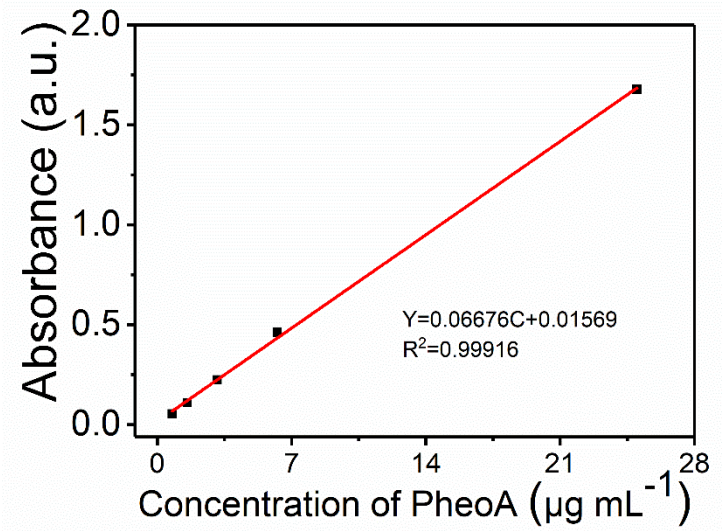


**Figure S4.3** The standard curve of PheoA dissolved in PBS solution containing 0.5% (v/v) Tween 80.

### 4.6 References

1. Li, X.; Lovell, J. F.; Yoon, J.; Chen, X., Clinical development and potential of photothermal and photodynamic therapies for cancer. *Nat. Rev. Clin. Oncol.* **2020,** *17*, 657-674.

2. Abbas, M.; Zou, Q.; Li, S.; Yan, X., Self-Assembled Peptide- and Protein-Based Nanomaterials for Antitumor Photodynamic and Photothermal Therapy. *Adv. Mater.* **2017,** *29*, 1605021.

3. Robertson, C. A.; Evans, D. H.; Abrahamse, H., Photodynamic therapy (PDT): A short review on cellular mechanisms and cancer research applications for PDT. *J Photochem. Photobiol. B: Biology* **2009,** *96*, 1-8.

4. Allison, R.; Downie, G.; Cuenca, R.; Hu, X.; Childs, C.; Sibata, C., Photosensitizers in clinical PDT. *Photodiagnosis Photodyn. Ther.* **2004,** *1*, 27-42.

5. Li, X.; Lee, S.; Yoon, J., Supramolecular photosensitizers rejuvenate photodynamic therapy. *Chem. Soc. Rev.* **2018,** *47*, 1174-1188. and

6. Liu, K.; Xing, R.; Zou, Q.; Ma, G.; Mohwald, H.; Yan, X., Simple Peptide-Tuned Self-Assembly of Photosensitizers towards Anticancer Photodynamic Therapy. *Angew. Chem. Int. Ed. Engl.* **2016,** *55*, 3036-9.

**7.** Liu, Y.; Ma, K.; Jiao, T.; Xing, R.; Shen, G.; Yan, X., Water-Insoluble Photosensitizer Nanocolloids Stabilized by Supramolecular Interfacial Assembly towards Photodynamic Therapy. *Sci. Rep.* **2017,** *7*, 42978.

8. Zhang, Y.; He, L.; Wu, J.; Wang, K.; Wang, J.; Dai, W.; Yuan, A.; Wu, J.; Hu, Y., Switchable PDT for reducing skin photosensitization by a NIR dye inducing self-assembled and photo-disassembled NPs. *Biomaterials* **2016,** *107*, 23-32.

9. Zhang, L.; Wu, S.; Qin, Y.; Fan, F.; Zhang, Z.; Huang, C.; Ji, W.; Lu, L.; Wang, C.; Sun, H.; Leng, X.; Kong, D.; Zhu, D., Targeted Codelivery of an Antigen and Dual Agonists by Hybrid NPs for Enhanced Cancer Immunotherapy. *Nano Lett.* **2019,** *19*, 4237-4249.

10. Rosenblum, D.; Joshi, N.; Tao, W.; Karp, J. M.; Peer, D., Progress and challenges towards targeted delivery of cancer therapeutics. *Nat. Comm.* **2018,** *9*, 1410.

11. Zhao, F.; Shen, G.; Chen, C.; Xing, R.; Zou, Q.; Ma, G.; Yan, X., Nanoengineering of Stimuli-Responsive Protein-Based Biomimetic Protocells as Versatile Drug Delivery Tools. *Chem. Eur. J.* **2014,** *20*, 6880-6887.

12. Zou, Q.; Chang, R.; Yan, X., Self-Assembling Proteins for Design of Anticancer Nanodrugs. *Chem. Asian J.* **2020,** *15*, 1405-1419.

13. Zhang, N.; Zhao, F.; Zou, Q.; Li, Y.; Ma, G.; Yan, X., Multitriggered Tumor-Responsive Drug Delivery Vehicles Based on Protein and Polypeptide Coassembly for Enhanced Photodynamic Tumor Ablation. *Small* **2016,** *12*, 5936-5943.

14. Baler, K.; Michael, R.; Szleifer, I.; Ameer, G. A., Albumin Hydrogels Formed by Electrostatically Triggered Self-Assembly and Their Drug Delivery Capability. *Biomacromolecules* **2014,** *15*, 3625-3633.

15. Wang, J.; Liu, K.; Xing, R.; Yan, X., Peptide self-assembly: thermodynamics and kinetics. *Chem. Soc. Rev.* **2016,** *45*, 5589-5604.

16. Yuan, C.; Levin, A.; Chen, W.; Xing, R.; Zou, Q.; Herling, T. W.; Challa, P. K.; Knowles, T. P. J.; Yan, X., Nucleation and Growth of Amino Acid and Peptide Supramolecular Polymers through Liquid–Liquid Phase Separation. *Angew. Chem. Int. Ed.* **2019,** *58*, 18116-18123.

17. Bai, Y.; Luo, Q.; Liu, J., Protein self-assembly via supramolecular strategies. *Chem. Soc. Rev.* **2016,** *45*, 2756-2767.

18. Zhou, L.; Lv, F.; Liu, L., In Situ-Induced Multivalent Anticancer Drug Clusters in Cancer Cells for Enhancing Drug Efficacy. *CCS Chemistry* **2019**, *1*, 97-105.

19. Li, S.; Zhang, W.; Xue, H.; Xing, R.; Yan, X., Tumor microenvironment-oriented adaptive nanodrugs based on peptide self-assembly. *Chem. Sci.* **2020,** *11*, 8644-8656.

20. Li, S.; Zou, Q.; Xing, R.; Govindaraju, T.; Fakhrullin, R.; Yan, X., Peptide-modulated self-assembly as a versatile strategy for tumor supramolecular nanotheranostics. *Theranostics* **2019,** *9*, 3249-3261.

21. Sun, H.; Chang, R.; Zou, Q.; Xing, R.; Qi, W.; Yan, X., Supramolecular Protein Nanodrugs with Coordination- and Heating-Enhanced Photothermal Effects for Antitumor Therapy. *Small* **2019,** *15*, 1905326.

22. Li, S.; Zou, Q.; Li, Y.; Yuan, C.; Xing, R.; Yan, X., Smart Peptide-Based Supramolecular Photodynamic Metallo-Nanodrugs Designed by Multicomponent Coordination Self-Assembly. *J.*

*Am. Chem. Soc.* **2018,** *140*, 10794-10802.
23. Zou, Q.; Yan, X., Amino Acid Coordinated Self-Assembly. *Chem. Eur. J.* **2018,** *24*, 755-761.
24. Zhang, H.; Kang, L.; Zou, Q.; Xin, X.; Yan, X., Coordination-assembled supramolecular nanoplatforms: structural modulation and theranostic applications. *Curr. Opin. Biotechnol.* **2019,** *58*, 45-52.
25. Liu, Y.; Zhao, L.; Shen, G.; Chang, R.; Zhang, Y.; Yan, X., Coordination self-assembly of natural flavonoids into robust NPs for enhanced in vitro chemo and photothermal cancer therapy. *Colloid. Surface. A.* **2020,** *598*, 124805.
26. Oh, I. H.; Min, H. S.; Li, L.; Tran, T. H.; Lee, Y. K.; Kwon, I. C.; Choi, K.; Kim, K.; Huh, K. M., Cancer cell-specific photoactivity of pheophorbide a-glycol chitosan NPs for photodynamic therapy in tumor-bearing mice. *Biomaterials* **2013,** *34*, 6454-63.
27. Moret, F.; Menilli, L.; Battan, M.; Tedesco, D.; Columbaro, M.; Guerrini, A.; Avancini, G.; Ferroni, C.; Varchi, G., Pheophorbide A and Paclitaxel Bioresponsive NPs as Double-Punch Platform for Cancer Therapy. *Pharmaceutics* **2021,** *13*, 1130.
28. Zhao, L.; Ren, X.; Yan, X., Assembly-induced superlarge redshifted absorption: A burgeoning way for organic near-infrared materials. *CCS Chemistry* **2021,** *3*, 1-32.
29. Zhao, L.; Li, S.; Liu, Y.; Xing, R.; Yan, X., Kinetically Controlled Self-Assembly of Phthalocyanine–Peptide Conjugate Nanofibrils Enabling Superlarge Redshifted Absorption. *CCS Chemistry* **2019,** *1*, 173-180.
30. Hering, J. A.; Innocent, P. R.; Haris, P. I., Automatic amide I frequency selection for rapid quantification of protein secondary structure from Fourier transform infrared spectra of proteins. *Proteomics* **2002,** *2*, 839-849.
31. Xing, R.; Yuan, C.; Li, S.; Song, J.; Li, J.; Yan, X., Charge-Induced Secondary Structure Transformation of Amyloid-Derived Dipeptide Assemblies from β-Sheet to α-Helix. *Angew. Chem. Int. Ed.***2018,** *57*, 1537-1542.
32. Keiderling, T. A., Protein and peptide secondary structure and conformational determination with vibrational circular dichroism. *Curr. Opin. Chem. Biol.* **2002,** *6*, 682-688.
33. Zhao, L.; Liu, Y.; Xing, R.; Yan, X., Supramolecular Photothermal Effects: A Promising Mechanism for Efficient Thermal Conversion. *Angew. Chem. Int. Ed.* **2020,** *59*, 3793-3801.
34. Zhang, H.; Liu, K.; Li, S.; Xin, X.; Yuan, S.; Ma, G.; Yan, X., Self-Assembled Minimalist Multifunctional Theranostic Nanoplatform for Magnetic Resonance Imaging-Guided Tumor Photodynamic Therapy. *ACS Nano* **2018,** *12*, 8266-8276.
35. Yoon, D. S.; Lee, M.-H.; Cha, D. S., Measurement of Intracellular ROS in Caenorhabditis elegans Using 2',7'-Dichlorodihydrofluorescein Diacetate. *Bio-protocol* **2018,** *8*, 2774.
36. Yang, M.; Yuan, C.; Shen, G.; Chang, R.; Xing, R.; Yan, X., Cyclic dipeptide nanoribbons formed by dye-mediated hydrophobic self-assembly for cancer chemotherapy. *J. Colloid Interface Sci.* **2019,** *557*, 458-464.

# Chapter 5 Conclusions and Future work

## 5.1 Conclusions

Based on that excessive ROS generation can lead to increased risk of chronic diseases and carcinogenesis and interfere with redox dynamics for self-survival, ROS in lesion site have received drawn wide attention as a new target for treating variety of different diseases. Therefore, we have designed ROS-regulating nanomaterials owing to all-in-one progress of ROS biology, ROS chemistry and ROS nanotechnology.

In Chapter 2, antioxidant NPs are prepared by co-assembly of flavonoid Myr and GSH in the presence of $Zn^{2+}$. As-obtained NPs not only overcome the disadvantages of Myr and GSH for improving their bioavailability, but also possess sustainable ROS scavenging activity for protecting cells from ROS damage.

In Chapter 3, CPP and Genipin are combined to covalently assemble robust GCPP NPs. Covalent-assembled GCPP NPs with antioxidant activity are fabricated for IBD treatment via oral administration. As-prepared GCPP NPs possess stable nanostructure in harsh pH/enzymatic conditions, which cannot be destructed by oral delivery for achieving high bioavailability of peptides Moreover, GCPP NPs present favorable therapeutic effect, which attributes to properties of controlled antioxidation to sustainably scavenging ROS and nano size preferentially accumulated at the inflamed colon site and remarkable advantage of promoted crypt regeneration. As-made GCPP NPs have been spotlighted as a potential antioxidant agent to treat ROS-related inflammation diseases.

In Chapter 4, supramolecular photosensitizer nanorods have been constructed by coordination assembly based on the combination of OVA, $Zn^{2+}$ and PheoA. Co-assembled OVA-$Zn^{2+}$-PheoA nanorods exhibit high encapsulation efficiency compared with loading strategy. Owing to the dynamic flexibility of noncovalent interactions, as-prepared nanorods can respond to acid pH in tumor cells for the controlled release of monomeric photosensitizer and corresponding generation of ROS, thus enhancing *in vitro* PDT. During *in vivo* experiment, nanorods can selectively accumulate in tumors and further diagnose tumor site for antitumor treatment.

## 5.2 Future work

The nosogenesis of many diseases, such as periodontal disease (PD), Neurodegenerative diseases, Atherosclerosis and Myocardial infarction, have been investigated to have tightly relationship with ROS. Therefore, ROS-based nanomedicines have been deemed as important strategy for disease therapy. Nowadays is an era of precision medicine, increasing number of nanodrugs with unique compositions, structures and functionalities are fabricated, which is an important step for meeting personalized medicine. Moreover, immunotherapy has been regarded as the most typical personalized therapeutic modality. Therefore, we need further integrate immunotherapy with ROS-based nanodrugs for optimized disease therapy.

During gradually preparing and optimizing new-generation nanomedicine, there are still new challenges remaining to be met. In the spirit of "confront soldiers with generals

and stem water with earth", we will surely that ROS-based nanomedicines will obtain leap-forward development and further clinical transformation in the future.

**List of publications**

1. **Ma, X**.; Xing, R.; Yuan, C.; Ogino, K.; Yan, X., Tumor therapy based on self-assembling peptides nanotechnology. *VIEW* **2020,** *1*, 20200020-13. (In chapter 1)

2**. Ma,X**.; Gong,H.; Ogino,K.; Yan,X.; Xing,R. Coordination-assembled myricetin nanoarchitectonics for sustainably scavenging free radicals. *Beilstein J. Nanotechnol.* **2022,** *13,* 284–291. (In chapter 2)

3. **Ma, X**.; Gong, H.; Liu, Y.; Ogino, K.; Xing, R.; Yan, X., Orally Administered Covalent-assembled Antioxidative Peptide NPs for Inflammatory Bowel Disease Therapy. *J. Colloid. Interf. Sci.* **2022**, *626*, 156-166. (In chapter 3)

4. **Ma, X.**; Liu, Y.; Li, S.; Ogino, K.; Xing, R.; Yan, X., Multicomponent Coassembled Nanodrugs Based on Ovalbumin, Pheophorbide a and $Zn^{2+}$ for in vitro Photodynamic Therapy. *Supramol. Mater.* **2022**, 100010-6. (In chapter 4)

**Reference paper:**

1. **Ma, X**.; Wu, Q.; Tan, L.; Fu, C.; Ren, X.; Du, Q.; Chen, L.; Meng, X., Chemical chaperone delivered nanoscale metal–organic frameworks as inhibitor of endoplasmic reticulum for enhanced sensitization of thermo-chemo therapy. *Chinese Chem. Lett.* 2022, 33, 1604-1608

**Acknowledgements**

In the twinkling of an eye, three years of doctoral career is coming to an end. This is most fulfilling life for me. I really appreciate many people that I have met during three years.

First and foremost, I would like to express my sincere appreciation to my supervisors, Prof. Kenji Ogino and Prof. Xuehai Yan. Thank Prof. Kenji Ogino for your careful treatment and attendance when I was in confusion. Thank Prof. Xuehai Yan for your advice and guidance during my PhD. During the doctoral period, I gradually cultivated the ability to independently think about scientific problems, designed experiments and verify results. I believe these processes must be favorable for my growth both in scientific research and in life road.

Secondly, I also need to express my special gratitude to Dr. Ruirui Xing, Dr. Peng Zhou, Dr. Chenqian Yuan, Dr. Luyang Zhao, Dr. Guizhen Shen, Dr. Shukun Li, Dr. Yanmei Liu, Dr. Haoning Gong, Dr. Yanchen Liu, Dr. Yazhou Liu and Dr. Wei Fan for their assistance with profound knowledge and rich experimental experience. Especially thanks to Dr. Jin Chen for patient assistance in life.

I am also grateful to my classmates, Rui Chang, Fengqiang Cao, Kaili Zhao, Kaiwei Chen, Dongrui Su, Rongke Gong, Xiaonan Li, Zhuoyi Liu. It is so glad to meet you and do research together, which make my life more colorful.

Last but not the least, I would like to express sincere appreciation to my family. I could not have achieved this PhD degree without their selfless support and positive encouragement.

Finally, I am grateful for the experts who attended the thesis defense for their careful guidance and valuable opinions.